# Supramolecular crosslinking of biomimetic poly(2-hydroxyethyl methacrylate) nanocomposite reinforced with multi-walled carbon nanotubes

Laura Lemetti

Master's thesis

UNIVERSITY OF HELSINKI

Department of Chemistry

Laboratory of Organic Chemistry

02/2016

HELSINGIN YLIOPISTO
HELSINGFORS UNIVERSITET
UNIVERSITY OF HELSINKI

| Tiedekunta/Osasto Fakultet/Sektion – Faculty | Laitos/Institution– Department |
|---|---|
| Faculty of Science | Department of Chemistry |

Tekijä/Författare – Author
Laura Lemetti

Työn nimi / Arbetets titel – Title
Supramolecular crosslinking of biomimetic poly(2-hydroxyethyl methacrylate) nanocomposite reinforced with multi-walled carbon nanotubes

Oppiaine /Läroämne – Subject
Organic chemistry

| Työn laji/Arbetets art – Level | Aika/Datum – Month and year | Sivumäärä/ Sidoantal – Number of pages |
|---|---|---|
| Master's thesis | 02/2016 | 101 |

Tiivistelmä/Referat – Abstract

Evolving technology sets new requirements to material development all the time. Many scientists are trying to meet these requirements by the means of biomimetics. Biomaterials, like spider silk and nacre, have exceptional properties which derive from their hierarchical organization and supramolecular interactions. Spider silk has attracted plenty of attention during the past decades. It has high tensile strength and very good elongation properties but in addition to these, researchers are interested in of the energy dissipating properties which arise from sacrificial bonding and hidden lengths in the protein structure.

Production of synthetic spider silk has been approached in several ways. Different nanocomposites consisting of polymers and carbon nanotubes have been studied extensively. In these nanocomposites, carbon nanotubes are used to mimic reinforcing β-sheets which enable high tensile strength of spider silk. Polymer is used to simulate the non-crystalline regions which give rise to high elongation of spider silk.

In this Master's thesis, a review of supramolecular concepts enabling biomimetic research is presented. Also chemical and physical structure and properties of spider silk and carbon nanotubes and their role in different biomimetic materials are presented. The experimental part of this thesis consists of functionalization of multi-walled carbon nanotubes and poly(2-hydroxyethyl methacrylate) with 2-ureido-4[1H]-pyrimidinone hexamethylene isocyanate. These materials were used to prepare nanocomposites via self-assembly. The aim of this study was to prepare two-component nanocomposite with high tensile strength.

Tensile tests on the nanocomposites were carried out and major improvement in the mechanical properties were observed. Even though the ultimate strength of the materials did not reach expected values, the composites functionalized with dimerizing ureidopyrimidinone-motifs resisted crack growth like predicted.

Avainsanat – Nyckelord – Keywords
Supramolecular, self-assembly, carbon nanotube, pHEMA, ureidopyrimidinone

Säilytyspaikka – Förvaringställe – Where deposited
HELDA/ eThesis

Muita tietoja – Övriga uppgifter – Additional information

# Table of contents

# ABBREVIATIONS

| | |
|---|---|
| ACS | Alumina-coated silica nanoparticles |
| BMIM | 1-butyl-3-methyl imidazolium |
| CVD | Chemical vapor deposition |
| DBTDL | Dibutyltin dilaureate |
| DDBS | Dodecylbenzene sulfonate |
| DMF | Dimethylformamide |
| DMSO | Dimethyl sulfoxide |
| FWCNT | Few-walled carbon nanotube |
| HEMA | 2-Hydroxyethylmethacrylate |
| MeOH | Methanol |
| MWCNT | Multiwalled carbon nanotube |
| NMR | Nuclear magnetic resonance spectroscopy |
| NOM | Natural organic matter |
| PEG | Polyethyleneglycol |
| PFH | Poly[9,9-dihexylfluorenyl-2,7-diyl] |
| PFO | Poly[9,9-dioctylfluorebyl-2,7-diyl] |
| SDBS | Sodium dodecylbenzene sulfonate |
| SEM | Scanning electron microscopy |
| SWCNT | Single walled carbon nanotube |
| UPy | 2-Ureido-4[1H]-pyrimidinone |
| UPy-$C_6$-NCO | 2-Ureido-4[1H]-pyrimidinone hexamethylene isocyanate |
| FT-IR | Fourier transform infrared spectroscopy |

# I LITERATURE PART

## 1. Introduction

Nature has shown its power by synthesizing materials that possess extraordinary mechanical properties which have never been obtained by man-made materials. Increasing interest in replicating the designs found in the nature have occurred during the past few years. Biomimicry studies biological processes and the function of biological material, aiming to produce synthetic material with similar properties.[1]

Biomaterials, like spider silk, nacre and bone, have unique properties which derive from their hierarchical organization[1] and supramolecular interactions. Supramolecular interactions between the composites results in precisely determined self-assembly and appearance of fine structures. Spider silk and nacre are both tough and durable; silk being stretchable and strong, nacre tough but not as brittle as the structure would indicate. These materials have inspired scientists in their research for years and research on this field will continue to evolve rapidly. Silk for example, has been used in medical and biomedical applications, parachutes and tissue regeneration.[2]

Scientists have already defined the amino acid sequences found in spider silk to some extent.[3] However, this is a challenging task due to the large variety of spider species which produce different silk proteins. Because the amino acid sequence is known to some extent, a possibility to prepare similar structures synthetically from amino acids exists. Advances in the field of protein engineering have allowed the synthesis of genetically engineered spider silk proteins. Still, producing spider silk proteins is rather laborious and yields are not very good.[1,4] Instead of mimicking the exact protein structure of the spider silk, studies concentrate on mimicking the nanostructure in spider silk. Scientists have studied the properties of different regions of spider silk and the interactions between these regions and try to transfer these properties into their nanocomposite design. Research on this field has gained massive interest in recent years. Several nanocomposites are built up from stiff nanoscale sheet-like reinforcements, which corresponds to the β-sheets in the spider silk structure, and synthetic polymers which resemble the soft and stretchable protein part of spider silk.

New nanocomposites are being developed and studied all over the world. As technology develops, new ways to meet the growing requirements considering the size and performance are needed. Devices should be thinner and lighter than before, work faster, and function without trouble. Carbon nanotubes (CNT) are very intriguing material considering nanocomposites. They could improve the durability and strength of the nanocomposites and bring additional functional properties like conductivity and better mechanical properties to them. Carbon nanotubes have been lately used in several new materials as the conducting phase. For example Wang *et al.*[5] produced self-supported film from ureidopyrimidinone (UPy) -functionalized carbon nanotubes using layer by layer -assembly. Du *et al.*[6] obtained a supramolecular hydrogel with self-healing properties by crosslinking oxidized carbon nanotubes and polyethylene polyamine by using hierarchical hydrogen bonding.

In this thesis, a brief review of supramolecular chemistry and the structure and properties of spider silk and carbon nanotubes are presented. The experimental part of this thesis describes surface modification of multi-walled carbon nanotubes, preparation of supramolecularly cross-linked nanotube/polymer nanocomposites and their characterization and determination of mechanical properties. The aim is to produce supramolecularly crosslinked nanomaterial, reinforced with carbon nanotubes, which structure would mimic the structure of spider silk. Our target is to develop a tough two-component nanocomposite with energy-dissipating fracturing mechanism. We use multi walled carbon nanotubes to mimic the β-sheets in the spider silk structure and ureidopyrimidinone to create sacrificial bonding between the carbon nanotubes and the polymer phase that resembles the non-crystalline protein phase of the spider silk (figure 1).[3,7,8]

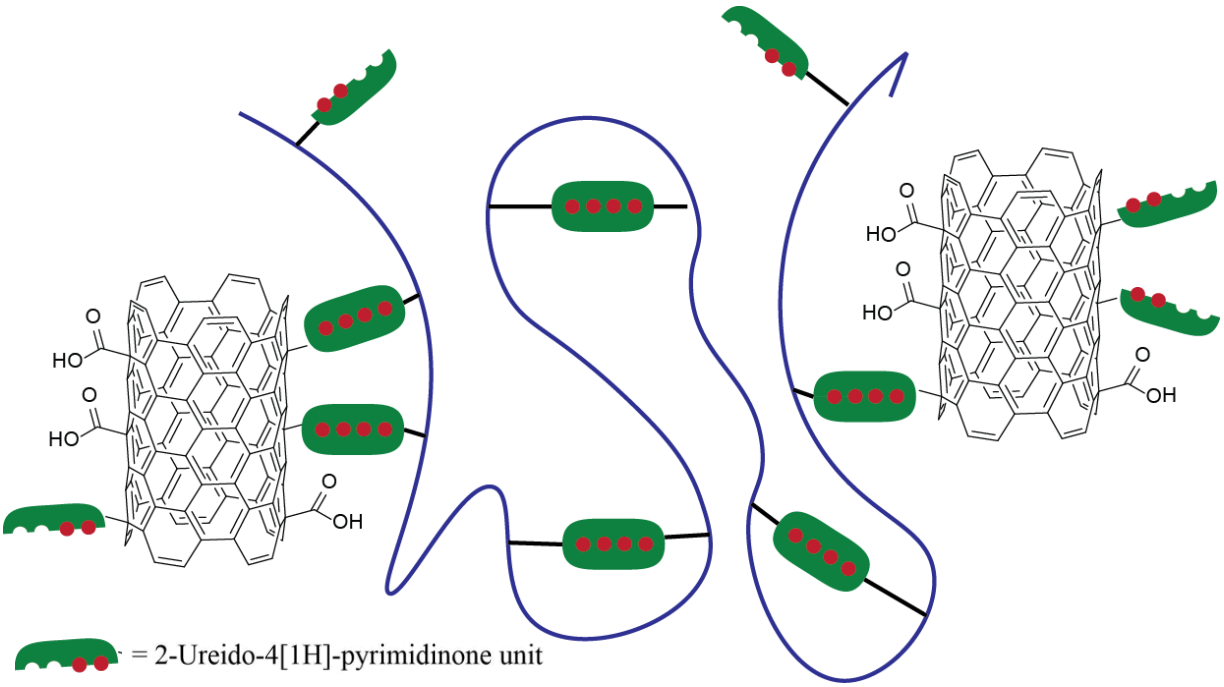


**Figure 1.** Schematic representation of the supramolecular complex between carbon nanotubes and polymer.

Similar design, using nanocellulose, has already been reported by McKee *et al.*[9]. They created a one-component nanocomposite while we are aiming at using two-component system which would bind together supramolecularly. McKee *et al.*[9] used cellulose nanocrystals which they grafted with polymethacrylate polymers with ureidopyrimidininone-groups as side chains. UPy-groups behave as sacrificial bonds when stress is applied on the material – these bonds are a very important part of the strength of spider silk.

# 2. Supramolecular chemistry

The background of biomimetic research and the experimental part of this thesis lies in the principles of supramolecular chemistry. Jean-Marie Lehn defines supramolecular chemistry as "chemistry of the intermolecular bond, covering the structures and functions of the entities formed by association of two or more chemical species".[10] According to Lehn, supramolecular chemistry has already been recognized in the mid-1930s. Back then, the term "Übermoleküle" was coined, meaning a supermolecule which forms when coordinatively saturated species interact with each other. Jean-Marie Lehn is considered to be a pioneer of supramolecular chemistry and he received the Nobel Prize in Chemistry in 1987 for research on the field of supramolecular chemistry.

Via supramolecular chemistry we could end up with very precisely designed, highly selective recognition between molecules. There are several cases in the field of biomedical[11–13] and electronic applications in which this is already utilized. For example supramolecular, DNA based nanomachines[14] or tweezers[15] in which change of conformation is used to convert energy to motion have been reported.

Supramolecular chemistry still has some big challenges that need to be overcome in order to build a working supramolecular complex. Strength of the complex, directionality and selectivity are important features when designing a new way to approach a problem, but these features may not necessary be easy things to overcome. The complex should not be too strong so that some reversibility could be reserved, and it should be selective, so that precisely the aimed outcome can be achieved.

## 2.1 Principles of supramolecular chemistry

Supramolecular chemistry is based on organic and inorganic molecules that are complementary and can interact with non-covalent forces with each other. These non-covalent interactions enable self-assembly and molecular recognition.[16] The aim, when designing supramolecular complexes, is to have segregation between different guests.

The lock-and-key principle was developed by Emil Fischer over hundred years ago to describe the way enzyme and substrate recognize each other (figure 2).[17] This principle is easy to understand and describes the recognition process of enzymes well.

Molecular recognition involves selection of the substrate and binding.[10] This leads to a host-guest complex, or supramolecule.[18] The complex might have a certain function which can for example lead to modification of the substrate. High recognition is usually feasible and to reach this, receptor and substrate should have contact over a large area.[10]

DNA and its complementary base pairs are most often used as an example of the phenomenal way nature uses self-assembly. Overall, biology gives us several good examples of very precise host-guest interaction and molecular recognition. Enzymatic reactions, antigen-antibody interactions and signal induction by neurotransmitters give some idea of how well supramolecular chemistry works in human body.[10]

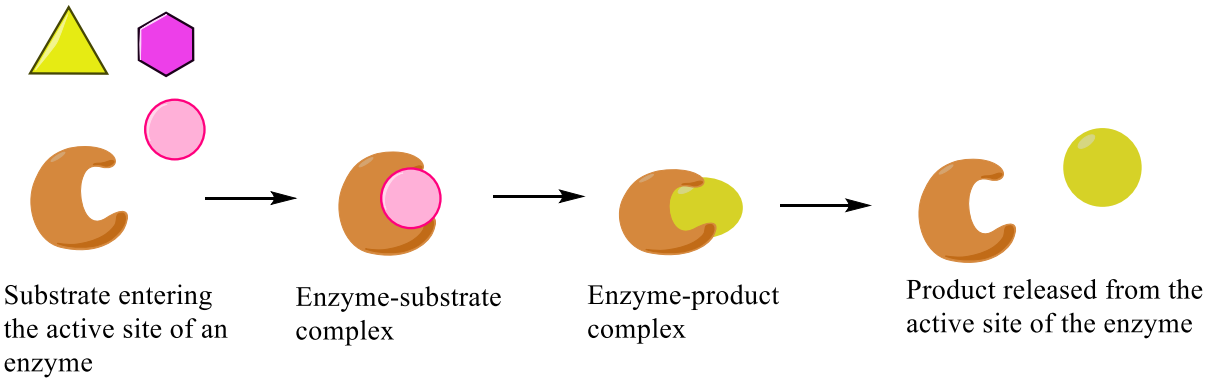


**Figure 2.** The lock-and-key principle developed by Emil Fischer.

Supramolecular complexes result from interaction between molecular receptor and a substrate.[10] In most cases, substrate is smaller than receptor. Preorganization is a very important part of complex formation in supramolecular chemistry. This means that before the host can bind a substrate, it must undergo some major changes in its conformation. In a host-guest complex, the host needs to be rigid enough for supramolecular recognition. If the host is too flexible, the preorganization might take too much time and energy and complexation is impossible. Rigidity on the other hand may cause problems if it exceeds certain extent; then complementary geometry of a guest might not be found.[19] Complementary electronic and geometric character of the host and the guest is required as well and for example crown ethers (figure 3) are highly discriminating with size of the guest. The larger the ring, the larger the guest can also be.

HSAB-theory (Hard and soft acids and bases) applies also in the formation of supramolecular complexes. This theory handles the properties of Lewis acids and bases. Hard species refer to small, highly electronegative and weakly polarizable species while soft ones refer to their opposites. The outcome of this theory is that hard acids tend to react rather with hard bases and soft acids with soft bases.[20] Considering supramolecular chemistry, hardness and softness of the host can be tuned for example in a crown ether ring by changing the acceptor atoms – if some oxygens are replaced with sulfur, the resulting complex prefers to bind softer guests like $Ag^+$.[20] On the other hand, [15]crown-5 would be complementary to $Na^+$ but [18]crown-6 (figure 3) is complementary to $K^+$ so also the size of the guest leads to discrimination and high selectivity.

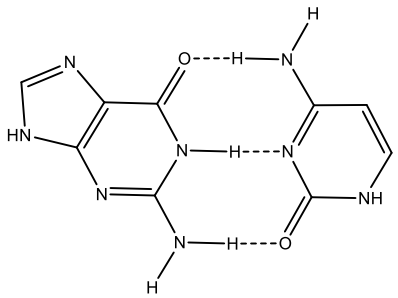

Hydrogen bonding between Guanine and cytosine

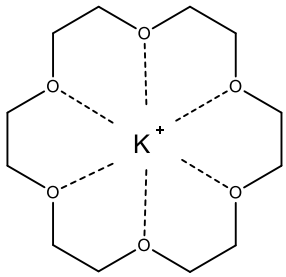

$K^+$ crown ether complex
ion-dipole interaction

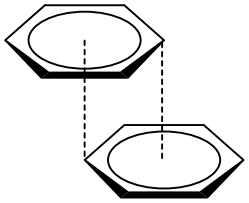

Face-to-face π-π stacking

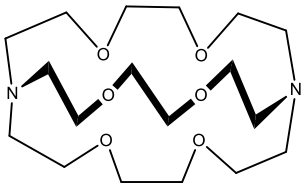

2.2.2. Cryptand

**Figure 3**: Examples of supramolecular complexes. Cryptand forms a cavity and can bind ions by ion-dipole interaction.[18]

Non-covalent forces are not always needed to form a supramolecular complex; topology can also be used to form interlocked complexes. Catenanes are formed from two or more rings that are interlocked mechanically (figure 4). They do not need any non-covalent interactions to keep this structure but for example ion-dipole interaction can be used to keep the rings in specific orientation. Rotaxanes are formed from a linear molecule which has one or more macrocycles threaded around it (figure 4).

Rotaxanes are capped with bulky groups at the end of the linear molecule so that the macrocycles cannot escape. Pseudorotaxanes do not have these caps at the end of the molecule. These mechanically interlocked structures are presented in figure 4.

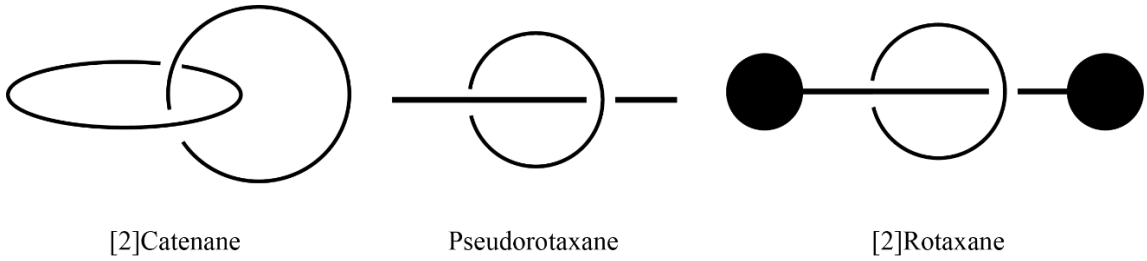


**Figure 4:** Mechanically interlocked complexes: catenane, pseudorotaxane and rotaxane.

## 2.2 Self-assembly

Self-assembly is a process in which molecules organize in a certain way due to intermolecular non-covalent forces. A simple two-component host-guest-complex forms by self-assembling if the media is suitable but much larger structures, like supramolecular polymers, can be designed as well. The driving forces for supramolecular self-assembling are non-covalent intramolecular interactions such as hydrogen bonding, host-guest interaction, hydrophobic or hydrophilic forces or π-π-interactions. Their bond energies vary from 5 kJ $mol^{-1}$ to 200 kJ $mol^{-1}$ (table 1). As can be seen, ion-dipole bond could be the strongest one, hydrogen bonds being only half of the maximum value of ion-dipole bond. Though, hydrogen bonding systems can be stronger as these bonds are directional to some extent and there can be several of them side by side.[21] Supramolecular chemistry usually covers complexes that are in equilibrium since non-covalent forces are weak and they can break and form again easily.[16]

**Table 1.** Bond energies of different non-covalent forces.[18]

| Interaction | Bond energy kJ mol$^{-1}$ |
|---|---|
| Ion-dipole interaction | 50-200 |
| Dipole-dipole interaction | 5-50 |
| Hydrogen bonding | 4-120 |
| Cation-π interaction | 5-80 |
| π-π stacking | 0-50 |
| Van der Waals forces | <5 |

π-π Stacking is a rather weak force but just like with H-bonding, cooperativity results in strong interaction between components. For example in the case of carbon nanotubes, π-π stacking and van der Waals forces[22] are present in such large quantities that it affects dispersibility of the nanotubes[23]. It is difficult to obtain a homogeneous dispersion because the solvent is not able to overcome the interaction between nanotubes, resulting in CNT agglomeration.

## 2.3 Thermodynamic and kinetic control

Control, or selectivity, of the reaction can be either thermodynamic or kinetic. Majority of supramolecular complexes are under thermodynamic control as a consequence of the reversible nature of bonding between the components of the system.[16] Thermodynamic control is based on the strength of the interaction between the host and a guest. The host is selective towards the guest that binds the strongest. Kinetic control on the other hand is based on the transformation rate of competing guests. High binding constant indicates thermodynamic control as strong binding hinders fast reaction. Elio and Sijbren[16] divide synthetic supramolecular systems into three categories according to their thermodynamics (figure 5):

1. Equilibrium assemblies. These systems last for long periods of time since they are thermodynamically very stable. For example mechanically interlocked structures or supramolecular polymers are under thermodynamic control.
2. Kinetically trapped assemblies. These systems are momentarily durable. Kinetically trapped assemblies are trapped in a local energy minimum and energy is required to transform them to more stable structures. Usually for example a catalyst is required to

form such a complex. Bilayer vesicles formed from phospholipids are most of the time under kinetic control. They are usually formed very fast in specific conditions but can easily transform to more stable species.

3. Far-from-equilibrium assemblies. To persist, these assemblies require energy constantly. If the system does not get the energy needed, it collapses and end up in a thermodynamic minimum state. Examples of this type of systems are scarce.

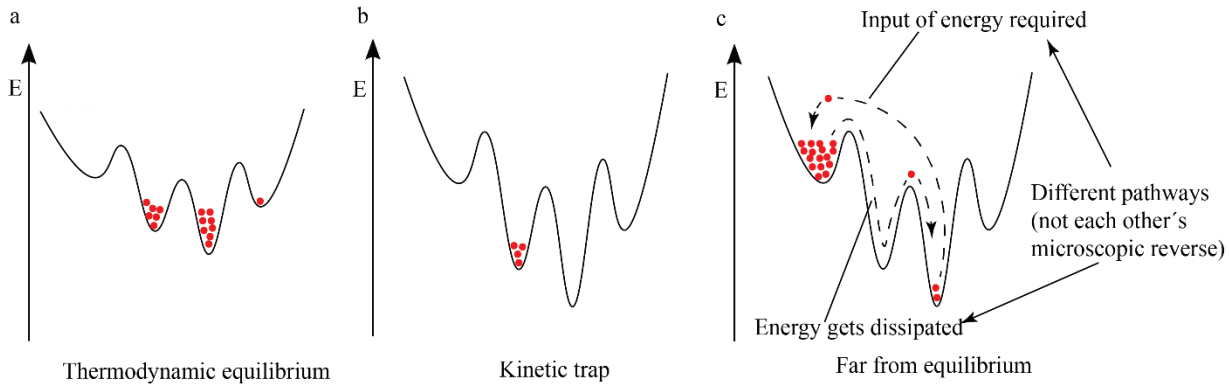


**Figure 5:** Energy profiles of thermodynamic and kinetic reactions.[16]

# 3. Spider silk

Spiders produce silk to protect their descendants from the environment but also to produce different shaped webs to capture prey.[24] Over 34 000 spider species are known[25] but orb-weaving spiders are researched the most[24] and dragline silk is the most profoundly studied silk[26,27]. Spiders produce silk with silk glands that are located in their abdomen.[3] According to Xu and Lewis[3], orb-web-spinning spiders have six different glands from which they can generate silk. These all different silks have differing properties but they all are composed solely of proteins.

Spider silk is often compared to steel and synthetic polymer Kevlar because by weight, spider silk has a tensile strength higher than steel and of the same order of magnitude as Kevlar.[3,24,28] In addition to that, spider silk also possesses very high elasticity; a property that synthetic Kevlar does not have.[28] The combined stiffness and elasticity of spider silk together result in toughness that has never been produced synthetically.[28]

## 3.1 Structure and properties of spider silk

Spider silk has a highly organized structure that consists of reinforcing β-sheet nanocrystals and non-crystalline, semiamorphous protein matrix.[2] Rousseau *et al.*[27] used scanning transmission X-ray microscopy to show, that the structure of the semiamorphous matrix is actually much more oriented than previously thought. This has been noticed in other studies as well.[8] Rousseau *et al.*[27] also found out that the polypeptide matrix is more greatly ordered at the surface of the fiber than at the core.

Spider silk could be understood as a block copolymer where the repeating amino acid sequences correspond to polymer blocks.[29] It is difficult to generalize the amino acid sequence of different spider silks due to the diversity of species. According to Xu and Lewis[3], the repeating unit of spider silk consists of maximum 34 amino acids but a more recent study by Huemmerich *et al.*[26] states that the repeating unit can include up to 60 amino acids. The repeating units are not tightly conserved, therefore plenty of variations in the sequences can be observed.

Alanine, serine and glycine are the dominating amino acids in the protein (figure 6). According to Beek *et al.*[8] almost 70 % of the primary amino acid sequence consists of alanine and glycine. Bulk of the material consists of non-crystalline regions in which the amino acid sequences are dominated by glycine and proline.[8,24] This region should not be called amorphous since it has a specific orientation even though it is not crystalline.[8] The semiamorphous protein phase of spider silk consists of $3_1$-helices and β-turn protein structures.[2]

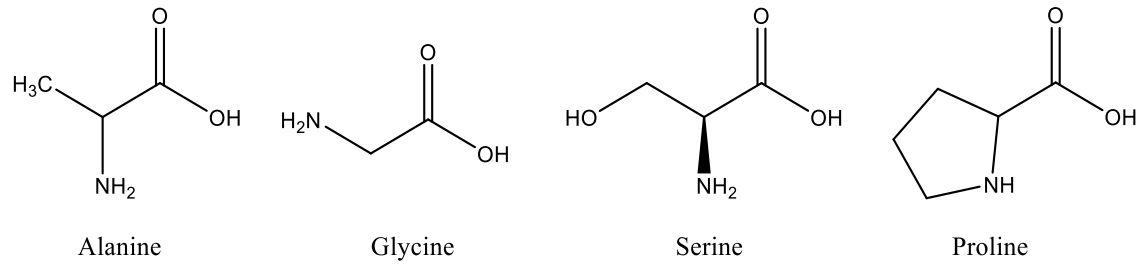


**Figure 6.** The most common amino acids in spider silk.

The crystalline region consists of β-sheets which are mostly formed of polyalanine or alternating alanine-glycine residues.[24,30] 40 % of alanine residues are found in crystalline form in β-sheets and this corresponds to approximately 10 % of the whole fiber. The rest of alanine is found from the non-crystalline regions.[31]

Poorly hydrated, consecutive alanine residues can interlock with adjacent chains via hydrophobic interactions and form β-sheets (figure 7).[30] β-sheets formed from glycine and alanine cannot interact the same way as alanine residues even though they form similar β-sheet structures. Therefore, interactions between Gly-Ala sectors are weaker than the hydrophobic interactions between alanine chains. These different β-sheets can be found from different spider silks depending on the purpose of the silk.[30]

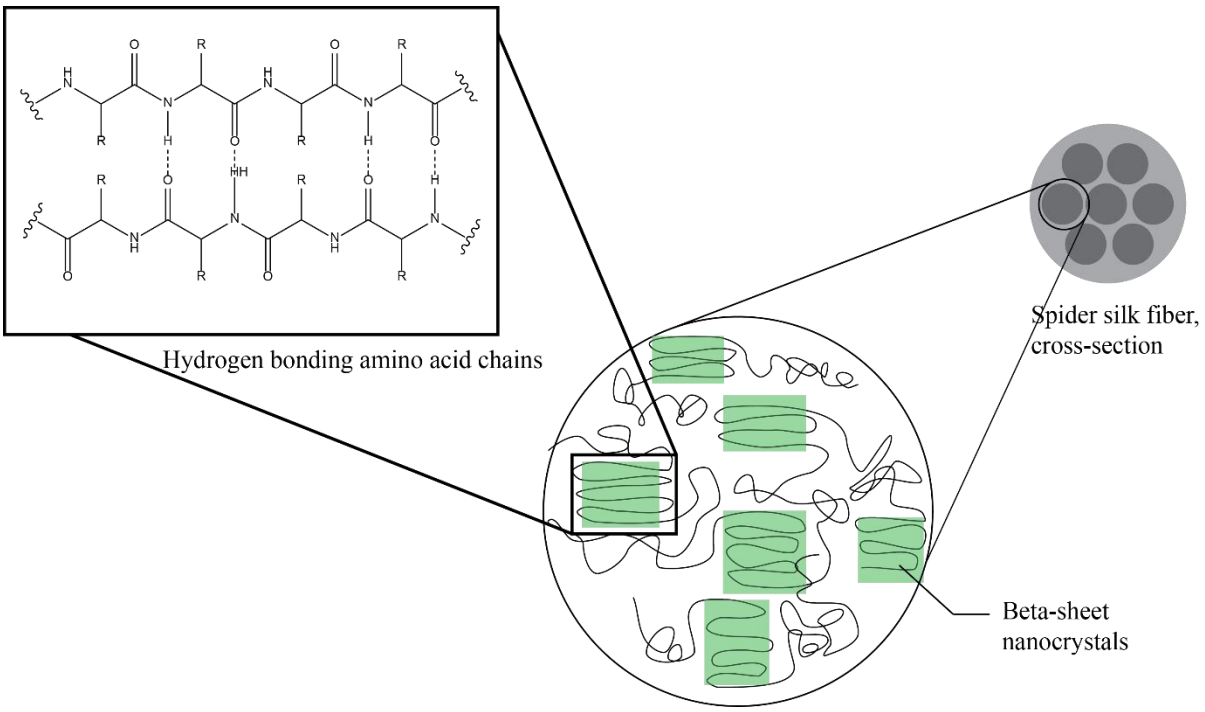


**Figure 7.** Schematic representation of the structure of spider silk. R-groups at the amino acids correspond to different side chains of amino acids found in spider silk.

Amino acids used in spider silk make two different proteins and they are called Spidroin I and Spidroin II.[8] From these, Spidroin I is more ordered and hydrophobic whereas Spidroin II is less ordered and hydrophilic.[32] In the final product, Spidroin I is homogeneously distributed in the core of the fiber and Spidroin II stays as heterogeneously distributed clusters at the most interior part of the core (figure 8). [24]

The core of the fiber, formed of Spidron I and Spidroin II, is then covered by a layer of skin consisting of some minor ampullate silk, then with a layer of glycoprotein and finally with some lipids (figure 8).[24] The glycoprotein layer participates the humidity control of the silk. Humidity affects the mechanical properties. When water is absorbed, silk dragline fiber shrinks.[33] The glygoprotein layer together with lipid layer protects the fiber from micro-organisms and therefore prevents degradation.[24]

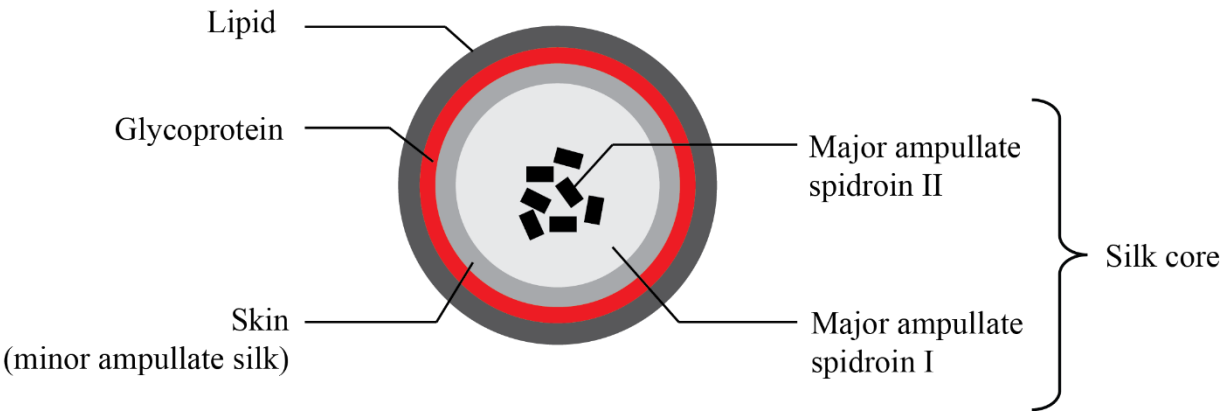


**Figure 8.** Schematic representation of Spidroin I and II.[24]

As already stated, spider silk has very good mechanical properties. These properties depend strongly on the crystallinity of the protein.[34] The crystallinity on the other hand, is controlled by the sequence of amino acids in the protein. Different regions have their own role when the material is deforming; β-sheet nanocrystals determine the mechanical properties of the fiber at large deformation whereas the non-crystalline matrix has the responsibility of the behavior of the material at small deformation.[2] Therefore, crystalline matrix is mostly responsible of spider silks ultimate tensile strength while semiamorphous regions are responsible of the stretching properties.[2]

The size of the β-sheets influences the tensile strength and elasticity of the spider silk fiber much. The smaller the crystalline β-sheets are, the lower the elastic modulus and the higher the tensile strength is.[2] Normal size of a β-sheet in natural spider silk is 3 $nm^2$, Grubb and Jelinski[31] report approximate dimensions of 2 x 5 x 7 nm.

The crack resisting properties arise from hydrogen bonding between the β-turns and $3_1$-helices in the semiamorphous parts of spider silk.[2] This hydrogen bonding leads to sacrificial bonds and hidden lengths which act as nanoscale toughening structures for the spider silk fibers (figure 9). When the spider silk fiber is stretched, the proteins of the semiamorphous regions are aligned and stretched along the pulling direction.[2] This way, the material is continuously dissipating energy and therefore resists deformation and suppresses development of catastrophic crack. This mechanism is made possible by the hidden lengths and sacrificial bonding which, according to McKee *et al.*[9], increase the process zones near the crack and as a consequence applied stress is

concentrated to a larger volume in the material. When the semiamorphous region has been stretched to its ultimate length, the crystalline β-sheets start to preserve higher strains.[2]

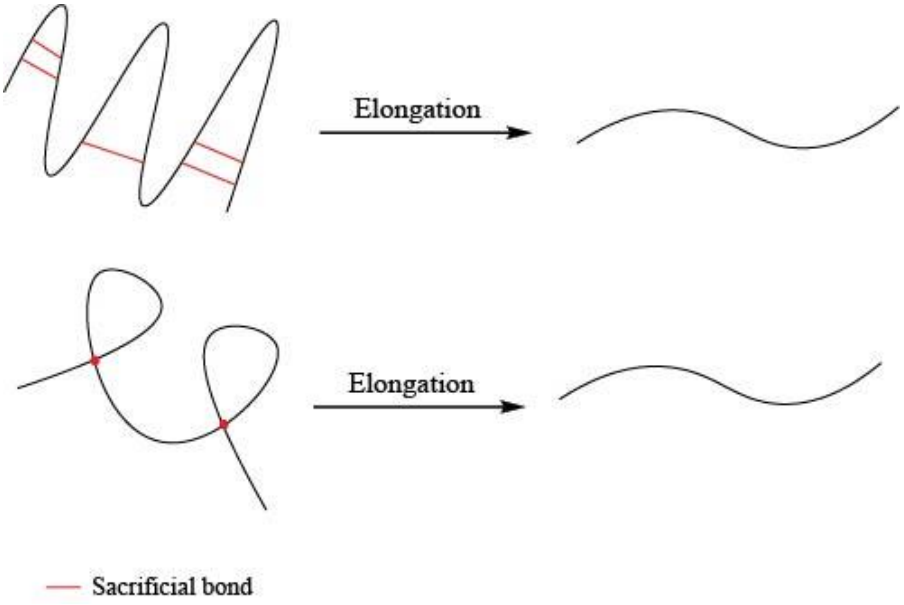


**Figure 9:** Schematic representation of the hidden length and sacrificial bonds in the polymer matrix. These hidden lengths allow stretching of the material before fracture. The work needed to stretch the material is higher due to sacrificial bonds, making the material tougher.

Spiders produce several different silks depending on the purpose where it is used. The frame and the radii usually consists of different silks compared to the spirals around the radii.[24,34] There are at least four different silk types that form the spider web (figure 10). Dragline silk (major ampullate silk) can be found from the frame and the radii and the dragline silk proteins are kept in the major ampullate gland at 50 % (w/v) concentration[26] at the most. Flagelliform silk can be found in the capture spiral, piriform silk is used as an attachment cement at the intersections of the capture spiral and the radii and minor ampullate silk can be found from the auxiliary spiral. Auxiliary spiral stabilizes the web while it is under construction before production of the capture spiral.

According to Denny's[34] observations, the frame silk would contain more and larger crystalline regions since the viscid silk does not have birefringent properties similar to the frame silk. He suggests that the amino acids with bulky side groups would be more distributed around the protein chain and due to this the protein would not be able to form such large and stable

crystalline sites. This would require different amino acid sequence from these silks. These differences in structure also lead to different physical properties which is understandable; the frame silk has to be harder and not so stretchable whereas the viscid silk can be extended more. Other studies support these findings. In the stiff spider dragline silk, 20 to 30 % of its volume consists of β-sheets.[35] More elastic vicid silk contains less than 5 % of crystal by volume. Study by Grubb and Jelinski[31] states that only 12 % of the silk fiber would be crystalline and one third well oriented but not crystalline material.

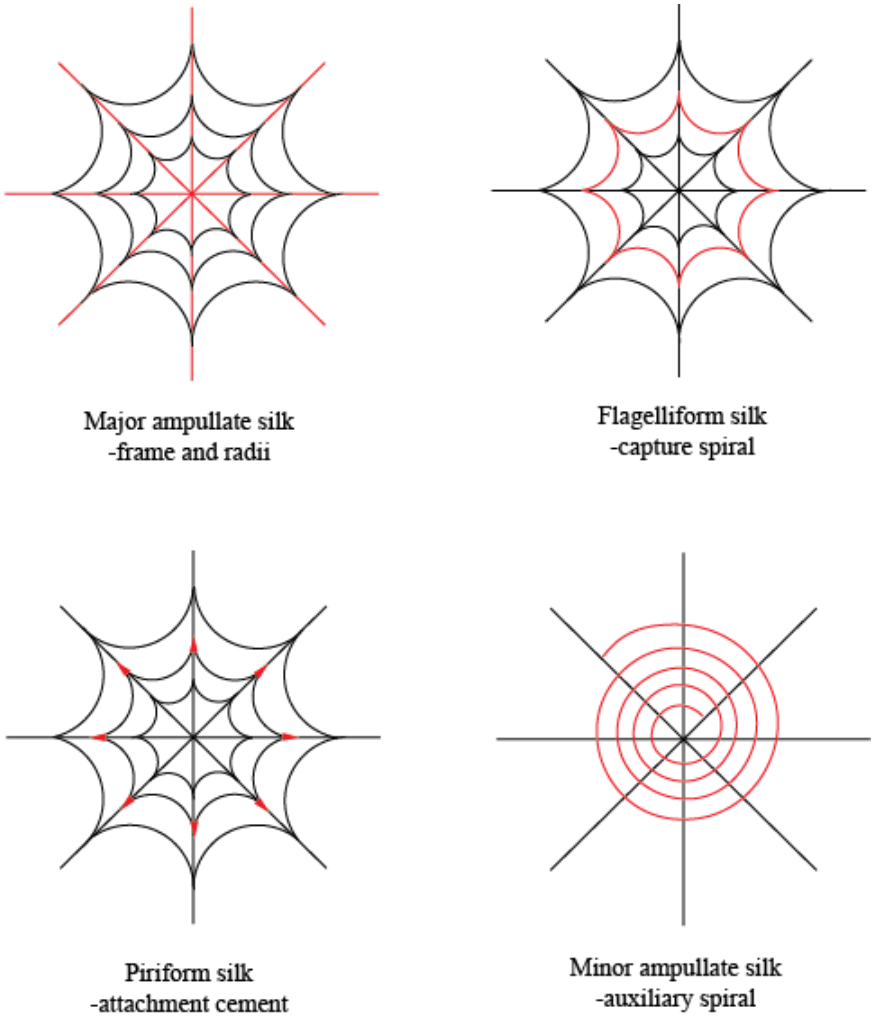


**Figure 10:** At least four different types of silk can be found from spired web structure.[24]

The ultimate stress for both, vicid silk and the frame silk is of almost the same order. For vicid silk it is approximately 1.1 GPa and for frame silk it varies from 0.8 to 1.4 GPa.[34]. Nova *et al.*[2] also report ultimate strength of almost 1.4 GPa.

The primary structure of spider silk is not the only factor contributing to the tough result; also the way and the speed with what silk is spinned out of the glands affects the secondary structure of the silk.[824] Therefore, spiders can influence the hierarchical structure of silk by changing the speed and so changing the time that the fiber has to align. Also humidity, nutrition and temperature affect the structure of spider silk.[24,33]

Gatesy *et al.*[25] argue with the claim that the spinning mechanism of spider silk would affect its mechanical properties more than the actual amino acid sequence. Motifs of amino acids, that have been preserved for over 125 million years through all the evolutionary changes, are most likely highly important to the outstanding mechanical properties of spider silk. They state that polyalanine residues could have been conserved in different spider silks already for over 240 million years.

When the spider silk fiber is drawn from the glands, it is transformed from liquid to solid state. This change is irreversible for both, Spidroin I and II.[3] Ionic strength, pH and concentration of lyotropic ions affect the irreversible change of spider silk from liquid to solid.[36] Dope passes first through the spinning duct. At this stage water and some ions are extracted from the protein solution while concentration of lyotropic ions is increased and pH lowered. Finally mechanical stress is applied when silk thread is pulled from the spider´s abdomen.[26] The sodium chloride concentration is high in the silk glands and only one phase is found in high silk protein concentrations (40 % w/v). High sodium chloride concentration deteriorates hydrophobic interactions between silk protein strands which results in inhibition of liquid-liquid phase separation and oligomer formation.[36] This is vital for the animal as it would be detrimental if liquid-solid phase separation did happen in the silk glands.

## 3.2 Spider silk mimetics

Due to its mechanical properties, biocompatibility and biodegradability, spider silk is the topic of extensive research. However, even though spider silk is tough and can be stretched, if it would be utilized in applications with heavy and continuous load, spider silk would need to act in its elastic region.[32] This would lead to a situation where the ultimate tensile strength would be useless because that property would only dominate at the plastic region.[32] For several different applications, it would be important to design a material which can take cyclic stress for long period of time and still have all the properties of spider silk.

Spider silk structure, and the ways it works, are already well known and have been utilized in several studies. The essential point in spider silk structure is sacrificial bonding and hidden lengths which are formed by hydrogen bonding. Utilization of hydrogen bonding has led to several self-healing materials since this non-covalent interaction may form again after breaking. Especially polymers are very interesting components for self-healing nanomaterials due to their elasticity, but molecularly engineered cross-linkers are needed to improve their tensile strength. Kushner *et al.*[37] introduced a biomimetic concept using UPy-motif to enhance mechanical properties of 3D network formed of crosslinked poly(n-butyl acrylate) polymer. In this study, UPy-motifs were covalently linked together by ring-closing metathesis. 6 % of UPy-linkers in the material led to more than 700 % increase in the tensile strength yet elongation was not reduced.

Qu *et al.*[38] reported a transparent, self-supported membrane made from polypeptide multi-block copolymer. Spontaneous self-assembly was observed and irreversible hydrogelation achieved when the conditions were modified to favor the conformational change from α-helices to β-strands. Nagapudi *et al.*[39] also approached the problem of biomimetic spider silk by constructing a polymer but in a rather different way. They synthesized a BAB-type block copolymer with plastic-like end blocks and elastomeric middle block which behaved as a protein-based thermoplastic elastomer. They suggest that such material could be used in applications for controlled drug release and cell encapsulation.

In addition to different polymer composites, it is possible to produce spider silk protein synthetically and use this to construct new nanomaterials. Bone and tissues of body behave as an example for synthesis of biomimetic materials. They also contain sacrificial bonding and hidden lengths which increase the fracture toughness of bone and mechanical properties of muscles.[40] Agnarsson *et al.*[41] used the humidity driven contraction properties of silk to construct a biomimetic muscle. They report that spider web based biomimetic muscle generates 50 times greater amount of work than equivalent mass of human muscle. Similar behavior can be seen in many other hydrophilic materials as well, but spider silk possesses exceptionally high modulus and therefore it is able to generate very high force. The best polymer-based synthetic muscles are activated by electric field and therefore scaling up is much more difficult than with humidity driven silk-muscle. Such nanomaterials could be used for example in sensors and actuators.[41]

Spider silk protein produced in bacteria was shown to yield mechanically very stable microcapsules.[42] Assembly was carried out in oil/water interface where conformational change from coil to β-sheet rich structure was observed. Other groups have also noticed that the conformational change from coil to β-sheet structure seems to be responsible of good properties.[38] Responsiveness of the microcapsules can be modified easily by functionalization of the capsules which leads to large amount of possible applications. Microcapsules may have applications among biomedical devices and delivering drugs or other active components. Large proteins can be controlled and functionalized better than short amphiphilic peptides and thus they are more suitable when constructing new nanocomposites.[42] Fibers[36], hydrogels[43], spheres[44,45] and films[46] can be made from recombinantly produced spider silk proteins.

# 4. Carbon nanotubes

Carbon nanotubes (CNTs) were first reported by Sumio Iijima in 1991 when they were discovered as a byproduct of fullerene synthesis.[47] Ever since, major development among nanosize carbon structures has occurred.

Carbon nanotubes have long cylindrical shape and they can be single-walled (SWCNT), few-walled (FWCNT) or multiwalled (MWCNT).[47] There are no such solvents that would dissolve pristine carbon nanotubes, therefore other ways, for example surfactants, are needed in order to get a homogeneous suspension of CNTs in solvent.[48] Another way to obtain a homogeneous suspension is oxidizing the carbon nanotubes in a solution of concentrated acids.[49] Surface functionalization by oxidation gives several other possibilities for further processing as well. Surface functionalization enables solution-phase purification and fractionation of nanotubes and also further functionalization of the surface with even larger side groups.[49]

## 4.1 Structure of carbon nanotubes

Carbon nanotubes can be thought as cylindrical structures made of graphene sheets (figure 11), multiwalled carbon nanotubes consisting of many coaxial layers.[50]. Carbon nanotubes consist of 3-coordinated carbons whose structure is between the pure $sp^2$ hybridized graphene and $sp^3$ hybridization of diamond. Carbon nanotubes have very low percentage of $sp^3$ bonds and due to this it resembles the structure of graphite.[48] To roll tube-like structure from a graphene sheet, continuous lattice structure is required. Therefore, there are only limited amount of ways a nanotube can be rolled out from a graphene sheet. Two of these have very high symmetry; armchair and zig zag forms. The ratio of $sp^2$ and $sp^3$ affects the reactivity of the carbon nanotube. Also the diameter of the tube affects the reactivity of the material. This arises from the fact that the deformation energy of $sp^2$ bond is inversely proportional to the diameter of the nanotube.[48]

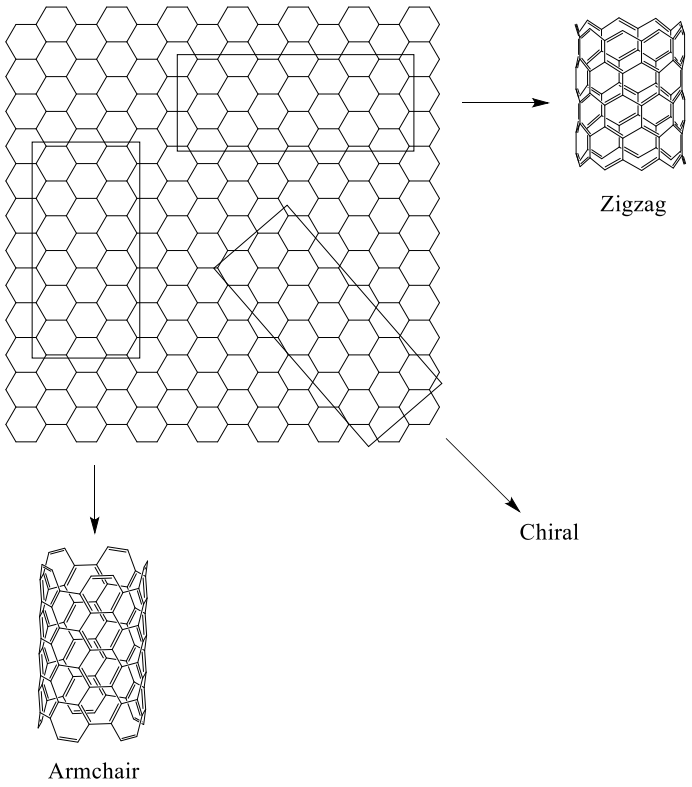


**Figure 11.** Relation between nanotubes and graphene sheets.[48]

Carbon nanotubes have very high aspect ratios. The diameter of SWCNTs normally varies approximately from 1 to 10 nm[48] and length can reach even 18.5 cm[51]. MWCNTs have outer diameter that varies from 2 to 100 nm.[52] The diameter is affected the most by the amount of walls, not by the diameter of the inner tube.[48] MWCNTs have been reported to be 5 to 50 μm[52,53] in length. Somewhat large variation in length or diameter of carbon nanotubes occur because different production methods give different physical properties. Multi-walled carbon nanotubes are reported to have a 0.34 nm gap between the layers; this corresponds to the basal plane separation in graphite.[47]

Multiwalled carbon nanotubes are more rigid than single-walled carbon nanotubes.[48] Multi-walled carbon nanotubes are also essentially frustrated because of neighboring shells, for it is impossible to satisfy the compatibility of the wrapping indices simultaneously with preserving the intershell spacing close to that of graphite interlayer spacing, which is 3.35 Å.[48]

## 4.2 Properties of carbon nanotubes

Carbon nanotubes with a helical twist (chiral) are semiconductive while achiral ones (armchair and zig zag) exhibit conductive properties like metals.[50,54] As a consequence, carbon nanotubes can have different structures which affects the electrical transport in the carbon nanotube drastically. Resistance in the tube results from locations with minimal electron density or strong tunnel barrier. These phenomena might be caused by defects in the structure or contamination in the sample.[50,55] In an ideal case, there would not be any defects on the surface of a carbon nanotube and this would lead to a ballistic electron transport but this is rarely the case. Ballistic behavior is observed only for the metallic carbon nanotubes with no defects.

Electrical properties of carbon nanotubes can be changed by bending them but in order to actually cause some changes in the local electronic structure, large stress is needed.[56] When the tubes are bent, the amount of topological defects increase and this increases the resistance of the nanotubes.[53,56] For single walled nanotubes the change in electrical properties depends on the structure of the nanotubes; zig-zag nanotubes become semi-conducting and armchair nanotubes remain conducting after bending.

Thinner multi-walled carbon nanotubes are more flexible than thick MWCNTs.[57] For multi-walled carbon nanotubes, the effects seen after bending are more powerful. This is because in single walled carbon nanotubes bending the tube does not cause enough strain and therefore not enough of atomic rearrangement is produced.[56] Bending the outermost layer inwards is restricted in multi-walled nanotubes and this leads to a higher strain compared to single walled tubes.[56] Bending causes drastic changes in the electron structure of the tubes and this affects the transmission properties of it.[53] Also twisting MWCNTs causes increased resistance. Semiconducting tubes are less symmetrical compared to metallic nanotubes; the amount of elastic deformations in the nanotube is higher in semiconducting ones.[56]

Thin SWCNTs bear high Young's modulus and high tensile strength because they are very stiff.[58] Young's modulus for multi walled carbon nanotubes has been reported to be even over 1 TPa[59] and tensile strength can vary from 11 to 63 GPa[60]. The bending modulus for multi-walled carbon nanotubes varies depending on the way they were produced. For example multi-walled carbon nanotubes produced by pyrolysis have more defects than the ones produced by arc-discharge and therefore they are softer.

This leads to even 15 times smaller bending modulus for the multi-walled carbon nanotubes produced by pyrolysis; the variation in Young's modulus between CNTs produced with these two methods is 2 GPa to 1.2 TPa (diameter smaller than 8 nm for the latter value).[61] Demczyk *et al.*[62] report Young's modulus of 0.80 TPa for MWCNTs produced by arc-discharge method.

Zhu *et al.*[63] studied the pressure resistance of multi-walled carbon nanotubes and the result was remarkable ~50 GPa. This also supports the theoretical predictions of high mechanical strength of carbon nanotubes.

Thermal conductivity of single walled carbon nanotubes has been noticed to be very high, some sources estimate it would be twice as much as the thermal conductivity of a diamond.[53] Single walled carbon nanotubes also have high thermal stability (up to 2800°C in vacuum).

## 4.3 Production of carbon nanotubes

Several different methods to produce carbon nanotubes are available. They all use very high temperatures and the reactions are performed in an inert atmosphere (either Ar or He). The three most common methods are laser ablation[64], arc-discharge and chemical vapor deposition (CVD).[65]

Production method may affect the amount of impurities in the material and the entanglement of the nanotubes.[53] Chemical entanglement occurs as surface-to-surface attraction or self-assembly, physical entanglement implies for example loops around other nanotubes.[53]

MWCNTs are easy to produce in large scale by chemical vapor deposition method because it is fairly simple and easy to scale up. CVD process can be carried out for example in a quartz reactor as Yeoh *et al.*[65] did. A schematic representation of the set-up is presented in figure 12.

To produce carbon nanotubes in a CVD reactor, a catalyst (Co-Mo/MgO) is placed to the reactor and the reactor is then heated to 800 °C with a nitrogen flow. When the required temperature is reached, mixture of methane and nitrogen is kept in the reactor for 30 minutes. Cooling down to room temperature is carried out again with a nitrogen flow. Catalyst is then removed by stirring the carbon nanotubes in mild nitric acid and the purified product is rinsed with distilled water until neutral and dried.

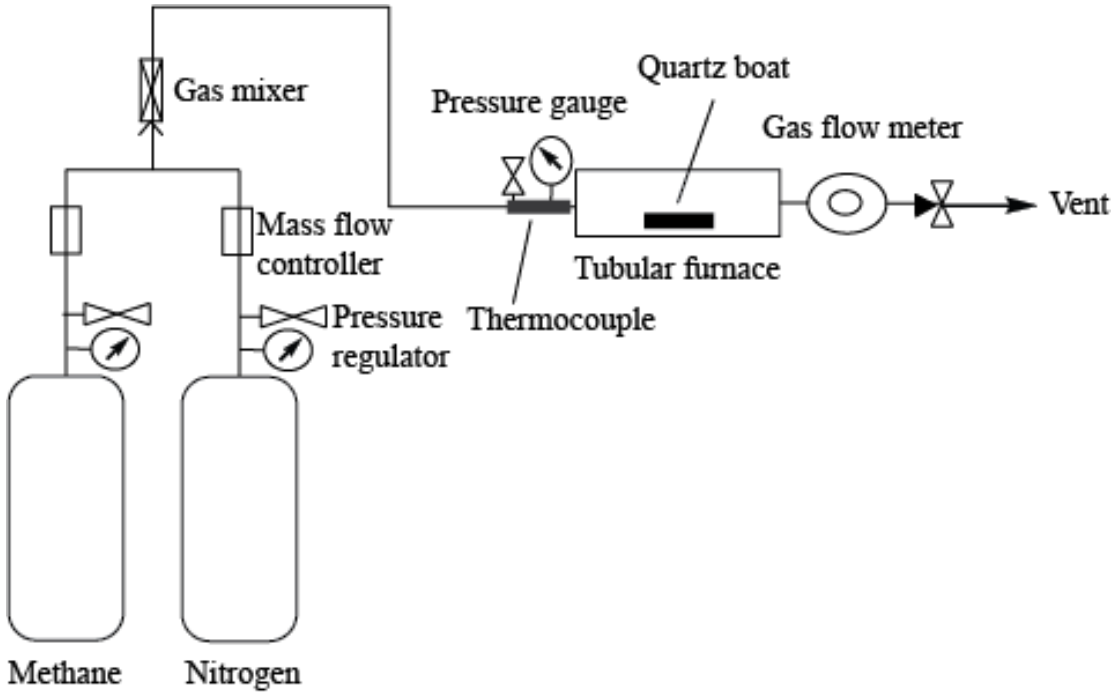


**Figure 12.** Schematic representation of the chemical vapor deposition set-up.[65]

## 4.4 Dispersing of carbon nanotubes in liquid media

As already mentioned, carbon nanotubes do not dissolve in any common solvents. In addition, obtaining a stable dispersion is very difficult due to high hydrophobicity, strong π-π stacking and van de Waals interactions between the tubes, resulting in entanglement. The more entangled the material is, the harder it is to disperse in a liquid media.[53] van der Waals interaction energies between nanotubes have been computed to vary between 200 and 500 eV per square micrometer depending on the size of the tubes.[66] Separation of single carbon nanotubes is important so that the highest performance in an application can be achieved. Dispersion of nanotubes is also crucial for their purification, functionalization and analysis.

Usually dispersing even a small amount of carbon nanotubes requires harsh conditions like sonication or treatment with strong acids and it might lead to degradation of the nanotubes.[23,49] The solvation process requires media which is able to disturb the strong π-π-stacking and van der Waals forces between the tubes (figure 13). Interaction between the tubes and the solvent has to be also strong enough to stabilize separated nanotubes.

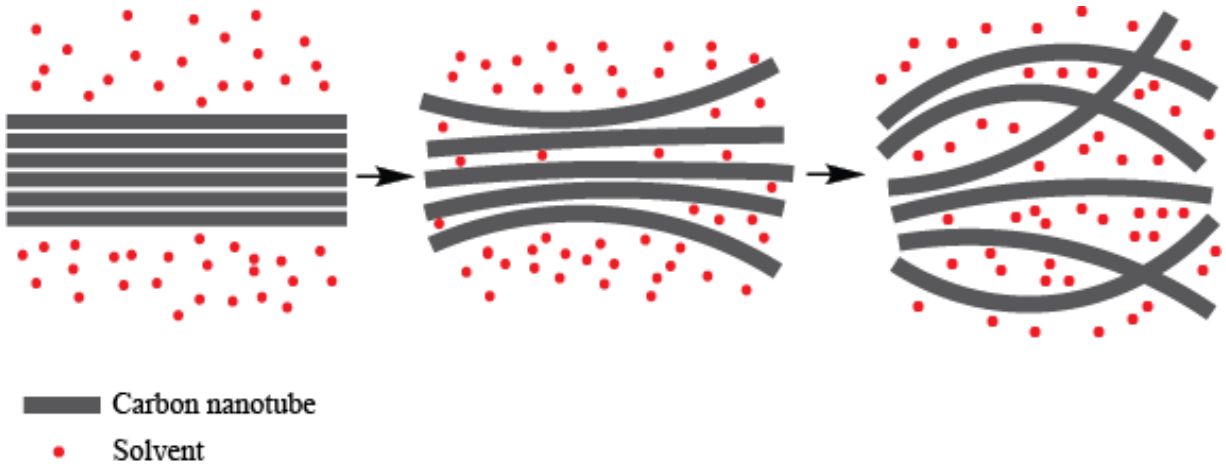


**Figure 13:** Schematic representation of dispersion of carbon nanotubes in a liquid media.[23]

### 4.4.1 Dispersing carbon nanotubes via physical modification

Physical modification of CNTs can be achieved by non-covalent stabilization. This can be carried out for example with surfactants like sodium dodecylbenzene sulfonate (SDBS) or with a polymers like poly[9,9-dioctylfluorenyl-2,7-diyl] or Nafion which has a polar side group and therefore can stabilize carbon nanotubes in specific conditions (figure 14).[67] Sonication is needed to achieve a stable dispersion.[22] The problem with surfactant assisted dispersions is their poor stability.

The structure of a polymer and the nature of the solvent affect solubility of CNTs much.[68] Solvent can induce conformational changes in the polymer and therefore change its physical properties. High density and polarity solvents lead to higher solubility of SWCNTs and aromatic polymers show great selectivity towards CNTs due to π-π stacking.[68] Size compatibility between surfactant and nanotubes is also important as stability decreases if the size of aromatic part of the polymer is too large compared to the diameter of the nanotube. In the case of PFO and PFH, locked structure enhances selectivity since conformation cannot change. Effect of side chains can be seen when comparing PFO and PFH; PFO shows greater solubility since longer side chains cover the nanotube surface more.

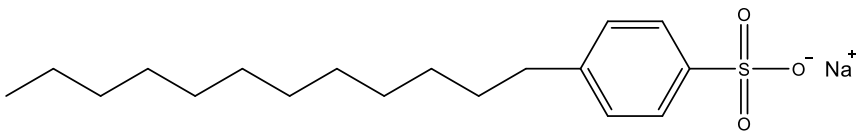

Sodium dodecylbenzene sulfonate

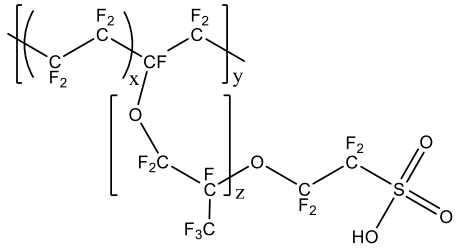

Nafion

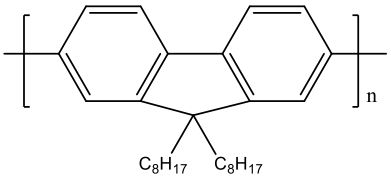

PFO
Poly[9,9-dioctylfluorenyl-2,7-diyl]

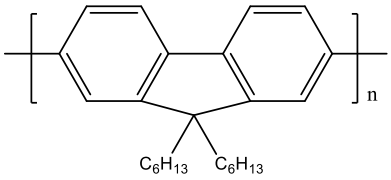

PFH
Poly[9,9-dihexylfluorenyl-2,7-diyl]

**Figure 14.** Chemical structures of sodium dodecylbenzene sulfonate, Nafion and aromatic polymers[68] used to disperse carbon nanotubes.

So far ionic liquids seem to be the only media that dissolves carbon nanotubes without additional surfactants. Ionic liquids are a very promising dissolving media and are under extensive research.[69–71] They are usually organic salts and carry a charge which gives them properties that common organic solvents do not have. Properties of ionic liquids can be modified easily by changing the chemical structure of one of the ions.[23]

Wang *et al.*[23] studied dispersing carbon nanotubes in ionic liquids. Ionic liquids are able to interact with carbon nanotubes via van der Waals forces. Wang *et al.*[23] suggested that the reason for the capability of ionic liquids to dissolve carbon nanotubes is their high dielectric constant which leads to efficient shielding of the π-π stacking of the nanotubes. The original orientation of ionic liquid is not changed too much by SWCNTs which means that the carbon nanotubes are surrounded by both polar and nonpolar parts of the solvent equally. They obtained a homogeneous dispersion by mechanical milling with concentration as high as 1 wt %.

In this research it was not possible to use ionic liquids since it is difficult to purify the products after dispersing them in ionic liquids. Since film production was the target, the solvent should be either evaporated or filtrated during the film preparation. Due to negligible vapor pressure of ionic liquids [72] evaporation would be impossible. Ionic liquids are also usually quite viscous which could complicate filtration.

Chronoamperometry has been demonstrated to give stable dispersion of stretched and aligned carbon nanotubes in epoxy resin.[73] An electrical field is applied in CNT/epoxy mixture using a large-surface electrode. Alignment of CNTs in epoxy resin affects their electrical conductivity. Carbon nanotubes are made to move in the mixture by addition of charge on their surface (CNT-$NH_3^+$ and CNT-$DDBS^-$). The advantages of this method are short dispersion time, no mechanical forces are required and nanotubes are aligned in the mixture during the process.

Alumina is widely used as a solid support in biomolecule immobilization. Tsai *et al.*[74] studied alumina-coated silica (ACS) nanoparticles as a solid support to disperse MWCNTs in an aqueous solution. 1 % w/t of ACS nanoparticles was enough to stabilize up to 20 mg/mL of MWCNTs. The phenomena is based on occurring halos as charged nanoparticles are added to negligibly charged micrometer-sized particles. Nanoparticle haloing has been studied also for example with silica spheres and hydrous zirconia nanoparticles.[75] Halos occur due to favorable interactions between charged particles and non-charged surface and repulsive Coulombic interactions between charged particles.[75]

Understanding the behavior of carbon nanotubes in aqueous media is important in terms of environmental and health issues as they will eventually end up into the nature.[22] Well suspended carbon nanotubes have higher mobility and so they are able to transfer further in environment and thus may cause ecological risks. Surfactants can be found from the nature in large quantities as they usually end up there after disposal. Natural organic matter (NOM) has also been reported to suspend CNTs in aqueous solutions[22,76,77] Yang *et al.*[22] noticed that stable dispersion achieved after sonication with a surfactant (SDBS) will re-aggregate when environmentally important cations like $Na^+$, $K^+$ and $Ca^{2+}$ are present. This observation suggests that carbon nanotubes do not give rise to large environmental risks as they will not travel long distances in considerable concentrations in the natural environment. Also, sonication is required in order to obtain a stable

dispersion and such agitation does not occur in the nature. The effect of mono- and divalent ions on CNT agglomeration has been the target of extensive research.[77,78]

### 4.4.2 Dispersing carbon nanotubes via chemical modification

Considering further processing, dispersing carbon nanotubes should be carried out so that fragmentation would not occur. This is possible with physical modification but very difficult with chemical modification. Chemical modification aims to covalent surface functionalization.

Oxidation with strong acids ($H_2SO_4$ and $HNO_3$) requires very harsh conditions but purifies the material at the same time.[49] Photo-oxidation would give higher oxygen content than oxidation with strong acids and requires milder conditions. Therefore photo-oxidation would not harm the nanotubes as much as acid treatment.[79] According to several sources, oxidation with strong acids places the functional groups at the open ends of single walled carbon nanotubes.[80,81] Some sources recon that functionalization happens also in the middle of the tube.[82,83] Since multi-walled carbon nanotubes have several layers, if the first one is broken because of the functionalization, it still will stay where it is because of the π-π-stacking of the layers. In this way it can be thought that multi-walled carbon nanotubes are also functionalized from the middle of the tube.

The oxygen content of the carbon nanotubes depend on the oxidation treatment and the nature of the nanotubes. Oxidation with acid treatment yields large difference between SWCNTs and MWCNTs. Oxidized MWCNTs have lower concentration of functional groups, only 6.2 % compared to 16.2 % of SWCNTs.[49] Photo-oxidation has been reported to give 11.3 % oxygen content for SWCNTs.[79]

## 4.5 Carbon nanotube based nanocomposites

Carbon nanotubes have been suggested to be very well suitable for applications like high-strength, conducting composites, sensors, energy storage, nanosize semiconductor devices and hydrogen storage.[58] Carbon nanotubes possess interesting mechanical and electronic properties, which combined with for example biological activity of proteins, could result in highly efficient biological nanocomposites.

When considering biological applications where carbon nanotubes are used, few things are important to bear in mind. Biocompatibility, specificity and selectivity are one of the most important ones. For example biological nanomaterial used in human body should be able to recognize only one type of molecules and repel the rest so that exactly the aimed outcome would be achieved.[84] Additionally, these materials should not cause any kind of harmful response in human body and therefore the material has to be biocompatible.

Enhancement in the stability of SWCNTs by biomacromolecules even at high salt concentrations was noticed by Saleh *et al.*[76]. SWCNTs associate with biomacromolecules because of their hydrophobic surface and this might cause a great risk considering their cytotoxicity and harmfulness for living organisms. Effect on the protein function resulting from interaction between SWCNTs and biomacromolecule depends on whether the biomacromolecule undergoes structural changes or not. Karajanagi *et al.*[85] studied two functionally different enzymes and found out that while the other preserved 30 % of its catalytic activity, the other lost it almost completely when adsorbed onto SWCNT. These observations are of great value when designing biochemical applications. Requirements considering biocompatibility and selectivity bring us to surface functionalization of nanocomposites; surface should be modified so that feasible interaction between nanomaterial and biosystem would be achieved.[84]

Shim *et al.*[84] show nanotube functionalization to achieve specific protein recognition. They studied specific and nonspecific binding of streptavidin protein on SWCNTs; without coating, nonspecific binding of streptavidin is observed. Polyethyleneglycol (PEG) is one of the most efficient and most frequently used coating to prevent nonspecific binding of proteins on surfaces.[84] This also reduces toxicity of CNTs. PEG can be adsorbed on SWCNTs irreversibly but coating is not completely uniform. A surfactant (Triton X-100 or X-405) was used to enhance the coating and this way nonspecific adsorbtion of streptavidin could be prevented. After inhibiting nonspecific binding, biotin was linked to the PEG chains; streptavidin is known to have high affinity to biotin and specific adsorbtion is achieved. Behavior of streptavidin with MWCNTs has also been studied.[86] According to Shim *et al.*[84], SWCNTs are promising material for detecting molecules in gas or liquid phase because they are susceptible for changes in the electrostatic surroundings.

Chen *et al.*[87] report a simple way to immobilize biological molecules onto nanotubes. The noncovalent functionalization of nanotube was conducted with a molecule including a pyrenyl group (figure 15) which interacts strongly with nanotube surface via π-π stacking resulting in irreversible functionalization. The molecule attached onto nanotubes also contains succinimidyl ester group which is prone to undergo nucleophilic substitution by primary and secondary amines. Therefore, reaction with proteins is highly favored and they can be immobilized on the surface of nanotubes.

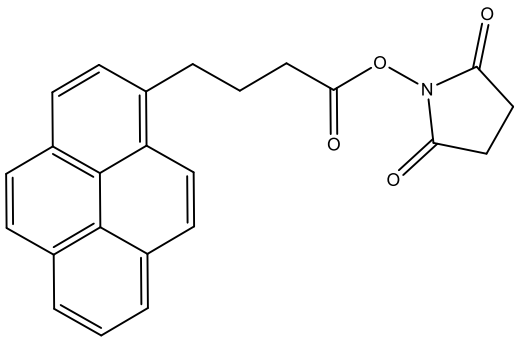


**Figure 15.** 1-pyrenebutanoic acid, succinimidyl ester

Application for efficient immunotherapy was presented by Fadel *et al.*[88] as they noticed big enhancement in T cell activation when antibodies were adsorbed onto SWCNT bundles. The antibody protein requires a suitable ligand so that T cell stimulation could be achieved and SWCNTs are competent possibilities due to their high large surface area which enables high local concentration of antibodies.

Carbon nanotubes have been suggested to possibly replace some metals used in electrical, thermal and mechanical applications.[89] Coatings on carbon nanotubes have been applied as insulating layer to create fibers for electrical microcabels.[89] Zetpol 2000 hydrogenated nitrile butadiene rubber gave uniform, only few microns thick insulating layer on CNTs. This coating is comparable to PVC coating on copper wires.

Thermal conductivity of a nanocomposite is an important property to handle as well, since even small change in operating temperature (order of 10 °C) can result in twice shorter lifetime of the device.[90] For MWCNTs thermal conductivity has been reported to be 3000 W/mK[91] and for SWCNTs experimental value is over 200 W/mK[92] but theoretical value has been suggested to be even 6600 W/mK[93]. 10 % improvement in thermal conductivity of poly(dimethyl siloxane)

composites was observed when dispersion state of the material was increased.[90] Increased dispersion state and alignment of CNTs also affects electrical conductivity positively.[94] Other sources report 60 % improvement in thermal conductivity in a mixture of MWCNTs and oil [95] (1.0 vol % of MWCNTs) and 25 % improvement in SWCNT/epoxy composites[96] (1.0 % wt SWCNT loading) but effect of dispersion state is not discussed in these.

Strength of a nanocomposite is largely based on good association of the matrix and CNTs. Good association prevents mechanical failure and therefore extends the lifetime of a nanocomposite.[97] Strong polymer/SWCNT composites can be built for example with layer-by-layer assembly which enables production of nanocomposites with high SWCNT concentrations (up to 50 wt %)[97] In layer-by-layer assembly, monolayers of individual components are adsorbed onto each other due to electrostatic and van der Waals interactions. By this technique, Mamedov *et al.*[97] were able to produce polyelectrolyte/SWCNT composite with ultimate tensile strength of 220 ± 40 MPa. Such homogeneous composites bearing high tensile strength could be used for example in prostheses. Phase separation is a problem when preparing nanocomposites with high loading of CNTs. Most often only 1-15 % loadings of CNTs are used in polymer matrices although over 50 % loadings would be needed in order to achieve significant improvement in mechanical performance.[97]

In addition to these above mentioned CNT/polymer-composites, carbon nanotubes can be used as conductive, transparent coatings on large variety of substrates.[98,99] SWCNTs seem to be better considering transparency and conductivity of the coating, but several factors affect the conductivity (defects, impurities and homogeneity of the coating). Even though it has been proposed that transparent SWCNT electrodes could replace indium tin oxide glass substrates due to higher conversion efficiency[100], difficulties to make coatings homogeneous enough will complicate their utilization in applications.

# 5. Ureidopyrimidinone

Ureidopyrimidinone[101–103] (figure 16) dimerizes via its 4[1H]pyrimidinone tautomer in solid and liquid state. This tautomer is preorganized due to intramolecular hydrogen bonding between urea- and pyrimidine-units which makes dimerization possible. Some examples of nanocomposites involving ureidopyrimidinone have been presented in previous chapters.

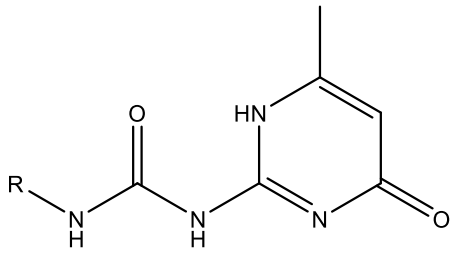


R = $(CH_2)_6$-NCO

**Figure 16:** 2-Ureido-4[1H]pyrimidinone hexamethylene isocyanate.

Double and triple hydrogen bonding arrays are familiar to us already from DNA base pairing (figure 17) and several triply hydrogen bonding units have been synthesized probably to mimic the strong binding properties that DNA possesses.[21,104] Lately, quadruple hydrogen bonding units have aroused interest more and more and ureidopyrimidinone is a good example of this category.

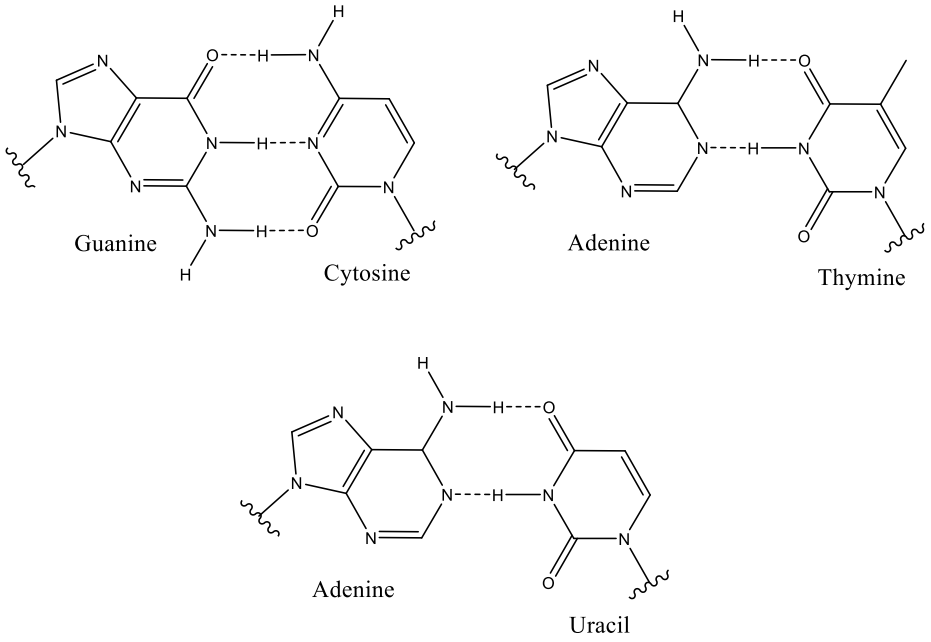


**Figure 17.** Hydrogen bonding between DNA base pairs.

Ureidopyrimidinone is fairly easy to synthezise which also makes it feasible in many applications.[101] 2-Ureido-4[1H]pyrimidinone hexamethylene isocyanate was used in these studies (figure 16) and three different tautomeric forms of it has been found (figure 18). Two of these are able to dimerize.[102] Ureidopyrimidinone contains a pyrimidine- and urea-units which in 4[1H]-pyrimidinone tautomer participate the formation of an intramolecular hydrogen bond making the molecule planar – this preorganization is needed in order to form a dimer via quadruple hydrogen bonding.[101,103]

4[1H]-pyrimidinone tautomer has a dimerization constant over $10^6$ $M^{-1}$ in chloroform[101], Söntjens *et al.*[103] report a value of $6 \times 10^7$ $M^{-1}$ in chloroform. In toluene the dimerization constant is even higher, $6 \times 10^8$ $M^{-1}$.[103]

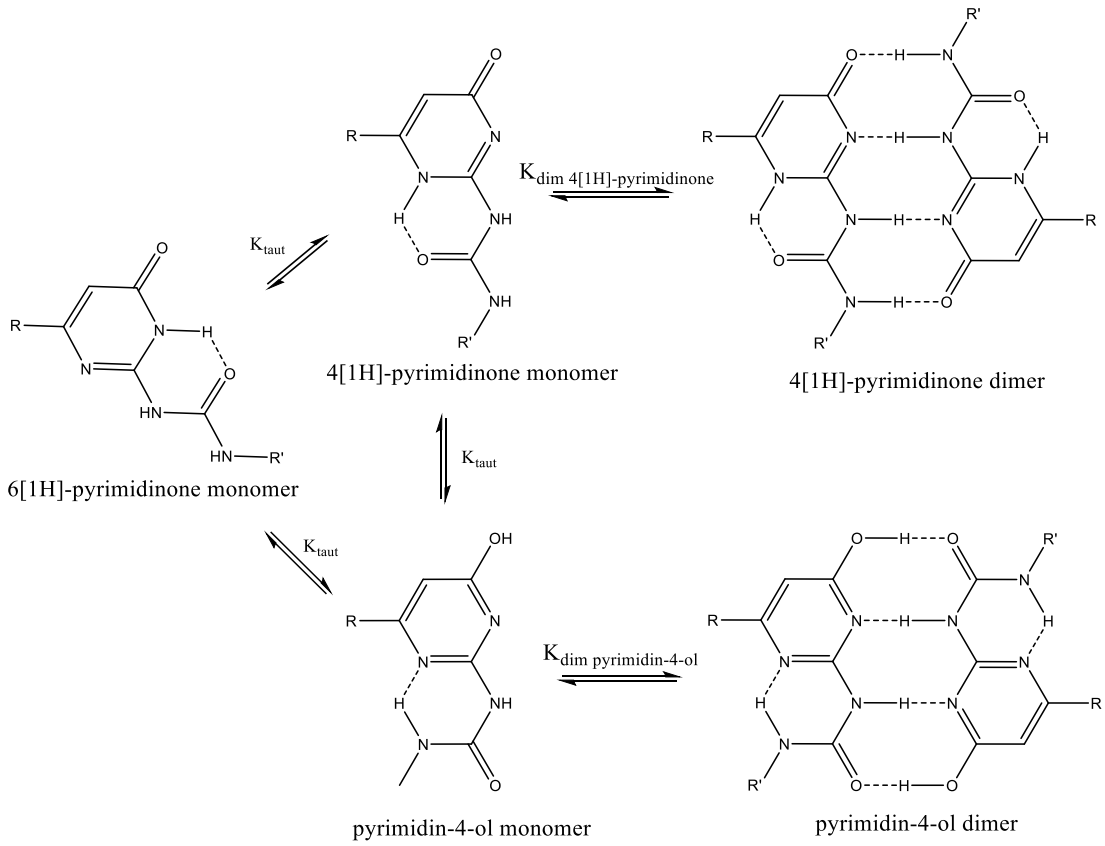


**Figure 18.** Tautomers of ureidopyrimidininone.[101,102]

In figure 18, the three tautomers of ureidopyrimidinone are presented. Of these three, 6[1H]-pyrimidinone is the most stable one.[101] Equilibrium between these three monomers is dependent on electronegativity of the substituents, polarity and hydrogen bonding ability of the solvent and the concentration of the solution.[101] In solid state there is 50:59 ratio of both tautomers, 4[1H]-pyrimidinone and pyrimidin-4-ol.[102]

When designing supramolecular complexes, the stability of the complex is a highly important aspect. Molecules that dimerize via hydrogen bonding can form different motifs of different arrangements of donor and acceptor atoms. Blight *et al.*[105] state that the binding forces should be the highest when the other component has only hydrogen-bond acceptors and the complementary component donors. Hydrogen bonding between preorganized motifs is very strong, but the secondary interactions have an important effect on the stability of the complex.[105]

Jorgensen and Pranata[104] noticed the effect of secondary interactions as well when studying the strength of interactions between triply hydrogen bonding complexes. Obvious change in the

strength of binding between species with two intramolecular hydrogen bonds and species with three intramolecular hydrogen bonds can be seen and easily explained. However, large differences between triply hydrogen bonding units was something Jorgensen and Pranata[104] did not expect. They concluded that the secondary interactions play a very important role in the formation and stability of the dimer. With quadruple binding, it gets more challenging to study and estimate the effect of secondary interactions.[105]

For quadruply hydrogen bonding motifs there are theoretically six different alternatives.[105,106] These six permutations are ADAD-DADA, AADD-DDAA and ADDA-DAAD, AAAD-DDDA, ADAA-DADD and AAAA-DDDD (D = donor, A = acceptor), but only the first three and the last one of these have been noticed to have strong enough binding constant to have some application in supramolecular chemistry.[105,106] As figure 19 presents, when all donors are located on one component and acceptors on the other (AAAA-DDDD permutation), we also get secondary attracting interactions which are presented as black arrows. This situation would be the most ideal considering the strength of the dimer. ADAD-DADA -complex would have the smallest binding constant due to repulsive interactions. 4[1H]-pyrimidinone monomer forms a stronger dimer than pyrimidin-4-ol because DDAA motif does not have as much repulsive forces as DADA motif.[102] Surprisingly, the dimerization constant of the DADA array is a lot higher than literature predicts for such arrays. This derives from preorganization of the molecule due to intramolecular hydrogen bond and also the presence of a strong O-H···O=C hydrogen bond affects the stability of the complex.[101]

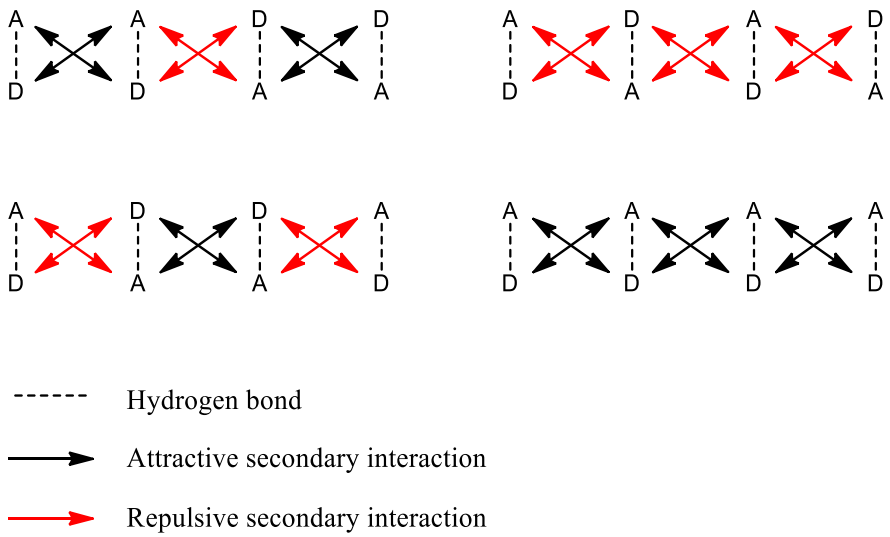


**Figure 19.** Schematic presentation of the repulsive and attractive forces in AADD, ADAD, ADDA and AAAA arrays.[105,101] Red arrows represent repulsive interactions.

Blight *et al.*[105] report an AAAA-DDDD$^+$ complex (figure 20) with unexpected stability in polar solvents and high dimerization constant. This complex stays as a dimer in for example DMSO/chloroform media whereas an ureidopyrimidinone dimer dissociated when just 30 % of DMSO was added to chloroform solution. Blight *et al.*[105] suggest that the exceptionally stable dimer in polar solvent may derive from the fact that it is hard to dissolve the monomeric compounds to polar solvents. The dimerization constant for this complex in dichloromethane is as high as $3 \times 10^{12}$ $M^{-1}$ and in 10 % DMSO/$CHCl_3$ it still is $3.4 \times 10^5$ $M^{-1}$.

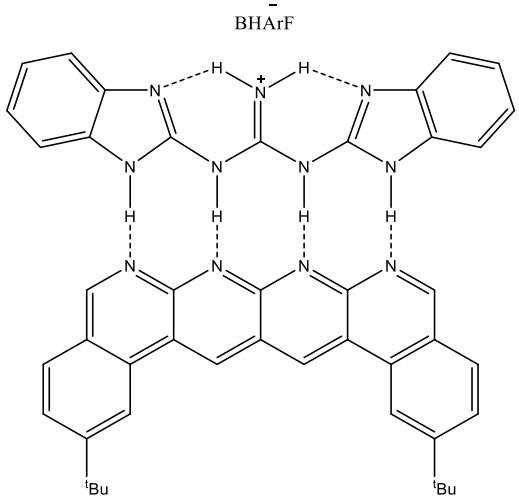


**Figure 20.** AAAA-DDDD$^+$ complex [105]

The positive charge on the donor species leads to stronger hydrogen bonding in the complex.[106] Due to tautomerism the positive charge can be on one of the donating nitrogens and therefore has an effect on hydrogen bonding.

## 5.1 Solvent and substituent effects

The polarity of the solvent affects the dimerization; it is more favorable in a solvent with lower polarity.[103] Dissociation of the dimer happens almost 15 times easier in chloroform than in toluene[103] The effect of water in the solvent has been previously thought to have a large effect on dimerization, but Söntjens *et al.*[103] showed that actually the dimerization constant of ureidopyrimidinone in wet chloroform is only 5 times lower than in dry chloroform. This is a result of the capability of water to interfere with the hydrogen bonding of the free monomers

In order to conduct a predictable supramolecular assembly, only one tautomer should be present in the solution.[101] Alexander *et al.*[102] studied the solvent induced tautomerization of the ureidopyrimidinone unit by functionalizing it with a ferrocene group at the 6-position of the heterocycle (figure 21). They became to a conclusion that solely the 4[1H]-pyrimidinone monomer exists in a chloroform solution. And in similar manner, in DMSO, only 6[1H]-pyrimidinone monomers are present. Beijer *et al.*[101] obtained similar results with alexander *et al.*[102]; in pure chloroform UPy forms DDAA dimer but if DMSO is present, an equilibrium between the monomeric form and the dimer is obtained.

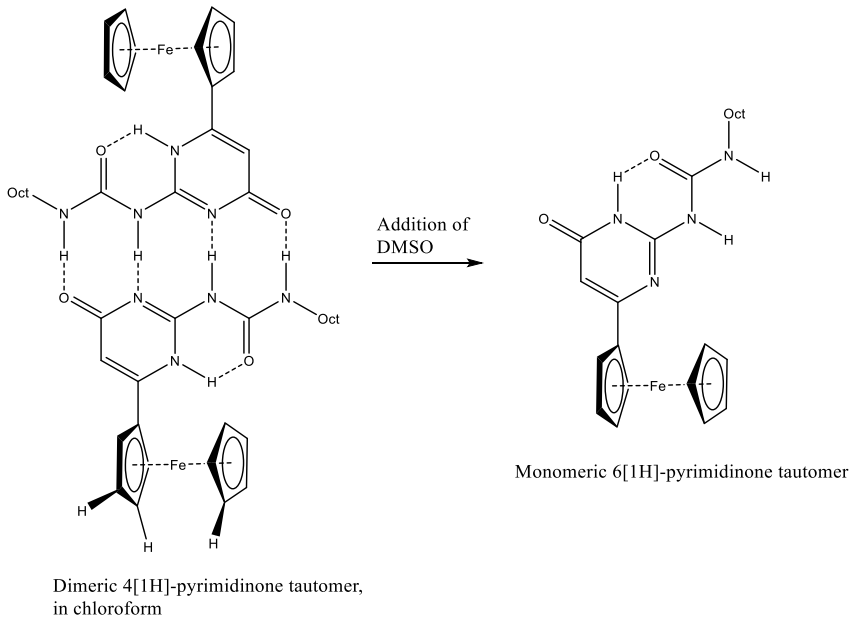


**Figure 21.** Ureidopyrimidinone moiety functionalized with a ferrocene group.

Already addition of 30 % DMSO to a chloroform solution of ureidopyrimidinone causes solvent induced tautomerization from 4[1H]-pyrimidinone to 6[1H]-pyrimidinone and the dimer dissociates.[102] DMSO is a strongly hydrogen bond accepting solvent and can disturb the intramolecular hydrogen bonding and so lower the amount of preorganization. When considering supramolecular chemistry, it is important to know ways to assemble and disassemble a supramolecular complex. Here, the fact that solvent induces tautomerization could be used to either form a dimer or to break one.

In addition to the effect of the solvent, also the character of the R and R'-sidegroups and the concentration affect the tautomerization.[102] Electronegative substituents at the 6-position of the heterocycle drive the tautomerization to go towards enol-form and due to this the intramolecular hydrogen bond forms in different position of the molecule and DADA hydrogen bonding array is obtained.[101]

# II EXPERIMENTAL

## 6. Introduction

In this Master's thesis, supramolecular assembling of carbon nanotubes and a polymer, both functionalized with 2-ureido-4[1H]-pyrimidinone, was studied. The target was to develop strong, electrically conducting composite material which would resist crack propagation. Several research groups have reported major improvements in mechanical, electrical and thermal properties of polymer materials after addition of carbon nanotubes.[83,107–109]

While carrying out the experimental part of this thesis, Micoli *et al.*[110] introduced supramolecular macrostructures of UPy-functionalized carbon nanotubes. In this research they used the dimerization properties of 2-ureido-4[1H]-pyrimidinone to accomplish self-assembly between carbon nanotubes and a block copolymer. A freestanding film or stable gel was obtained depending on the polymer used and rheology experiments show that addition of UPy stabilizes the polymer network. This design was similar to our approach.

A week after the publication by Micoli *et al.*[110], another with very similar idea was released by Guo *et al.*[111]. In this study, electrically conductive material was prepared from adamantine-derivatized poly(2-hydroxyethyl methacrylate) and cyclodextrin-derivatized SWCNTs via host-guest interaction. This design has its advantages over our design because adamantine cannot interact with itself, but only with cyclodextrins, present on the surface of the carbon nanotubes. Therefore, supramolecular complex can only form between nanotube and the polymer, not between two nanotubes or two polymers. Regardless of clever design of the nanocomposites presented by Micoli *et al.* and Guo *et al.* their mechanical properties were poor compared to the material we synthesized.

In our system, we do not have certainty that the supramolecular complex would form between nanotubes and the polymer as planned. Since we can have three different interactions; nanotube-nanotube, polymer-polymer or nanotube-polymer, there is notably smaller possibility to actually have the desired nanotube-polymer interactions. Experimental part introduces chemicals used, syntheses that were carried out, possible purification of materials and characterization of products.

# 7. Measurements and instrumentation

Starting materials and products were characterized with Fourier transform infra-red spectroscopy and/or nuclear magnetic resonance spectroscopy. Morphological characterization was carried out using electron microscopy and mechanical properties were determined using tensile testing of films produced from the final products.

## 7.1. Fourier Transform Infra-Red (FT-IR) Spectroscopy

Nicolet 380 Spectrometer (Thermo Fischer Scientific) was used to measure FT-IR spectra of all starting materials and products. Transmission mode was used with a 2 $cm^{-1}$ resolution. The spectra were averaged over 64 scans.

Pristine polymers were measured as such without any pretreatment. Ureidopyrimidinone derivatives were dialyzed in methanol and dried prior to measuring. This was done to remove the catalyst and possible unreacted UPy-isocyanate. Methanol was chosen as a solvent because it is easy to remove after dialysis.

## 7.2. Nuclear Magnetic Resonance (NMR) Spectroscopy

The NMR spectra were recorded with Bruker Avance 400 MHz spectrometer. Measurements were carried out in liquid state and deuterated dimethyl sulfoxide (DMSO-$d_6$ 99.96 % of D) or deuterated methanol (MeOH-$d_4$ 99.96 % of D) was used as a solvent.

$^1$H-NMR spectra were recorded from all of the samples with $2^7$ scans. The length of the $\pi/2$ pulse was 6.0 µs, flip angle 30$^o$ and recycled delay 2 s. 64 K data points in the time domain were collected and this was zero filled to 128 K prior to Fourier Transformation.

Approximately 6 mg/mL of the sample was dissolved for $^1$H-NMR measurements and the chemical shifts corresponding to DMSO-$d_6$ was found at 2.50 ppm (HOD at 3.3 ppm) and to MeOD at 3.33 ppm and 4.87 ppm.[112]

## 7.3. Scanning Electron Microscopy (SEM)

Scanning electron microscopy (SEM) measurements were carried out with Zeiss Sigma VP microscope at 2 kV voltage. The samples were attached on a SEM pin stub on carbon tape. Au/Pd coating was applied on the samples under vacuum at 20 mA for 3 min prior to imaging.

## 7.4. Tensile testing

Mechanical tests were carried out with Kammrath & Weiss tensile tester. Samples were 2.25mm wide and 200-400 µm (evaporated) or 90-200 µm (heat pressed) thick.

As the pristine polymer stretches much, samples without carbon nanotubes were 5 mm long and most of the ones containing carbon nanotubes 10 mm long. Inequalities in the thickness of films are most likely a result of slightly inclined bottom of the Teflon cups or uneven ventilation in the fume hood that was used for evaporation.

Before the actual measurements, samples were equilibrated at 50 % relative humidity at least for 16 h. Due to operating inside the measurement box during measurements, humidity changed ± 2 % from the equilibration humidity and this might cause some small error to the results. Especially since poly(2-hydroxyethyl methacrylate) is a hygroscopic polymer.

Fewer samples were obtained from some films due to breaking of the edges while peeling the film off from Teflon cup. This reduced the diameter of the film. The overall result from these films is of course not as reliable as it could be. 5 to 9 samples gives reliable results and this was obtained from almost all samples. The total amount of samples was reduced in some cases also because 10 mm samples did not break in the limits of the machine and due to this the rest were cut into 5 mm samples.

# 8. Materials and methods

All reactions were carried out in clean and dry glassware under nitrogen atmosphere. Reagents and solvents were purchased from commercial sources. Dibutyltin dilaurate (DBTDL, 95 % purity) was obtained from Sigma Aldrich and used without further purification just like all used solvents (technical and analytical grade, chloroform, *N*,*N*-dimethylformamide, dimethyl sulfoxide, methanol).

Multiwalled carbon nanotubes and poly(2-hydroxyethyl methacrylate) (pHEMA) molecular weights 20 kDa and 1 MDa (figure 22) were obtained from Sigma Aldrich. The multi-walled carbon nanotubes used in this research had following dimensions; outer diameter 10 nm ± 1 nm , inner diameter 4.5 nm ± 0.5 nm and length 3 - ~6 µm. These MWCNTs were made by catalytic chemical vapor deposition (CVD) method (CoMoCAT®). HEMA-PEG-HEMA block copolymer (figure 23) was synthesized by Salla Välimäki and 2-Ureido-4[1H]pyrimidinone hexamethylene isocyanate by Teemu Myllymäki.

Dialyses were performed with Spectra/Por dialysis membranes with suitable pore sizes. Ultra-Turrax was used to mix carbon nanotube and polymer solutions prior to film preparation, one minute on the slowest mode was used.

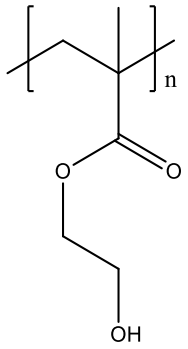


**Figure 22.** Poly(2-hydroxyethyl methacrylate)

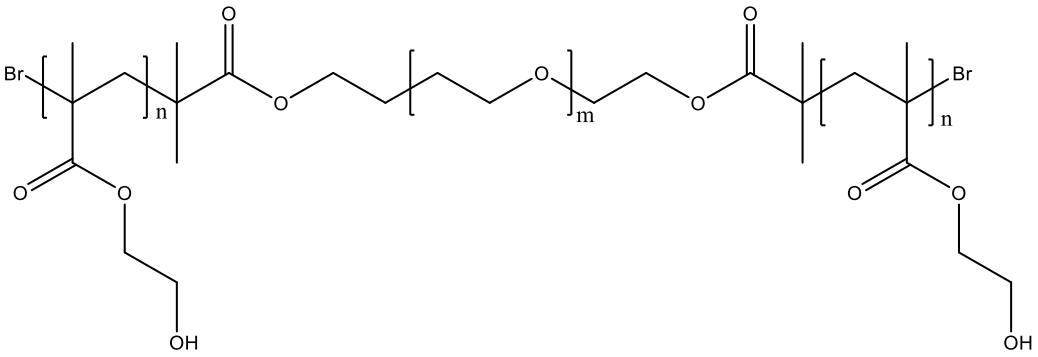


**Figure 23.** HEMA-PEG-HEMA block copolymer.

## 8.1. Oxidation of carbon nanotubes

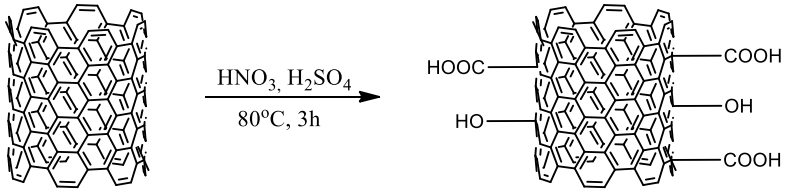


Depending on the production methods, commercially purchased carbon nanotubes may contain large amounts of impurities, like amorphous carbon or metals like Co or Mo from used catalysts.[82,113] Purification may be conducted in several ways and oxidation is one of those.[82,113] Chemical functionalization methods, filtration, acid reflux[114], gas oxidation[114] or different chromatography[115] techniques are other possibilities.[82]

Oxidation was a good option for us since there was a need to further functionalize the surface of the carbon nanotubes. Purification of the material also serves the greater purpose as impurities might affect the properties of the composites prepared later. Surfactants can be utilized to obtain a homogeneous dispersion[67] but in this research they were not an option. Additional surfactants might not be stable during the whole process and they do not give an option of further surface functionalization.

Oxidation of carbon nanotubes was carried out as described in the publication by Hung *et al.*[49]. 1 g of carbon nanotubes was weighed into a round bottom bottle. 150 mL of concentrated $H_2SO_4$ and 50 mL of concentrated $HNO_3$ were mixed and poured carefully on the carbon nanotubes followed by heating at 80 °C for 3 h 20 min.

After 3 h, the reaction mixture was cooled immediately by immersing in an ice bath and the solution was centrifuged for 1 h at 5000 G. Supernatants were removed and washed with water until sediment did not form anymore. Centrifugation for 10 min at 5000 G was enough to obtain clear supernatant.

When clear supernatant was not obtained anymore, dilute HCl was added to the tubes dropwise in order to induce precipitation. After centrifugation supernatant was poured off again, water was added to dilute the dispersion and then HCl again to precipitate the material. Presence of $SO_4^{2-}$ ions was tested from the supernatant by addition of $BaCl_2$ – white precipitate occurs if $SO_4^{2-}$ still is present. Washing was continued until solution did not contain sulfates.

$$SO_4^{2-}\,(aq) + BaCl_2\,(s) \rightarrow BaSO_4 \downarrow + 2Cl^-\,(aq)$$

A fine suspension was obtained after the purification procedure. The concentration of this suspension was 7 g/L. It is of the same order with the solubility that Hung *et al.*[49] obtained, 3.13 g/L.

The only evidence of actual functionalization was the formation of a suspension, no FT-IR spectra could be recorded. Formation of a suspension indicates that the surfaces of carbon nanotubes have been oxidized. Hung *et al.*[49] were able to obtain IR spectra for their products but could not point out major changes in the spectra between oxidized and neat MWCNTs; they also refer to the obvious solubility to water as an evidence of successful functionalization.

The attempt to quantify the amount of acid groups was tried by titration but it did not succeed. Several different ratios of functional groups for oxidized carbon nanotubes have been reported. Hung *et al.*[49] got following concentrations for –C(O)C-, -C=O and –C-O- 6.2, 4.2 and 13.0 %. Rosario-Castro *et al.*[116] gave 15.1, 6.2 and 16.2 % for hydroxyls, carbonyls and carboxyl compounds on single walled CNTs.

## 8.2 Synthesis of ureidopyrimidinone derivative of oxidized carbon nanotubes

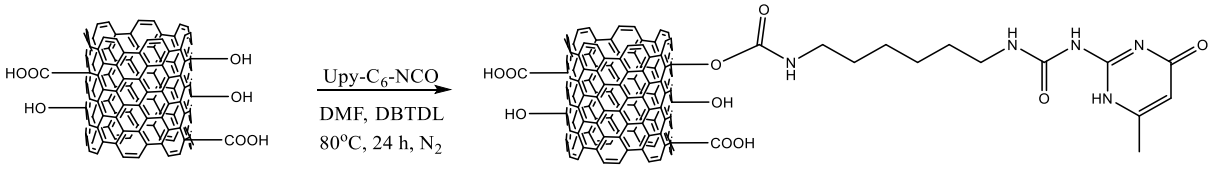


This reaction was tried to carry out in chloroform first like Wang *et al.* [5] performed their synthesis on MWCNTs but it did not succeed.

Oxidized carbon nanotubes were dialyzed from water to DMF before the reaction. The target was to derivatize all the hydroxyl groups on the nanotube surface. As determining the amount of functional groups by titration did not work, some idea was taken from the literature (see previous chapter).

4ml of the CNT water dispersion was dialyzed, this should contain roughly 28 mg of CNTs. Excess UPy was used and 0.1 mL of DBTDL was used as a catalyst. Reaction was performed at 80°C for 24 h. Unreacted UPy and catalyst were removed by dialysis after the reaction.

No FT-IR spectra could be recorded.

## 8.3 Synthesis of ureidopyrimidinone derivative of HEMA-PEG-HEMA

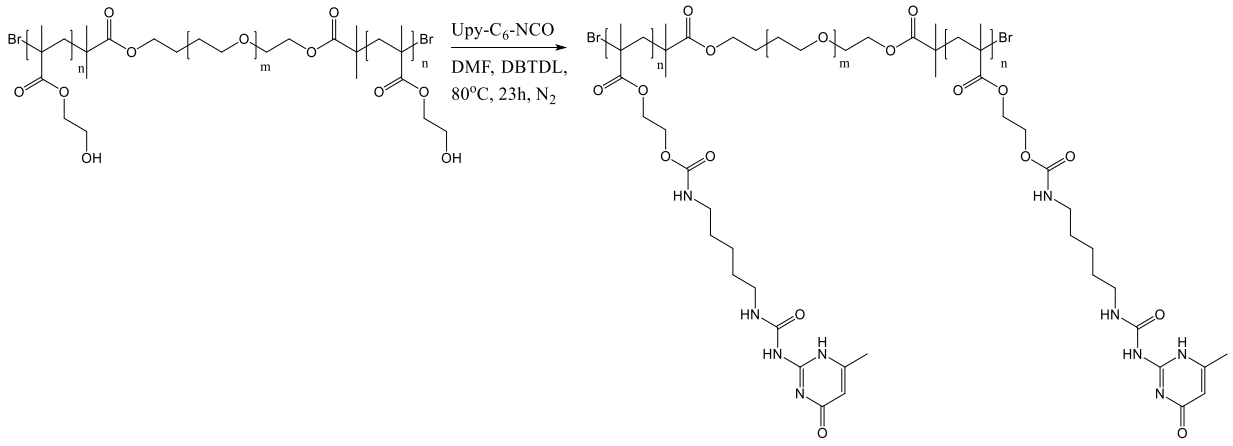


The target was to derivatize 10 % of the hydroxyl groups at the polymer. 194.5 mg of the polymer was dissolved in DMF (30 mL) and UPy-$C_6$-NCO (36.47 mg) and a catalyst (DBTDL, 0.1 mL) was added. Stirring under nitrogen at 80 °C for 23 h.

The solution was used as such without further purification.

**$^1$H-NMR of UPy-isocyanate (δ ppm):** 11.54, 9.71, 7.38, 5.78, 3.37, 3.34 (HOD), 3.14, 2.51 (DMSO-$d_6$), 2.11, 1.56, 1.46, 1.32

**$^1$H-NMR of HEMA-PEG-HEMA (δ ppm):** 4.87 (MeOD), 4.23, 4.08, 3.80, 3.66, 3.50, 3.33 (MeOD), 2.21, 2.04, 1.97, 1.35, 1.31, 1.14, 0.98, 0.12

**$^1$H-NMR of UPy-derivative of HEMA-PEG-HEMA (δ ppm):** 7.00, 5.75, 4.83, 3.90, 3.59, 3.48, 3.34 (HOD), 2.96, 2.90, 2.68, 2.51 (DMSO-$d_6$), 2.34, 2.12, 2.10, 1.79, 1.44, 1.30, 1.26, 1.24, 0.95, 0.78

## 8.4 Synthesis of ureidopyrimidininone derivatives of pHEMA

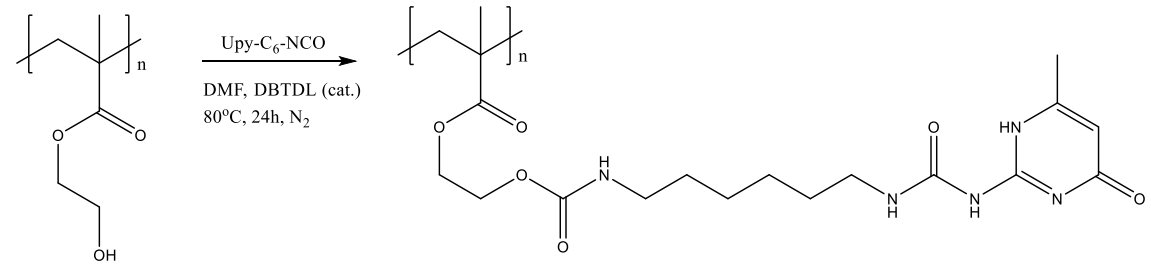


n = 20 000 or 1 000 000

Two different derivatives were made from both polymers, 20 kDa and 1 MDa pHEMA. 1 % and 10 % of the hydroxyls were derivatized.

**FT-IR 20 kDa pHEMA υ $cm^{-1}$:** 3410 (-OH, polymeric), 2941 ($-CH_2-$), 1715 ($CO_2R$), 1450 ($-CH_3$), 1387 ($-CH_3$), 1244 (-OH), 1149 ($-CO_2-$), 1070 ($-CO_2-$), 1021, 947, 897, 848, 747 ($-CH_2-$), 510, 469

**FT-IR 1 MDa pHEMA υ $cm^{-1}$:** 3400 (-OH, polymeric), 2946 ($-CH_2-$), 1714 ($CO_2R$), 1450 ($-CH_3$), 1387 ($-CH_3$), 1244 (-OH), 1149 ($-CO_2-$), 1070 ($-CO_2-$), 1021, 944, 898, 848, 747 ($-CH_2-$), 512

### 8.4.1 1 % derivatives

1 g of polymer was first dissolved in 20 mL of DMF and when the solution was clear, 0.0224 g (0.0234 g and 0.0229 g) of UPy-$C_6$-NCO was added to the polymer solutions. At this point additional 10 mL of DMF was added to reduce the viscosity of the solution. Mixture was heated first at 60 °C until UPy-$C_6$-NCO dissolved and then the catalyst (dibutyltin dilaureate, 0.1 mL) was added. After catalyst addition, the temperature was raised to 80 °C for 24 h. Reaction was done under nitrogen atmosphere as isocyanate is sensitive to moisture. After 24 h mixture was allowed to attain room temperature and it turned cloudy. After some time it turned clear again.

Catalyst addition was done as the last step since this speeds up the reaction between alcoholic OH-group and isocyanate. Niyogi *et al.*[117] noticed that if the catalyst is added before isocyanate, the catalyst forms such a strong complex with the alcohol, that the reaction rate is reduced. When catalyst is added after isocyanate, immediate complexation between these three components is observed and reaction proceeds fast.

**FT-IR of 1 % pHEMA-UPy derivative (20 kDa pHEMA): υ $cm^{-1}$:** 3391 (-OH, polymeric), 2944 ($-CH_2-$), 1715 ($-CO_2-$) and (RO-CONH-R), 1660 ($(RNH)_2CO$), 1557 (RO-CONH-R), 1454 ($-CH_2-$), 1387 ($-CH_3$), 1245 (-OH), 1150 ($-CO_2-$), 1071 ($-CO_2-$), 1021, 945, 897, 848, 747 ($-CH_2-$), 518, 467

**$^1$H-NMR spectra of 1 % pHEMA-UPy (20 kDa pHEMA) (δ ppm):** 7.96, 6.55, 4.82, 4.12, 3.90, 3.59, 3.33 (HOD), 3.18, 3.17, 2.90, 2.74, 2.51 (DMSO-$d_6$), 1.78, 1.49, 0.95, 0.78

**$^1$H-NMR spectra of 1 % pHEMA-UPy (1 MDa pHEMA) (δ ppm):** 11.56, 9.69, 7.34, 7.02, 5.77, 4.82, 4.12, 3.90, 3.59, 3.35 (HOD), 3.28, 2.96, 2.51 (DMSO-$d_6$), 2.10, 1.79, 1.44, 1.27, 0.95, 0.78

### 8.4.2 10 % derivatives

1 g of polymer was dissolved in 30 mL of DMF. Tenfold amount of UPy-$C_6$-NCO was added to the solutions (0,221 g and 0,223 g). Due to a larger amount of UPy-$C_6$-NCO, 10 ml of DMF was also added. This time both mixtures were put to 80 °C oil bath straight and the catalyst (0,1 mL) was added when UPy had dissolved. Reaction for 24 h under nitrogen atmosphere.

Both, 1 % and 10 % derivatives were decided to use as such. Drying the material might have led to problems with redissolution.

**FT-IR of 10 % pHEMA-UPy derivative (1 MDa pHEMA) υ $cm^{-1}$:** 3369 (-OH, polymeric), 2935 ($-CH_2-$), 1698 ($-CO_2-$ ) and (RO-CONH-R), 1652 ($(RNH)_2CO$), 1557 (RO-CONH-R), 1455 ($-CH_2-$), 1387 ($-CH_3$), 1245 (-OH), 1149 ($-CO_2-$), 1070 ($-CO_2-$), 1021, 965, 898, 845, 746 ($-CH_2-$), 518, 471

**$^1$H-NMR spectra of 10 % pHEMA-UPy (20 kDa pHEMA) (δ ppm):** 7.96, 4.82, 4.12, 3.90, 3.58, 3.35 (HOD), 3.18, 2.90, 2.74, 2.51 (DMSO-$d_6$), 1.79, 1.46, 1.25, 0.95, 0.78

**$^1$H-NMR spectra of 10 % pHEMA-UPy (1 MDa pHEMA) (δ ppm):** 11.56, 9.69, 7.96, 7.02, 5.77, 4.82, 3.90, 3.58, 3.35 (HDO), 3.18, 2.90, 2.74, 2.50 (DMSO-$d_6$), 2.12, 1.79, 1.44, 1.29, 1.24, 0.95, 0.78

All the FT-IR spectra from polymer and it´s derivatives are very similar, the fingerprint region does not really differ significantly from each other. pHEMA has an ester moiety at each monomer which results in an intense signal (1715 $cm^{-1}$)[112].

The only obvious difference between  can be seen in the ureidopyrimidinone derivatives (Appendix A, attachments 3 and 4); the carbonyl peak has shifted slightly and another peak occurs around 1660 $cm^{-1}$, right next to the carbonyl peak. This corresponds to the urea ($(RNH)_2CO$) structure in the ureidopyrimidinone sidechain. Also peak characteristic to isocyanate (-NCO; 2250-2275 strong, 1350 weak) are not present in attachments 3 and 4 which indicates that the reaction would have happened.

The almost non-existent differences at the fingerprint region of FT-IR can also be explained by the fact that the added amount of ureidopyrimidinone is very small compared to the amount of a very large polymer and therefore signals of the polymer cover signals from UPy.

NMR spectra for polymers that have very high molar mass can cover majority of the signals occurring from functional groups – in this case from ureidopyrimidinone. Also J-coupling cannot be seen since most of the peaks are broad. The easiest way to observe that functionalization has happened is to integrate the peak corresponding to OH-group and see if the intensity has decreased. The change in the integral of the OH-signal is very small and can be observed only for 10 % derivatives (appendix A, attachments 13 and 14)

# 9. Films

Two sample preparation methods were used to obtain the films. Evaporation at 80 °C from a Teflon cup and heat pressing. If films were heat pressed, they were first dried by evaporating the solvent at 80 °C.

Heat pressing was used to compare, if pressing the material at certain pressure above its glass transition temperature would change its mechanical properties. Moreover, obtaining a smooth film after dialysis of 10 % pHEMA-UPy derivative from DMF to methanol was not possible by evaporation as the material precipitated during dialysis. Another approach to make a film from this material was required and heat pressing suited this purpose well. Heat pressing has some advantages over evaporating. Obtaining a smooth and even film is probably the most important one. When the film is produced by evaporation only, it is highly probable that it is uneven and heterogeneous.

The temperature for heat pressing was chosen to be 110 °C since this is above the glass transition temperature of pHEMA and the transparencies used to protect the material from the pressing clamps did not start to melt. Mohomed *et al.*[118] reported a glass transition temperature of 99.2 °C for pHEMA. Glass transition temperature is dependent on the water content of the sample and as pHEMA is highly hygroscopic[119], its $T_g$ can change a lot depending on the moisture content. Glass transition temperature is a temperature above which the material is rubber-like and below hard and brittle. This behavior is characteristic for amorphous materials or regions since they do not have sharp melting point like crystalline materials do.

All the films were heat pressed for 90 min at 110 °C at 2 metric tons and after this they were let to cool down to room temperature while still pressed.

## 9.1 Pristine carbon nanotubes

The very first films were made from ureidopyrimidinone functionalized carbon nanotubes. They were prepared by filtration. One film was prepared straight by filtration of a DMF solution and other by dialysis against chloroform and filtration after the solvent exchange. Freestanding films were obtained from both but they were very brittle and no further experiments were conducted.

## 9.2 Carbon nanotubes and HEMA-PEG-HEMA

HEMA-PEG-HEMA was not an ideal starting material for film trials to begin with due to limited quantity of the material. Two solutions were done, both containing 50 mg of the polymer and 1 % w/w of CNT-UPy. The solutions were mixed for 48 h. The first solution was evaporated as such from a Teflon cup at 90$^{o}$C (in the end temperature was raised to 100$^{o}$C to ensure drying) and the second solution was dialyzed against methanol and then evaporated. In DMF the mixture stayed as a suspension but in methanol a precipitate occurred. The polymer does dissolve in methanol.

DMF solution gave a fairly homogeneous film, though when watched against a light, some aggregates could be seen. Methanol solution on the other hand gave clearly phase separated film with regions containing carbon nanotubes and regions containing the polymer. Sonication before solvent evaporation could have given more homogeneous film. Neither of these films was used for tensile testing.

## 9.3 Carbon nanotubes and pHEMA

Several films of pHEMA were made first to check differences between the two molecular weights, 20 kDa and 1 MDa. It turned out quickly that molecular weight of 20 kDa is too low and this polymer gives only very brittle films that cannot be removed from a Teflon surface as one piece. Due to this it was not used in the measurements and only 1 MDa pHEMA was suitable.

All films made are collected to table 2.

**Table 2.** All prepared films. pHEMA refers to 1 MDa polymer. E= evaporation, EH= evaporation followed by heat pressing, *Dialysis from DMF to methanol prior to heat pressing.

| **Component 1** | **Component 2** | **Ultra-turrax** | **Method** | **Mech. testing** |
|---|---|---|---|---|
| pHEMA | - | - | E | + |
| 1% pHEMA-UPy | - | - | E | + |
| 10% pHEMA-UPy | - | - | E | + |
| pHEMA | 1% w/w Ox-CNT | + | E | + |
| 1% pHEMA-UPy | 1% w/w CNT-UPy | + | E | + |
| 1% pHEMA-UPy | 5% w/w CNT-UPy | + | E | + |
| 10% pHEMA-UPy | 1% w/w CNT-UPy | + | EH | + |
| 1% pHEMA-UPy | 1% w/w CNT-UPy | + | EH | + |
| 10% pHEMA-UPy | 1% w/w CNT-UPy | + | E | + |
| 10% pHEMA-UPy | 5% w/w CNT-UPy | + | E | - |
| 10% pHEMA-UPy | - | - | EH | + |
| 10% pHEMA-UPy | - | - | EH* | - |
| pHEMA (20 kDa) | 5% w/w GLY | - | E | - |
| pHEMA (20 kDa) | 10 % w/w GLY | - | E | - |

# 10. Results

More comprehensive stress-strain curves from each measurement are presented in the appendices (appendix C, attachments 15-23). They show, how coherent results was obtained from each sample. From these results, the most representative curves have been chosen and they are compared and discussed in this chapter.

Figure 24 shows the most representative stress-strain curves from all measured films. The dark blue curve shows the control sample of 1 MDa pHEMA at 50 % humidity. Non-derivatized pHEMA elongates over 220 % and has a yield strength of 2 MPa. When pristine pHEMA reaches its maximum elongation and strain, it breaks down catastrophically. Unmodified pHEMA stretches a great deal and is also responsible for the stretching properties in all of the composites.

From figure 24, a large change between heat pressed and evaporated films can be observed as well. Without a doubt, the heat pressed films are the strongest ones (black curve). This strengthening, that heat pressing causes, has its prize; samples elongate 50 % less than the ones prepared by evaporation.

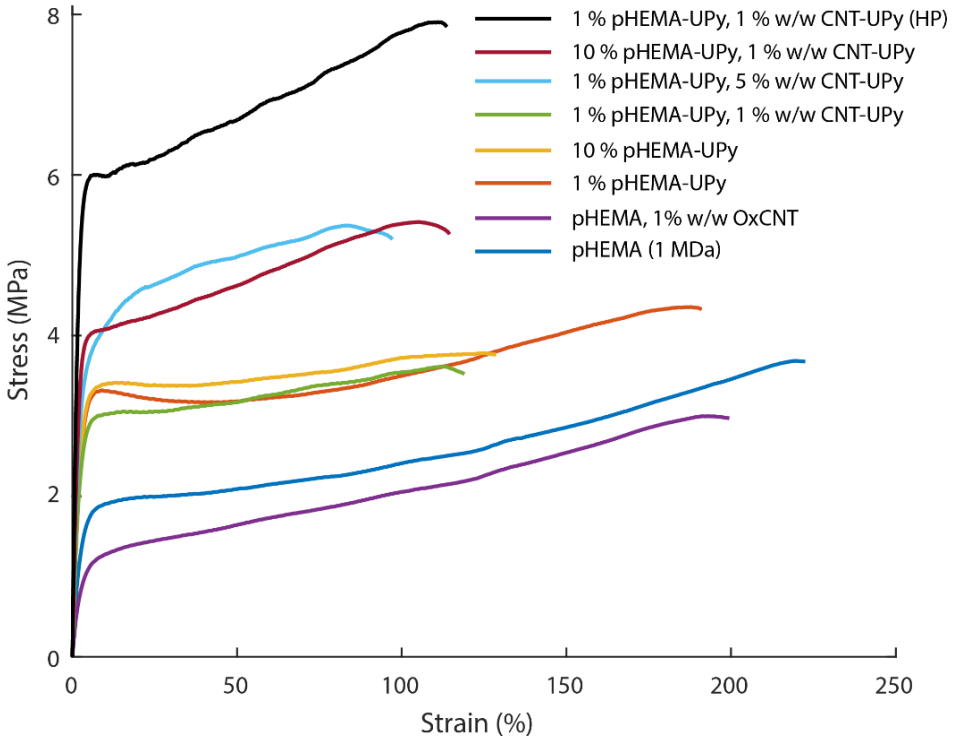


**Figure 24.** The most representative samples from mechanical testing of the pHEMA-UPy / MWCNT-UPy nanocomposites. Heat pressed sample denoted with HP.

The lowest yield strength is found from the pHEMA/oxCNT nanocomposite which does not contain ureidopyrimidinone at all (purple curve, figure 24). Compared to pristine pHEMA, the yield strength of pHEMA / oxCNT composite is decreased 50 % to 1 MPa but this film still elongates almost as much as unmodified pHEMA. This indicates that there are only very weak interactions, if at all, between the polymer and the carbon nanotubes. They both contain hydroxyl groups which could form hydrogen bonds between these two components. Most likely this is not happening or the interaction is not strong enough to affect the mechanical properties of the composite.

Addition of ureidopyrimidinone to the polymer increases the yield strength by 50 % from 2 MPa to 3 MPa and ultimate strength from 3 MPa to 4 MPa (figure 25). In the case of 1 % modification, it does not change the elongation too much; material stretches just 10 % less than unmodified pHEMA. In the case of 10 % modification, elongation is reduced by 40 %.

Compared to pristine pHEMA, the yield strength of 1 % ureidopyrimidinone derivative raises on average 1 MPa higher but less strain hardening occurs in the UPy-derivatives than in pristine

pHEMA (appendix C, attachments 15 and 16). The strain hardening behavior is strongest in pristine pHEMA as the yield strength is 2 MPa but ultimate strength is 4 MPa. The main differences between 1 % and 10 % ureidopyrimidinone derivatives is that 10 % derivative does not show such strain hardening behavior as 1% derivative does (appendix C, attachments 16 and 17). 10 % ureidopyrimidinone derivative shows the most crack resisting behavior and it can be seen from its stress-strain curve how after reaching the ultimate strength, the stress value starts to slowly get smaller. This indicates crack propagation rsistivity in the material.

pHEMA and its ureidopyrimidinone derivatives give fairly coherent results; samples cut from one component stretch to similar measures and they are also coherently strong (appendix C, attachments 15-17). Carbon nanotube composites give more incoherent results and this derives from inhomogeneities in the material. For example pristine pHEMA film is easier to make homogeneous compared to the composite of the polymer and carbon nanotubes. Even though the CNT-composite solutions are mixed with Ultra-turrax, they still might not be homogeneous enough to give coherent results.

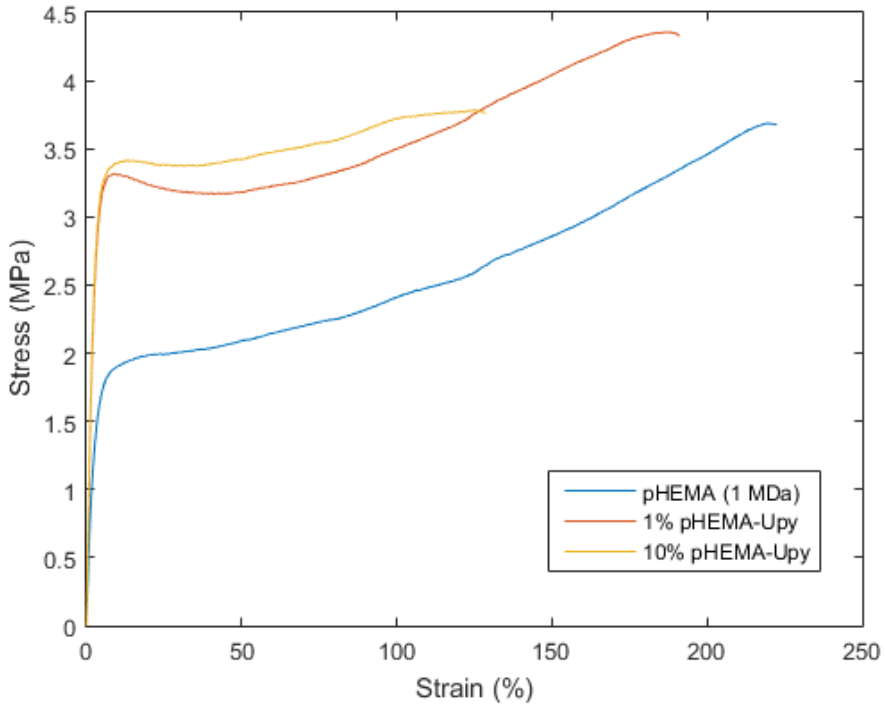


**Figure 25.** The effect of functionalization on the mechanical properties of pHEMA

Ureidopyrimidinone units are assumed to form dimers when solvent is removed. This dimerization increases the interaction between the components in the material and at the same time the rigidity of the material increases. The 10 % derivative stretches over 50 % less than the 1 % derivative. Bringing slightly more rigidity to the structure was thought to raise the yield strength and the ultimate strength without losing the elongation properties, and it did indeed, but not as much as planned.

Figure 26 shows the crack resisting behavior of 10 % pHEMA-UPy derivative when stretched. Pristine pHEMA breaks down catastrophically, but its ureidopyrimidinone-derivatives do not. In addition to energy dissipating features, the 10 % derivative has an interesting property; it develops a saw-tooth-like pattern on its edges.

As can be observed, the material is not completely homogeneous. This heterogeneity is most likely due to crystallization after drying the material. Partial crystallinity of the material may also lead to these saw-tooth-edges in the sample as the crystalline part break down while sample is elongated enough. Pristine pHEMA with 1 MDa molecular weight is crystalline. 10 % derivatization with ureidopyrimidininone is not very high percentage of the total molecular weight and might not disturb crystallization when solvent is removed slowly.

Similar behavior was not observed for the 1 % ureidopyrimidinone-derivative. These films were clear and smooth. They did develop cracks slowly but did not have the sawtooth-pattern at the edges. The actual crack usually develops right next to the clamps that hold the sample, or even under them so that the development cannot be seen, as almost happened with this sample.

**Figure 26:** 10 % pHEMA-UPy

The effect of ureidopyrimidinone derivatization and addition of carbon nanotubes on the mechanical propertied of the nanocomposite is shown in figure 27. Addition of oxidized carbon

nanotubes to unmodified pHEMA does not affect elongation much but led to otherwise poor results. The nanocomposite made from 10 % pHEMA-UPy and 1 % w/w of MWCNT-UPy has a yield strength twice as high as unmodified pHEMA and four times higher than pHEMA/oxCNT –composite, yet it still shows as high elongation as unmodified pHEMA. Composites containing ureidopyrimidinone also show crack resisting properties as the curve turns strongly down after reacting the ultimate strength and it continues going down for some time before breaking.

10 mm samples were prepared first from pHEMA/oxCNT composite, but they did not break in the limits of the tensile tester. Because of this, rest of the samples were shortened to 5mm. Both of the lengths gave similar results, curves from 10 mm samples are presented in appendix C, attachment 18.

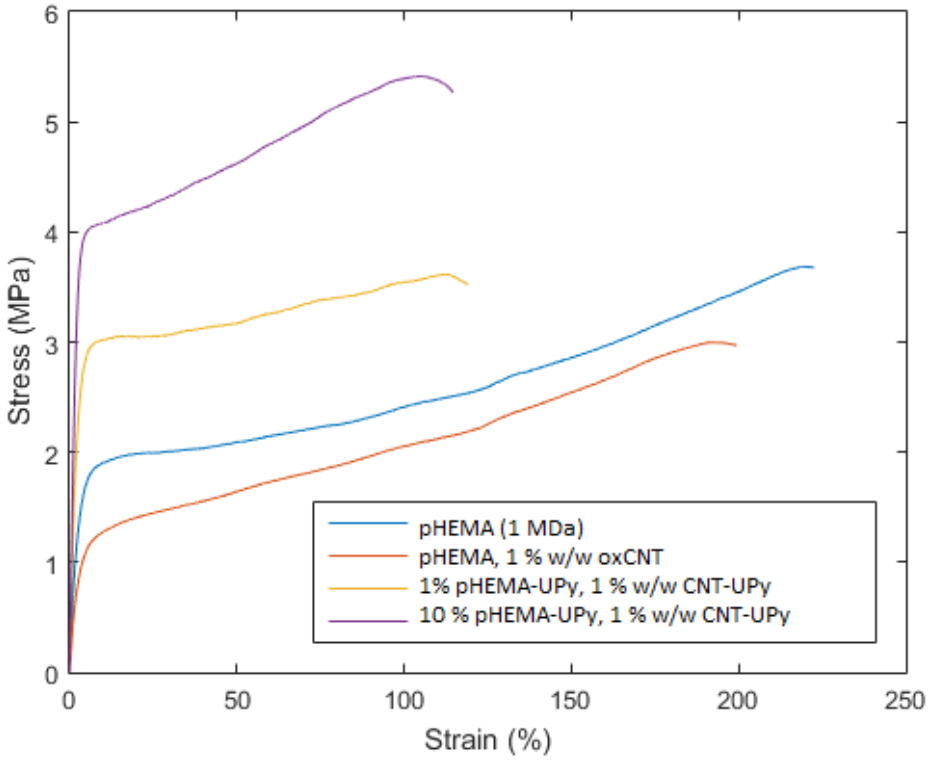


**Figure 27:** The effect of ureidopyrimidinone derivatization and carbon nanotube addition on the properties of the film.

1 % pHEMA-UPy/ 1 % CNT-UPy did not show as good results when considering mechanical properties but they show interesting behavior what comes to their crack propagation and crack growth while stretched (figure 28). Also the composite with 10 % pHEMA-UPy does develop cracks which grow slowly when the sample is stretched more. Behavior of the cracks was not entirely uniform, some of the samples developed such a double crack as in the picture 28. In these samples only one crack developed first but another started to develop to the other side, right next to the first one, when stretched more.

The difference between the polymer-UPy derivatives and carbon nanotube composites is that the material including CNTs does not develop the saw-tooth edge. The effect of crystallinity of the material was discussed earlier and one reason for not seeing a saw-tooth pattern at the edges of carbon nanotube composites might be the fact that when carbon nanotubes are mixed with the polymer, it disturbs the crystallization and the sample is more amorphous. If functionalization with ureidopyrimidinone was not enough to break the crystallinity of the material, the proper mixing with carbon nanotubes most likely is enough to break the lattice structure of the polymer.

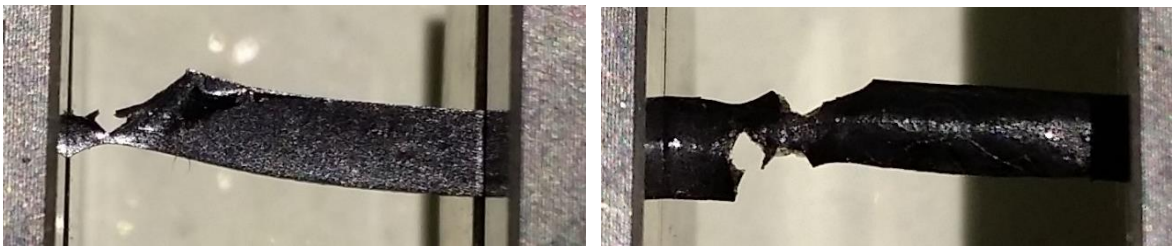

**Figure 28:** a) 1 % pHEMA-UPy / 1 % w/w CNT-UPy composite b) heat pressed 10 % pHEMA-UPy / 1 % w/w CNT-UPy composite

One of the aims was to make concentration series from both pHEMA-UPy derivatives with 1 %, 5 % and 10 % w/w of carbon nanotubes. This did not succeed, since already addition of 5 % w/w of CNT-UPy to 10 % pHEMA-UPy made the film brittle and we were unable to measure any tensile properties. The surface was very uneven as well and this would have affected the results a lot. 1 % pHEMA-UPy derivative gave measureable film with 5 % w/w of CNT-UPy. Compared to the 1 % w/w CNT-UPy composite with the same polymer derivative, this material has 2 MPa higher ultimate strength and shows a lot more strain hardening (figure 29). This result

is coherent with the hypothesis that addition of carbon nanotubes would make the material stronger.

1 % pHEMA-UPy / 1 % CNT-UPy composite gave fairly coherent results considering stress values; the variation is between 2.5 and 3.5 MPa (appendix C, attachment 19). Elongation on the other hand is not coherent at all as there is a 50 % difference between the smallest and highest elongation.

The aim to make concentration series from both polymers did not succeed, as already stated. 1 % pHEMA-UPy derivative gave measureable film with 5 % w/w of CNT-UPy (appendix C, attachment 16). The results from this composite are much more coherent than from the composite containing 1 % w/w CNT-UPy. The 1 % pHEMA-UPy / 5 % w/w CNT-UPy composite gave very similar results with the 10 % pHEMA / 1 % CNT-UPy composite (appendix C, attachments 20 and 21). The one with less carbon nanotubes can be stretched a bit more but strain values and variation among the samples are very similar in both cases.

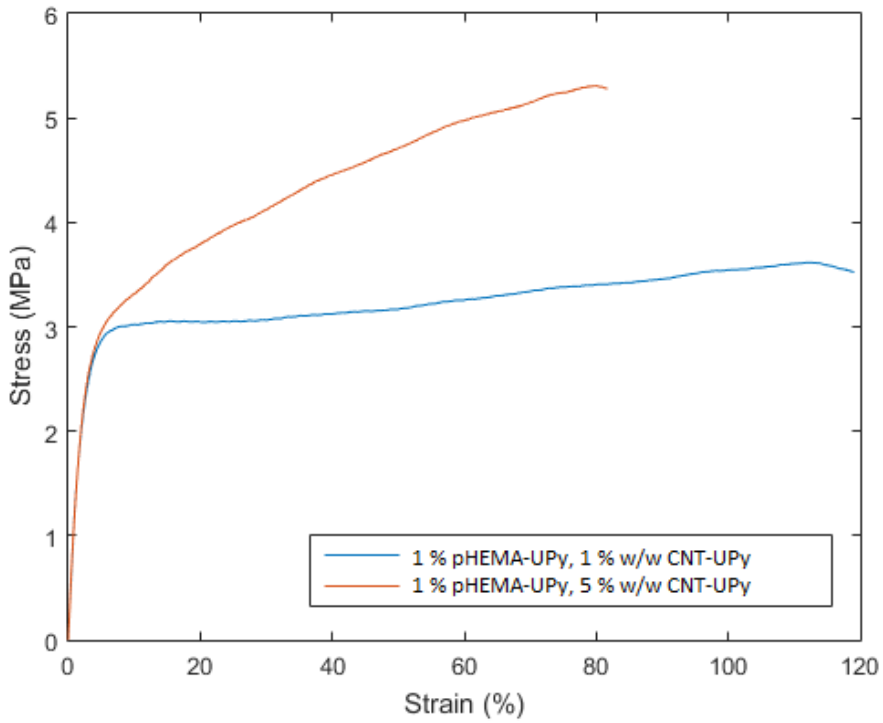


**Figure 29.** The effect of the amount of carbon nanotubes on the mechanical properties of the composites.

Figure 30 represents the effect that heat pressing has on the properties of one composite. In this material, heat pressing does not really affect the strain too much, but big improvement can be seen in the stress values. Heat pressed 5 mm samples show the most strain hardening of all the samples measured. The difference in yield strength between 5 mm samples is 4 MPa, heat pressed film being the tougher one. Difference in ultimate strength is as high as 9 MPa as heat pressed films shows much more strain hardening. The stress-strain curve of heat pressed 5 mm sample is very different than the behavior of heat pressed 10 mm sample. In shorter samples the deformation speed is higher and most likely the strain hardening also becomes more predominant due to that.

The stress-strain profile of the heat pressed 10 mm sample is very similar to the 5 mm evaporated composite but it has approximately 3 MPa higher stress values. The strengthening of heat pressed composites comes with the expense of the strain since those values drop drastically. Heat pressed films also give very incoherent results considering the elongation and due to this are not very well comparable to the films produced by evaporation (appendix C, attachments 22 and 23). Stress on the other hand does not have much larger variations than in the evaporated films.

Another problem occurred with the heat pressed films as well. Too fast cooling down could possibly cause buckling and distortion to the films. Even though all heat pressed films were let to cool down to room temperature over several hours while still pressed, after sample preparation they started to buckle and several samples could not be measured. Buckling causes the samples to not be straight anymore but it also shortens them which leads to unreliable results.

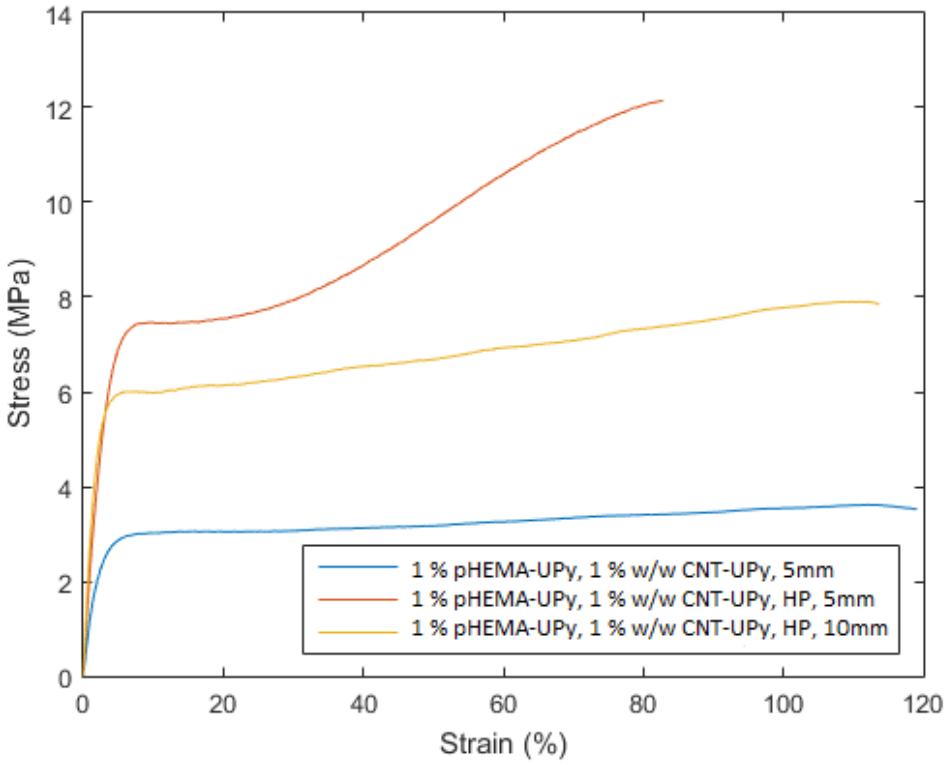


**Figure 30:** 1 % pHEMA-UPy/ 1 % w/w CNT-UPy composites, evaporated and heat pressed (HP).

## 10.1. Scanning Electron Microscopy (SEM)

1 % ureidopyrimidinone derivative seems to have two different regions. Figure 30 shows a very peculiar structure, this is not seen in any other composites. The cross section shows that the lower part of this film has a honeycomb-like structure. Similar pattern is not seen in the 10 % ureidopyrimidinone derivative of pHEMA (figure 31).

Upper part of the film is denser than the lower part; it also has holes but they are like squeezed and remind thin capillaries. This honeycomb structure more likely derives from the film preparation method than is a feature of the material. Even though the evaporation temperature (80 °C) is not even close to the boiling point of DMF, for example small amounts of water in the mixture could lead to formation of bubbles and so to the observed structure.

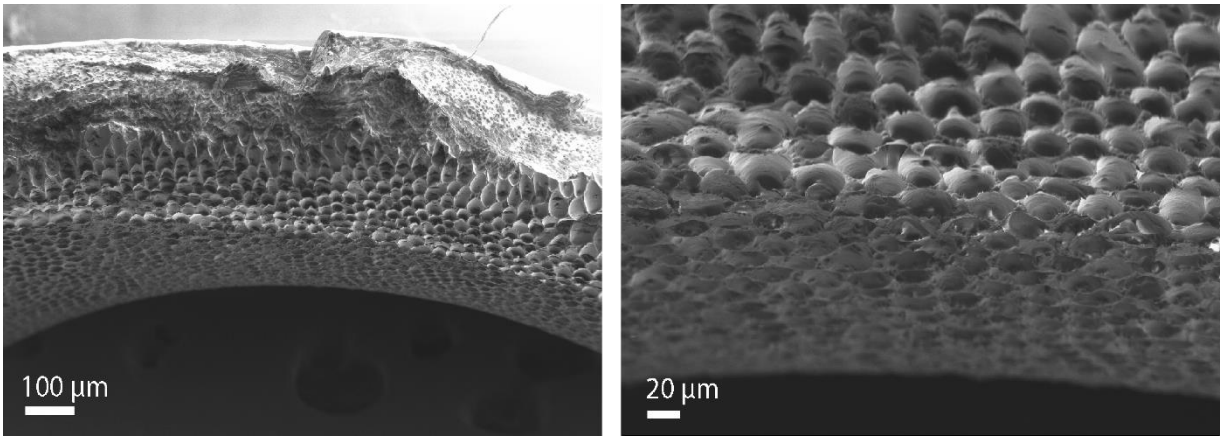


**Figure 31.** 1 % pHEMA-UPy

10 % ureidopyrimidinone derivative has holes in the cross-section of the film as well (figure 32). The figure 26 also shows several small cracks at the side of the film. This is most likely part of the saw-tooth-pattern that was noticed while carrying out the tensile testing.

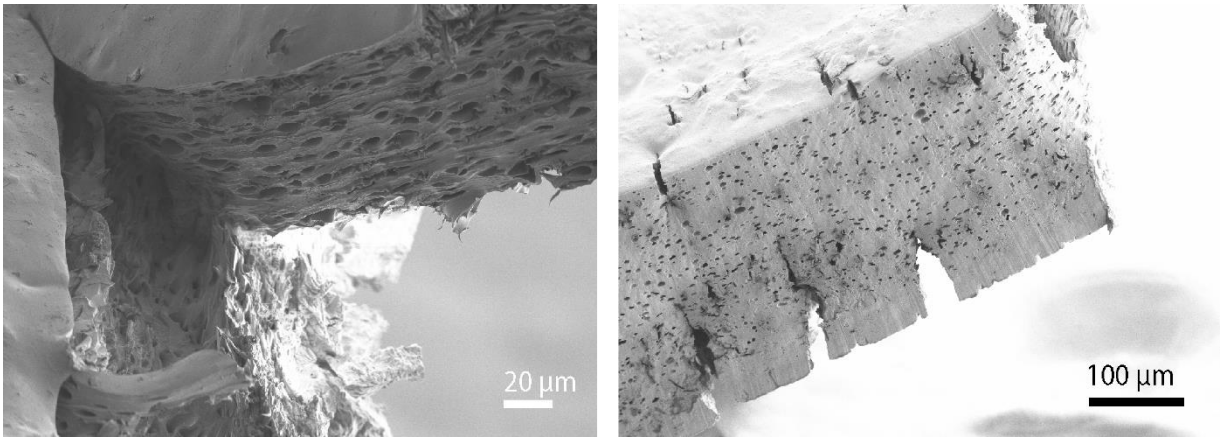


**Figure 32.** 10 % pHEMA-UPy

The film with 10 % pHEMA-UPy and 1 % w/w of CNT-UPy (figure 33) has a very similar structure compared to the 10 % pHEMA-UPy film (figure 32). The cross section of the crack seems to be sharper than in 10 % pHEMA-UPy and it does not have small cracks which causes the saw-tooth-pattern in 10 % pHEMA-UPy.

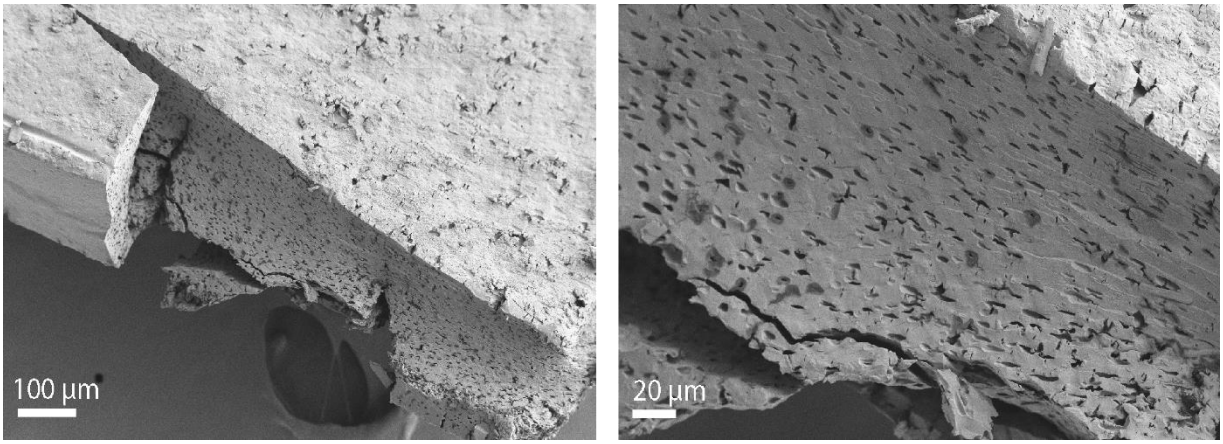


**Figure 33.** 10 % pHEMA-UPy/1 % CNT-UPy

1 % pHEMA-UPy/1 % CNT-UPy composite (figure 34) has a fairly different structure compared to the other films. The structure of the crack zone indicates slow growth of a cut as some regions have broken earlier than the others. The surface of the sample is rougher and unlike the situation with composites containing 10 % pHEMA-UPy derivative, 1 % pHEMA-UPy/1 % CNT-UPy composite reminds less the structure of 1 % pHEMA-film. It also has holes and they look like they would be squashed but compared to the composite without carbon nanotubes, the honeycomb-structure is missing.

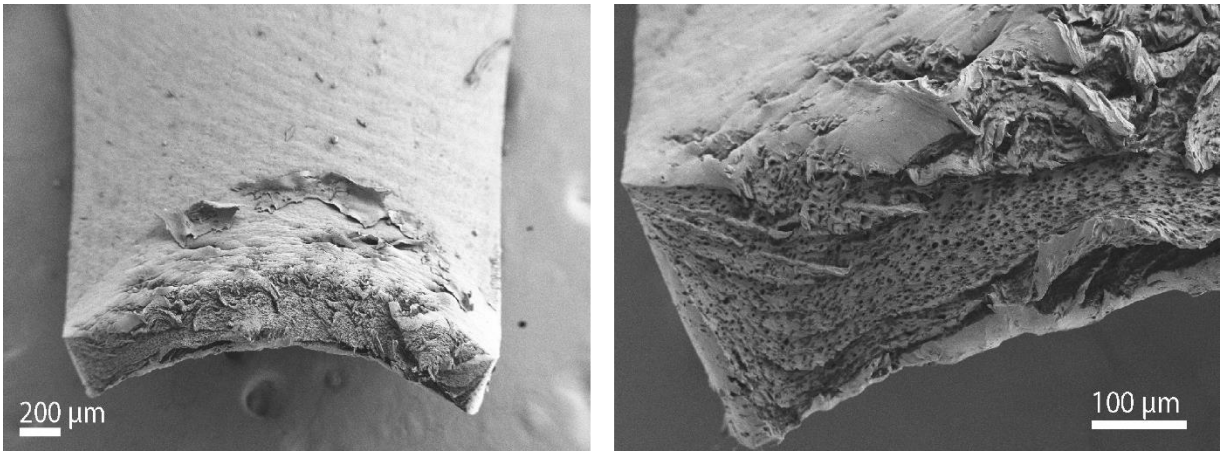


**Figure 34.** 1 % pHEMA-UPy/1 % CNT-UPy

Dialysis in methanol and heat pressing changed the structure drastically as expected. Figure 35 shows that this material is much smoother than the previously discussed ones. After methanol dialysis and heat pressing, the sample also does not show holes in the cross section. This material broke down catastrophically and due to that only one sample was measured. Compared to the

figure 34, the cross section in figure 35 looks very smooth. This implies a sudden crack rather than slow crack development and stretching.

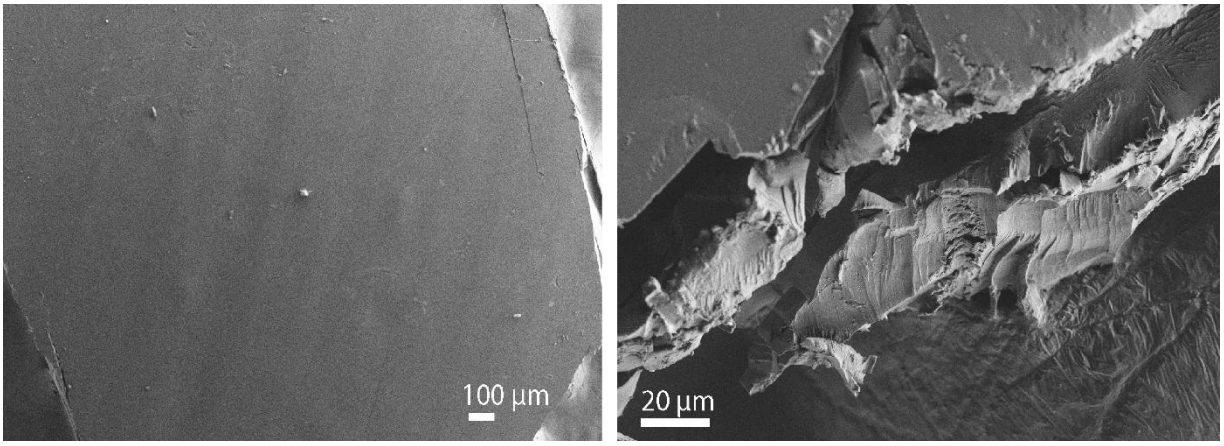


**Figure 35.** 1 % pHEMA-UPy dialyzed in methanol.

# 11. Conclusions

In this thesis, exceptionally strong binding of ureidopyrimidinone dimers and high tensile strength of multi-walled carbon nanotubes were used to obtain supramolecularly reinforced polymer/MWCNT nanocomposite. Addition of UPy to the polymer seems to raise the stress values but does not affect the strain much. On the other hand, addition of carbon nanotubes to the material increases the strength but this happens on the expense of the strain – the material does not elongate as much anymore. Major improvement in the mechanical properties (yield strength up to 300 % and ultimate strength up to 260 %) of the nanocomposite materials was achieved and this evidences benign association between UPy groups in carbon nanotubes and pHEMA. This association could result in outstanding stress transfer between the nanocomponents.[83]

Even though films prepared did not show as good mechanical properties as hoped, the crack propagation showed the kind of behavior as aimed. pHEMA seems to be responsible for the elongation properties of the films. However, addition of ureidopyrimidinone clearly results in slow crack propagation because this property is not seen in composites without UPy.

In the future, this design could be developed more by incorporating another polymer with slightly different properties. Supramolecular crosslinking could also be carried out with some other interaction, like heterodimers, host-guest inclusion complex or some other complementary heterogeneous molecules. This way it could be guaranteed, that the complex forms between the aimed components. Association between components, and further mechanical properties, could be enhanced by some other approach in film preparation; layer-by-layer assembly has been reported to give highly homogeneous nanocomposites from polymer and CNTs without phase separation issues.[97]

de Greef *et al.*[120] observed reduction in association constant of ethylene glycol substituted UPy moieties in apolar solvent. This reduction was dependent on the length of aliphatic spacer between the ethylene glycol unit and UPy moiety. The aliphatic chain shields the hydrogen bonding moiety from ethylene glycol which can behave as an acceptor and therefore disturb the dimerization process. Similar effect could disturb the dimerization in our design as well. pHEMA contains ester moiety which can behave as hydrogen bond acceptor and as the linker

between the polymer and UPy is only 6 carbons long, shielding from the polymer does not happen.

High tensile strength, good electrical and thermal properties and nanoscale size are all features which are demanded from composite materials as technology develops and size of electronic devices decreases. Carbon nanotubes possess these properties and CNT/polymer composites and other supramolecular structures containing CNTs have already been studied extensively but new ideas are needed. As the structure and mechanisms of biomaterials are understood better and new information on this area is trundling in, new ways to construct nanocomposites will be developed. In this thesis, synthesis of novel, biomimetic nanocomposite with 10 times better mechanical properties compared to previously reported similar composites[111], was presented. This sample preparation method and smart design has potential to be developed even further to obtain functional nanocomposites with better mechanical properties.

# 12. References


1. Guan, Z. & Kushner, A. M. Modular design in natural and biomimetic soft materials. *Angew. Chemie - Int. Ed.* **50,** 9026–9057 (2011).

2. Nova, A., Keten, S., Pugno, N. M., Redaelli, A. & Buehler, M. J. Molecular and Nanostructural Mechanisms of Deformation , Strength and Toughness of. *Nano Lett.* **10,** 2626–2634 (2010).

3. Xu, M. & Lewis, R. V. Structure of a protein superfiber : Spider dragline silk J |. *Proc. Natl. Acad. Sci. United States Am.* **87,** 7120–7124 (1990).

4. Hardy, J. G. & Scheibel, T. R. Production and Processing of Spider Silk Proteins. *J. Polym. Sci. Part A Polym. Chem.* **47,** 3957–3963 (2009).

5. Wang, S. *et al.* Self-Assembled Multiwalled Carbon Nanotube Films Assisted by Ureidopyrimidinone-Based Multiple Hydrogen Bonds. *J. Appl. Polym. Sci.* **131,** 1–8 (2014).

6. Du, R. *et al.* Hierarchical hydrogen bonds directed multi-functional carbon nanotube-based supramolecular hydrogels. *Small* **10,** 1387–1393 (2014).

7. Vollrath, F. & Porter, D. Spider silk as archetypal protein elastomer. *Soft Matter* **2,** 377–385 (2006).

8. Beek, J. D. Van, Hess, S., Vollrath, F. & Meier, B. H. The molecular structure of spider dragline silk : Folding and orientation of the protein backbone. *Proc. Natl. Acad. Sci. United States Am.* **99,** 10266–10271 (2002).

9. McKee, J. R. *et al.* Molecular engineering of fracture energy dissipating sacrificial bonds into cellulose nanocrystal nanocomposites. *Angew. Chemie - Int. Ed.* **53,** 5049–5053 (2014).

10. Lehn, J. Supramolecular Chemistry-Scope and Perpectives Molecules, Supermolecules and Molecular Devices. *Angew. Chem. Int. Ed.* **27,** 89–112 (1988).

11. Dong, R. *et al.* Functional Supramolecular Polymers for Biomedical Applications. *Adv. Mater.* **27,** 498–526 (2015).

12. Modi, S. *et al.* A DNA nanomachine that maps spatial and temporal pH changes inside living cells. *Nat. Nanotechnol.* **4,** 325–330 (2009).

13. Mozhdehi, D. & Guan, Z. Design of supramolecular amino acids to template peptide folding. *Chem. Commun. (Camb).* **49,** 9950–9952 (2013).

14. Kamiya, Y. & Asanuma, H. Light-Driven DNA Nanomachine with a Photoresponsive Molecular Engine. *Acc. Chem. Res.* **47,** 1663–1672 (2014).

15. Yurke, B., Turber, A. J., Mills, A. P. J., Simmel, F. C. & Neumann, J. L. A DNA-fuelled molecular machine made of DNA. *Nature* **406,** 605–608 (2000).

16. Elio, M. & Sijbren, O. Supramolecular systems chemistry. *Nat. Nanotechnol.* **10,** 111–119 (2015).

17. Behr, J. P. *The Lock-and-Key principle. The State of the Art - 100 years on*. (J. Wiley & Sons, Chichester, 1994).

18. Steed, J. W. & Atwood, J. L. *Supramolecular Chemistry*. (Wiley, 2002).

19. Hunter, C. A. & Sanders, J. K. M. The Nature of pi-pi interactions. *J. Am. Chem. Soc.* **112,** 5525–5534 (1990).

20. Steed, J. W. & Atwood, J. L. in *Supramolecular Chemistry* 142–143 (John Wiley & Sons, Ltd., 2002).

21. Prins, L. J., Reinhoudt, D. N. & Timmerman, P. Noncovalent synthesis using hydrogen bonding. *Angew. Chemie - Int. Ed.* **40,** 2382–2426 (2001).

22. Yang, K., Yi, Z., Jing, Q. & Lin, D. Dispersion and aggregation of single-walled carbon nanotubes in aqueous solutions of anionic surfactants. *J. Zhejiang Univ. Sci. A* **15,** 624–633 (2014).

23. Wang, J., Chu, H. & Li, Y. Why single-walled carbon nanotubes can be dispersed in imidazolium-based ionic liquids. *ACS Nano* **2,** 2540–2546 (2008).

24. Heim, M., Römer, L. & Scheibel, T. Hierarchical structures made of proteins . The complex architecture of spider webs and their constituent silk proteins. *Chem. Soc. Rev.* **39,** 156–164 (2009).

25. Gatesy, J., Hayashi, C., Motriuk, D., Woods, J. & Lewis, R. Extreme Diversity , Conservation , and Convergence of Spider Silk Fibroin Sequences. *Science (80-. ).* **291,** 2603–2606 (2001).

26. Huemmerich, D. *et al.* Primary Structure Elements of Spider Dragline Silks and Their Contribution to Protein Solubility †. *Biochemistry* **43,** 13604–13612 (2004).

27. Rousseau, M., Cruz, D. H., West, M. M., Hitchcock, A. P. & Pézolet, M. Nephila clavipes Spider Dragline Silk Microstructure Studied by Scanning Transmission X-ray Microscopy. *J. Am. Chem. Soc.* **129,** 3897–3905 (2007).

28. Termonia, Y. Molecular Modeling of Spider Silk Elasticity. *Macromolecules* **27,** 7378–7381 (1994).

29. Becker, N. *et al.* Molecular nanosprings in spider capture-silk threads. *Nat. Mater.* **2,** 278–283 (2003).

30. Hayashi, C. Y., Shipley, N. H. & Lewis, R. V. Hypotheses that correlate the sequence , structure , and mechanical properties of spider silk proteins. *Int. J. Biol. Macromol.* **24,** 271–275 (1999).

31. Grubb, D. T. & Jelinski, L. W. Fiber Morphology of Spider Silk : The Effects of Tensile Deformation. *Macromolecules* **30,** 2860–2867 (1997).

32. Brown, C. P., Rosei, F., Traversa, E. & Licoccia, S. Spider silk as a load bearing biomaterial: tailoring mechanical properties via structural modifications. *Nanoscale* **3,** 870–876 (2011).

33. Liu, Y. I., Shao, Z. & Vollrath, F. Relationships between supercontraction and mechanical properties of spider silk. *Nat. Mater.* **4,** 901–905 (2005).

34. Denny, B. Y. M. The Physical properties of spider´s silk and their role in the design of orb-webs. *J. Exp. Biol.* **65,** 483–506 (1976).

35. Guerette, P. A., Ginzinger, D. G., Weber, B. H. F. & Gosline, J. M. Silk Properties Determined by Gland-Specific Expression of a Spider Fibroin Gene Family. *Science (80-. ).* **272,** 112–115 (1996).

36. Exler, J. H., Hümmerich, D. & Scheibel, T. The Amphiphilic Properties of Spider Silks Are Important for Spinning. *Angew. Chemie - Int. Ed.* **46,** 3559–3562 (2007).

37. Kushner, A. M., Gabuchian, V., Johnson, E. G. & Guan, Z. Biomimetic Design of Reversibly Unfolding Cross-Linker to Enhance Mechanical Properties of 3D Network Polymers. *J. Am. Chem. Soc.* **129,** 14110–14111 (2007).

38. Qu, Y., Payne, S. C., Apkarian, R. P. & Conticello, V. P. Self-Assembly of a Polypeptide Multi-Block Copolymer Modeled on Dragline Silk Proteins. *J. Am. Chem. Soc.* **122,** 5014–5015 (2000).

39. Nagapudi, K. *et al.* Protein-Based Thermoplastic Elastomers. *Macromolecules* **38,** 345–354 (2005).

40. Lieou, C. K. C., Elbanna, A. E. & Carlson, J. M. Sacrificial bonds and hidden length in biomaterials : A kinetic constitutive description of strength and toughness in bone. *Phys. Rev. E* **88,** 1–10 (2013).

41. Agnarsson, I., Dhinojwala, A., Sahni, V. & Blackledge, T. A. Spider silk as a novel high performance biomimetic muscle driven by humidity. *J. Exp. Biol.* **212,** 1990–1994 (2009).

42. Hermanson, B. K. D., Huemmerich, D., Scheibel, T. & Bausch, A. R. Engineered Microcapsules Fabricated from Reconstituted Spider Silk. *Adv. Mater.* **19,** 1810–1815 (2007).

43. Rammensee, S., Huemmerich, D., Hermanson, K. D., Scheibel, T. & Bausch, A. R. Rheological characterization of hydrogels formed by recombinantly produced spider silk. *Appl. Phys. A* **82,** 261–264 (2006).

44. Slotta, U. K., Rammensee, S., Gorb, S. & Scheibel, T. An Engineered Spider Silk Protein Forms Microspheres. *Angew. Chemie - Int. Ed.* **47,** 4592–4594 (2008).

45. Lammel, A., Schwab, M., Slotta, U., Winter, G. & Scheibel, T. Processing Conditions for the Formation of Spider Silk Microspheres. *ChemSusChem* **1,** 413–416 (2008).

46. Huemmerich, D., Slotta, U. & Scheibel, T. Processing and modification of films made

from recombinant spider silk proteins. *Appl. Phys. A* **82,** 219–222 (2006).

47. Iijima, S. Helical microtubules of graphitic carbon. *Nature* **354,** 56–58 (1991).

48. Gogotsi, Y. *Nanomaterials Handbook*. (2006).

49. Hung, N. T., Anoshkin, I. V., Dementjev, a. P., Katorov, D. V. & Rakov, E. G. Functionalization and solubilization of thin multiwalled carbon nanotubes. *Inorg. Mater.* **44,** 219–223 (2007).

50. Bockrath, M., Cobden, D. H., Mceuen, P. L., Chopra, N. G. & Zettl, A. Single Electron Transport in Ropes of Carbon Nanotubes. *Science (80-. ).* **275,** 1922–1925 (2008).

51. Wang, X. *et al.* Fabrication of Ultralong and Electrically Uniform Single-Walled Carbon Nanotubes on Clean Substrates. *Nano Lett.* **9,** 3137–3141 (2009).

52. Coleman, J. N., Khan, U., Blau, W. J. & Gun'ko, Y. K. Small but strong : A review of the mechanical properties of carbon nanotube – polymer composites. *Carbon N. Y.* **44,** 1624–1652 (2006).

53. Hilding, J., Grulke, E. a., George Zhang, Z. & Lockwood, F. Dispersion of Carbon Nanotubes in Liquids. *J. Dispers. Sci. Technol.* **24,** 1–41 (2003).

54. Ozin, G. A. & Arsenault, A. C. *Nanochemistry: A chemical approach to nanomaterials*. (RSC Publishing, 2005).

55. Bachtold, A. *et al.* Scanned Probe Microscopy of Electronic Transport in Carbon Nanotubes Figure 1. *Phys. Rev. Lett.* **84,** 6082–6085 (2000).

56. Tekleab, D. & Carroll, D. L. Strain-induced electronic property heterogeneity of a carbon nanotube. *Phys. Rev. B* **64,** 1–5 (2001).

57. Ruoff, R. S. & Lorents, D. C. Mechanical and thermal properties of carbon nanotubes. *Carbon N. Y.* **33,** 925–930 (1995).

58. Baughman, R. H., Zakhidov, A. A. & De Heer, W. A. Carbon Nanotubes — the Route Toward Applications. *Science (80-. ).* **297,** 787–792 (2002).

59. Wong, E. W., Sheehan, P. E. & Lieber, C. M. Nanobeam Mechanics: Elasticity,

Strength, and Toughness of Nanorods and Nanotubes. *Science (80-. ).* **277,** 1971–1976 (1997).

60. Yu, M. *et al.* Strength and Breaking Mechanism of Multiwalled Carbon Nanotubes Under Tensile Load. *Science (80-. ).* **287,** 637–640 (2000).

61. Wang, Z. L. *et al.* Mechanical and electrostatic properties of carbon nanotubes and nanowires. *Mater. Sci. Eng. C* **16,** 3–10 (2001).

62. Demczyk, B. G. *et al.* Direct mechanical measurement of the tensile strength and elastic modulus of multiwalled carbon nanotubes. *Mater. Sci. Eng. A* **334,** 173–178 (2002).

63. Zhu, Y. Q. *et al.* Collapsing carbon nanotubes and diamond formation under shock waves. *Chem. Phys. Lett.* **287,** 689–693 (1998).

64. Guo, T., Nikolaev, P., Thess, A., Colbert, D. T. & Smalley, R. E. Catalytic growth of single-walled nanotubes by laser vaporization. *Chem. Phys. Lett.* **243,** 49–54 (1995).

65. Yeoh, W., Lee, K., Chai, S., Lee, K. & Mohamed, A. R. Synthesis of high purity multi-walled carbon nanotubes over Co-Mo / MgO catalyst by the catalytic chemical vapor deposition of methane. *New Carbon Mater.* **24,** 119–123 (2009).

66. Girifalco, L. A., Hodak, M. & Lee, R. S. Carbon nanotubes, buckyballs, ropes, and a universal graphitic potential. *Phys. Rev. B - Condens. Matter Mater. Phys.* **62,** 13104–13110 (2000).

67. Lin, Y. *et al.* Advances toward bioapplications of carbon nanotubes. *J. Mater. Chem.* **14,** 527 (2004).

68. Hwang, J. *et al.* Polymer Structure and Solvent Effects on the Selective Dispersion of Single-Walled Carbon Nanotubes. *J. Am. Chem. Soc.* **130,** 3543–3553 (2008).

69. King, A. W. T., Asikkala, J., Mutikainen, I., Järvi, P. & Kilpeläinen, I. Distillable Acid – Base Conjugate Ionic Liquids for Cellulose Dissolution and Processing. *Angewante Chemie* **50,** 6301–6305 (2011).

70. Granström, M. *et al.* Tosylation and acylation of cellulose in 1-allyl-3-methylimidazolium chloride. *Cellulose* **15,** 481–488 (2008).

71. Lozano, L. J. *et al.* Recent advances in supported ionic liquid membrane technology. *J. Memb. Sci.* **376,** 1–14 (2011).

72. Greaves, T. L. & Drummond, C. J. Protic Ionic Liquids : Properties and Applications. *Chem. Rev.* **108,** 206–237 (2008).

73. Prolongo, S. G., Meliton, B. G., Del Rosario, G. & Ureña, A. Simultaneous dispersion and alignment of carbon nanotubes in epoxy resin through chronoamperometry. *Carbon N. Y.* **50,** 5489–5497 (2012).

74. Tsai, Y. *et al.* Dispersion of carbon nanotubes in low pH aqueous solutions by means of alumina-coated silica nanoparticles. *Carbon N. Y.* **45,** 2823–2827 (2007).

75. Tohver, V., Smay, J. E., Braem, A., Braun, P. V & Lewis, J. A. Nanoparticle halos : A new colloid stabilization mechanism. *Proc. Natl. Acad. Sci. United States Am.* **98,** 8950–8954 (2001).

76. Saleh, N. B., Pfefferle, L. D. & Elimelech, M. Influence of Biomacromolecules and Humic Acid on the Aggregation Kinetics of Single-Walled Carbon Nanotubes. *Environ. Sci. Technol.* **44,** 2412–2418 (2010).

77. Lin, D. *et al.* The effect of ionic strength and pH on the stability of tannic acid-facilitated carbon nanotube suspensions. *Carbon N. Y.* **47,** 2875–2882 (2009).

78. Bouchard, D., Zhang, W., Powell, T. & Rattanaudompol, U. Aggregation Kinetics and Transport of Single-Walled Carbon Nanotubes at Low Surfactant Concentrations. *Environ. Sci. Technol.* **46,** 4458–4465 (2012).

79. Lebrón-Colón, M. *et al.* Surface oxidation study of single wall carbon nanotubes. *Nanotechnology* **22,** 1–5 (2011).

80. Hamon, M. A. *et al.* Dissolution of Single-Walled Carbon Nanotubes. *Adv. Mater.* **11,** 834–840 (1999).

81. Chen, J. *et al.* Solution Properties of Single-Walled Carbon Nanotubes. *Science (80-. ).* **282,** 95–98 (1998).

82. Ciobotaru, C.-C., Damian, C. M. & Iovu, H. Single-wall carbon nanotubes purification

and oxidation. *Sci. Bull.* **75,** 55–66 (2013).

83. Kokil, A. *et al.* Introduction of Multiple Hydrogen Bonding for Enhanced Mechanical Performance of Polymer-Carbon Nanotube Composites. *J. Macromol. Sci.* **48,** 1016–1021 (2011).

84. Shim, M., Wong Shi Kam, N., Chen, R. J., Li, Y. & Dai, H. Functionalization of Carbon Nanotubes for Biocompatibility and Biomolecular Recognition. *Nano Lett.* **2,** 285–288 (2002).

85. Karajanagi, S. S., Vertegel, A. A., Kane, R. S. & Dordick, J. S. Structure and Function of Enzymes Adsorbed onto Single-Walled Carbon Nanotubes. *Langmuir* **20,** 11594–11599 (2004).

86. Balavoine, F. *et al.* Helical Crystallization of Proteins on Carbon Nanotubes : A First Step towards the Development of New Biosensors. *Angew. Chemie - Int. Ed.* **38,** 1912–1915 (1999).

87. Chen, R. J., Zhang, Y., Wang, D. & Dai, H. Noncovalent Sidewall Functionalization of Single-Walled Carbon Nanotubes for Protein Immobilization. *J. Am. Chem. Soc.* **123,** 3838–3839 (2001).

88. Fadel, T. R. *et al.* Enhanced Cellular Activation with Single Walled Carbon Nanotube Bundles Presenting Antibody Stimuli. *Nano Lett.* **8,** 2070–2076 (2008).

89. Alvarez, N. T. *et al.* Polymer Coatings of Carbon Nanotube Fibers for Electric Microcables. *Nanomaterials* **4,** 879–893 (2014).

90. Hong, J., Lee, J., Hong, C. K. & Shim, S. E. Effect of dispersion state of carbon nanotube on the thermal conductivity of poly ( dimethyl siloxane ) composites. *Curr. Appl. Phys.* **10,** 359–363 (2010).

91. Kim, P., Shi, L., Majumdar, A. & McEuen, P. L. Thermal Transport Measurements of Individual Multiwalled Nanotubes. *Phys. Rev. Lett.* **87,** 1–4 (2001).

92. Hone, J. *et al.* Electrical and thermal transport properties of magnetically aligned single wall carbon nanotube films. *Appl. Phys. Lett.* **77,** 666–668 (2000).

93. Berber, S., Kwon, Y. & Tománek, D. Unusually High Thermal Conductivity of Carbon Nanotubes. *Phys. Rev. Lett.* **84,** 4613–4616 (2000).

94. Bal, S. Influence of dispersion states of carbon nanotubes on mechanical and electrical properties of epoxy nanocomposites. *J. Sci. Ind. Res. (India).* **66,** 752–756 (2007).

95. Choi, S. U. S., Zhang, Z. G., Yu, W., Lockwood, F. E. & Grulke, E. A. Anomalous thermal conductivity enhancement in nanotube suspensions. *Appl. Phys. Lett.* **79,** 2252–2255 (2001).

96. Biercuk, M. J. *et al.* Carbon nanotube composites for thermal management. *Appl. Phys. Lett.* **80,** 2767–2769 (2002).

97. Mamedov, A. A. *et al.* Molecular design of strong single-walled carbon nanotube/polyelectrolyte multilayer composites. *Nat. Mater.* **1,** 190–195 (2002).

98. Kaempgen, M., Duesberg, G. S. & Roth, S. Transparent carbon nanotube coatings. *Appl. Surf. Sci.* **252,** 425–429 (2005).

99. Li, Z. *et al.* Comparative Study on Different Carbon Nanotube Materials in Terms of Transparent Conductive Coatings. *Langmuir* **24,** 2655–2662 (2008).

100. Pasquier, A. Du, Unalan, H. E., Kanwal, A., Miller, S. & Chhowalla, M. Conducting and transparent single-wall carbon nanotube electrodes for polymer-fullerene solar cells. *Appl. Phys. Lett.* **87,** 1–3 (2005).

101. Beijer, F. H., Sijbesma, R. P., Kooijman, H., Spek, A. L. & Meijer, E. W. Strong dimerization of ureidopyrimidones via quadruple hydrogen bonding. *J. Am. Chem. Soc.* **120,** 6761–6769 (1998).

102. Alexander, A.-M. *et al.* Probing the solvent-induced tautomerism of a redox-active ureidopyrimidinone. *Chem. Commun. (Camb).* 2246–2248 (2007).

103. Söntjens, S. H. M., Sijbesma, R. P., van Genderen, M. H. P. & Meijer, E. W. Stability and Lifetime of Quadruply Hydrogen Bonded 2-Ureido-4[1 H ]-pyrimidinone Dimers. *J. Am. Chem. Soc.* **122,** 7487–7493 (2000).

104. Jorgensen, W. L. & Pranata, J. Importance of secondary interactions in triply hydrogen

bonded complexes: guanine-cytosine vs uracil-2,6-diaminopyridine. *J. Am. Chem. Soc.* **112,** 2008–2010 (1990).

105. Blight, B. a, Hunter, C. a, Leigh, D. a, McNab, H. & Thomson, P. I. T. An AAAA–DDDD quadruple hydrogen-bond array. *Nat. Chem.* **3,** 244–248 (2011).

106. Wilson, A. J. Hydrogen bonding: Attractive arrays. *Nat. Chem.* **3,** 193–194 (2011).

107. Lebrón-Colón, M. *et al.* Reinforced Thermoplastic Polyimide with Dispersed Functionalized Single Wall Carbon Nanotubes. *ACS Appl. Mater. Interfaces* **2,** 669–676 (2010).

108. Zhang, X. *et al.* Poly ( vinyl alcohol )/ SWNT Composite Film. *Nano Lett.* **3,** 1285–1288 (2003).

109. Sandler, J. *et al.* Development of a dispersion process for carbon nanotubes in an epoxy matrix and the resulting electrical properties. *Polymer (Guildf).* **40,** 5967–5971 (1999).

110. Micoli, A. *et al.* Supramolecular Macrostructures of UPy-Functionalized Carbon Nanotubes. *Chem. - A Eur. J.* **21,** 14179–14185 (2015).

111. Guo, K. *et al.* Conductive Elastomers with Autonomic Self-Healing Properties. *Angew. Chemie Int. Ed.* **54,** 12127–12133 (2015).

112. Hase, T. *Tables for Organic Spectrometry*. (Otatieto, 1992).

113. Rosario-Castro, B. I. *et al.* Combined electron microscopy and spectroscopy characterization of as-received , acid purified , and oxidized HiPCO single-wall carbon nanotubes. *Mater. Charact.* **60,** 1442–1453 (2009).

114. Chiang, I. W., Brinson, B. E., Smalley, R. E., Margrave, J. L. & Hauge, R. H. Purification and Characterization of Single-Wall Carbon Nanotubes. *J. Phys. Chem.* **105,** 1157–1161 (2001).

115. Niyogi, S. *et al.* Chromatographic Purification of Soluble Single-Walled Carbon nanotubes (s-SWNTs). *J. Am. Chem. Soc.* **123,** 733–734 (2001).

116. Rosario-Castro, B. I., Contés, E. J., Pérez-Davis, M. E. & Cabrera, C. R. Attachment of single-wall carbon nanotubes on platinum surfaces by self-assembling techniques. *Rev.*

*Adv. Mater. Sci.* **10,** 381–386 (2005).

117. Niyogi, S., Sarkar, S. & Adhikari, B. Catalytic activity of DBTDL in polyurethane formation. *Indian J. Chem. Technol.* **9,** 330–333 (2002).

118. Mohomed, K., Gerasimov, T. G., Moussy, F. & Harmon, J. P. A broad spectrum analysis of the dielectric properties of poly ( 2-hydroxyethyl methacrylate ). *Polymer (Guildf).* **46,** 3847–3855 (2005).

119. Kim, S. J. *et al.* Successive Grafting of PHEMA and PIPAAm onto Cell Culture Surface Enables Rapid Cell Sheet Recovery. *Tissue Eng. Regen. Med.* **10,** 139–145 (2013).

120. de Greef, T. F. a *et al.* The influence of ethylene glycol chains on the thermodynamics of hydrogen-bonded supramolecular assemblies in apolar solvents. *Chem. Commun. (Camb).* 4306–4308 (2008).

# III APPENDICES

## Appendix A. Fourier Transform Infrared Spectroscopy

**Attachment 1.** FT-IR spectra of 20 kDa pHEMA

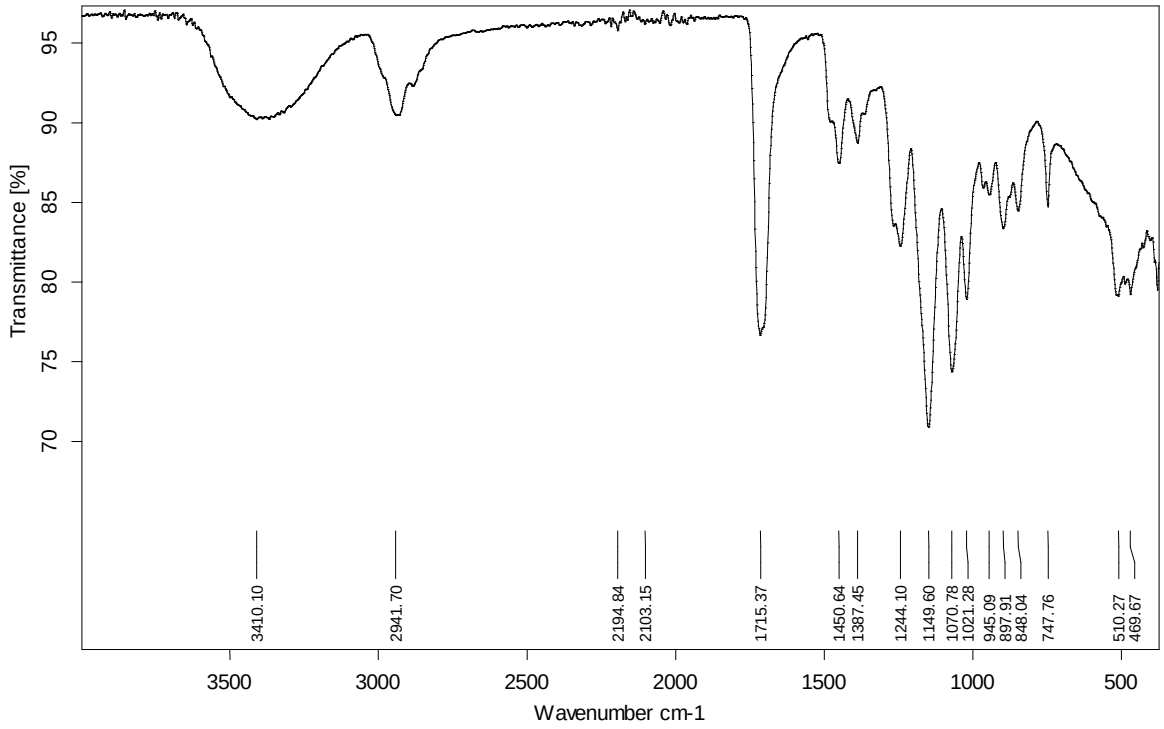


FT-IR 20 kDa pHEMA $\upsilon$ $cm^{-1}$:

3410 (-OH, polymeric), 2941 (-$CH_2$-), 1715 ($CO_2$R), 1450 (-$CH_3$), 1387 (-$CH_3$), 1244 (-OH), 1149 (-$CO_2$-), 1070 (-$CO_2$-), 1021, 947, 897, 848, 747 (-$CH_2$-), 510, 469

**Attachment 2.** FT-IR spectra of 1MDa pHEMA

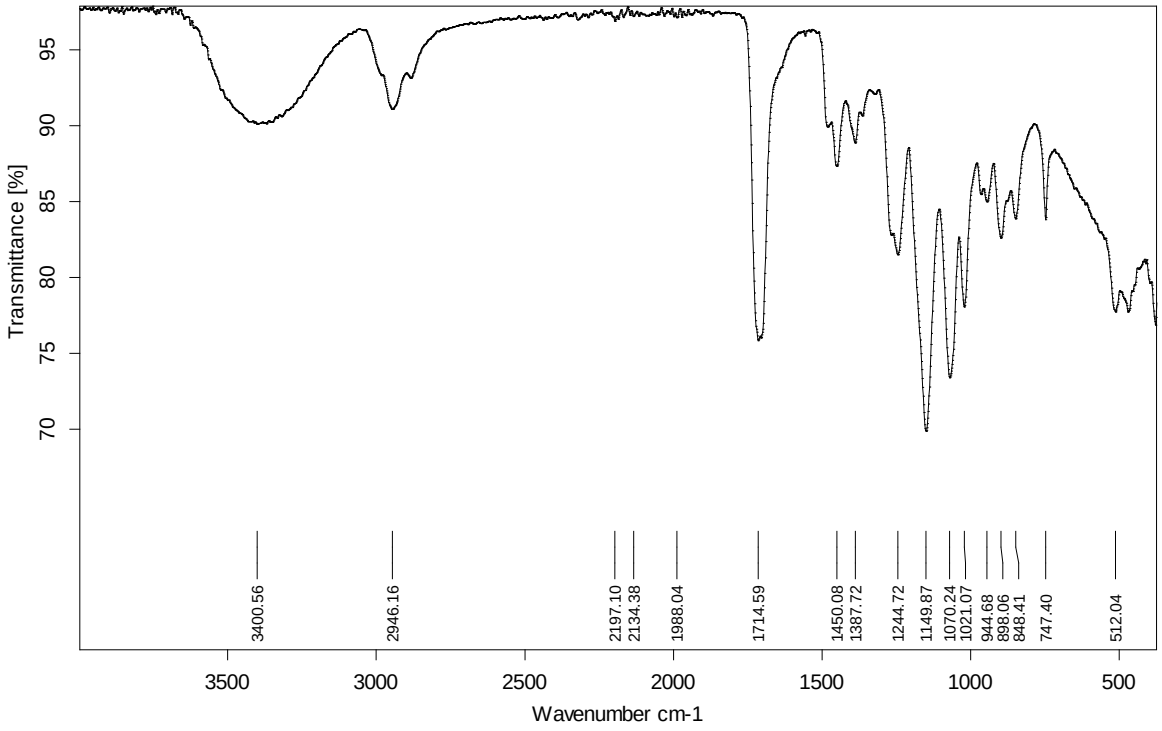


FT-IR 1 MDa pHEMA $\upsilon$ $cm^{-1}$:

3400 (-OH, polymeric), 2946 ($-CH_2-$), 1714 ($CO_2R$), 1450 ($-CH_3$), 1387 ($-CH_3$), 1244 (-OH), 1149 ($-CO_2-$), 1070 ($-CO_2-$), 1021, 944, 898, 848, 747 ($-CH_2-$), 512

**Attachment 3.** FT-IR spectra of 1 % pHEMA-UPy derivative.

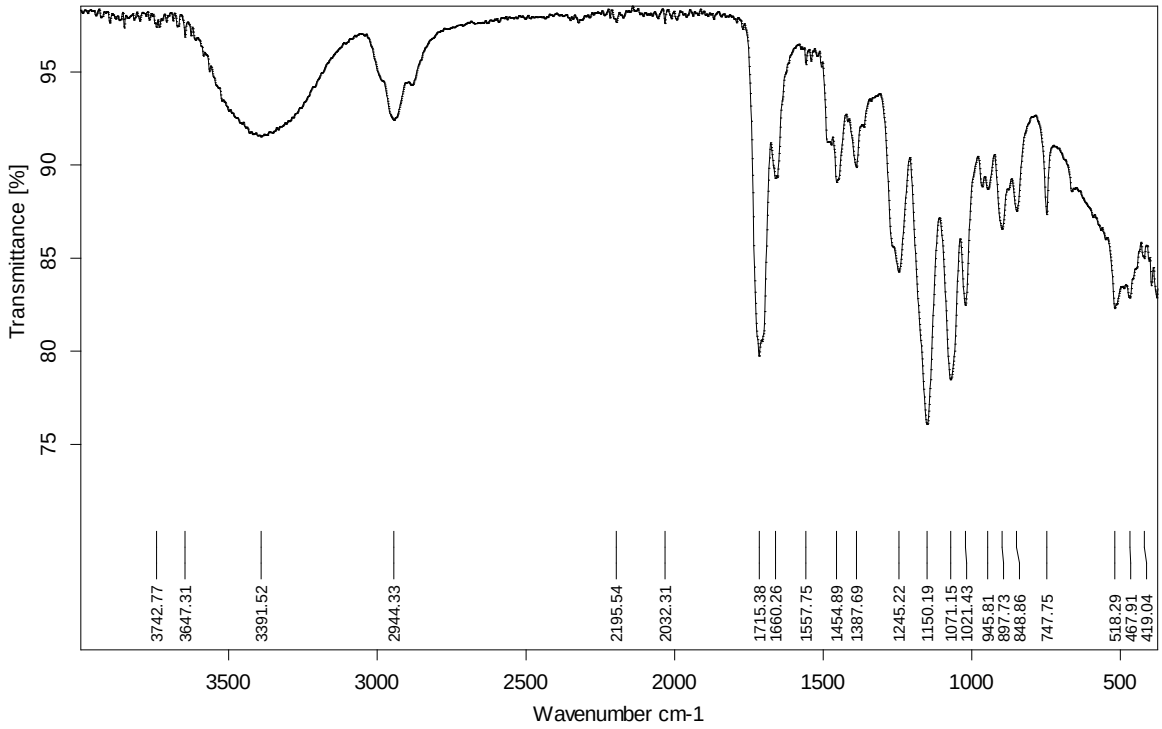


FT-IR: υ $cm^{-1}$: 3391 (-OH, polymeric), 2944 ($-CH_2-$), 1715 ($-CO_2-$) and (RO-CONH-R), 1660 ($(RNH)_2CO$), 1557 (RO-CONH-R), 1454 ($-CH_2-$), 1387 ($-CH_3$), 1245 (-OH), 1150 ($-CO_2-$), 1071 ($-CO_2-$), 1021, 945, 897, 848, 747 ($-CH_2-$), 518, 467

**Attachment 4.** FT-IR spectra of 10 % pHEMA-UPy derivative.

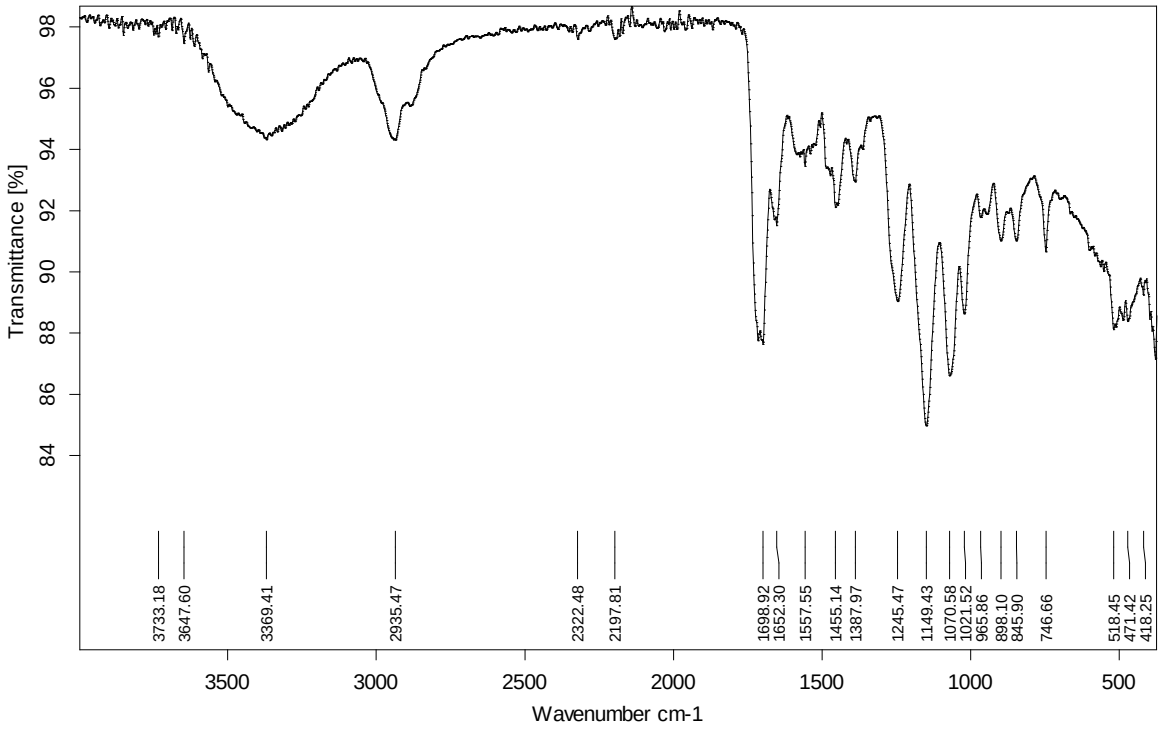


FT-IR υ $cm^{-1}$: 3369 (-OH, polymeric), 2935 ($-CH_2-$), 1698 ($-CO_2-$ ) and (RO-CONH-R), 1652 ($(RNH)_2CO$), 1557 (RO-CONH-R), 1455 ($-CH_2-$), 1387 ($-CH_3$), 1245 (-OH), 1149 ($-CO_2-$), 1070 ($-CO_2-$), 1021, 965, 898, 845, 746 ($-CH_2-$), 518, 471

## B. Nuclear Magnetic Resonance spectroscopy

**Attachment 5.** $^{1}$H-NMR spectra of pristine UPy-NCO (in DMSO-$d_6$)

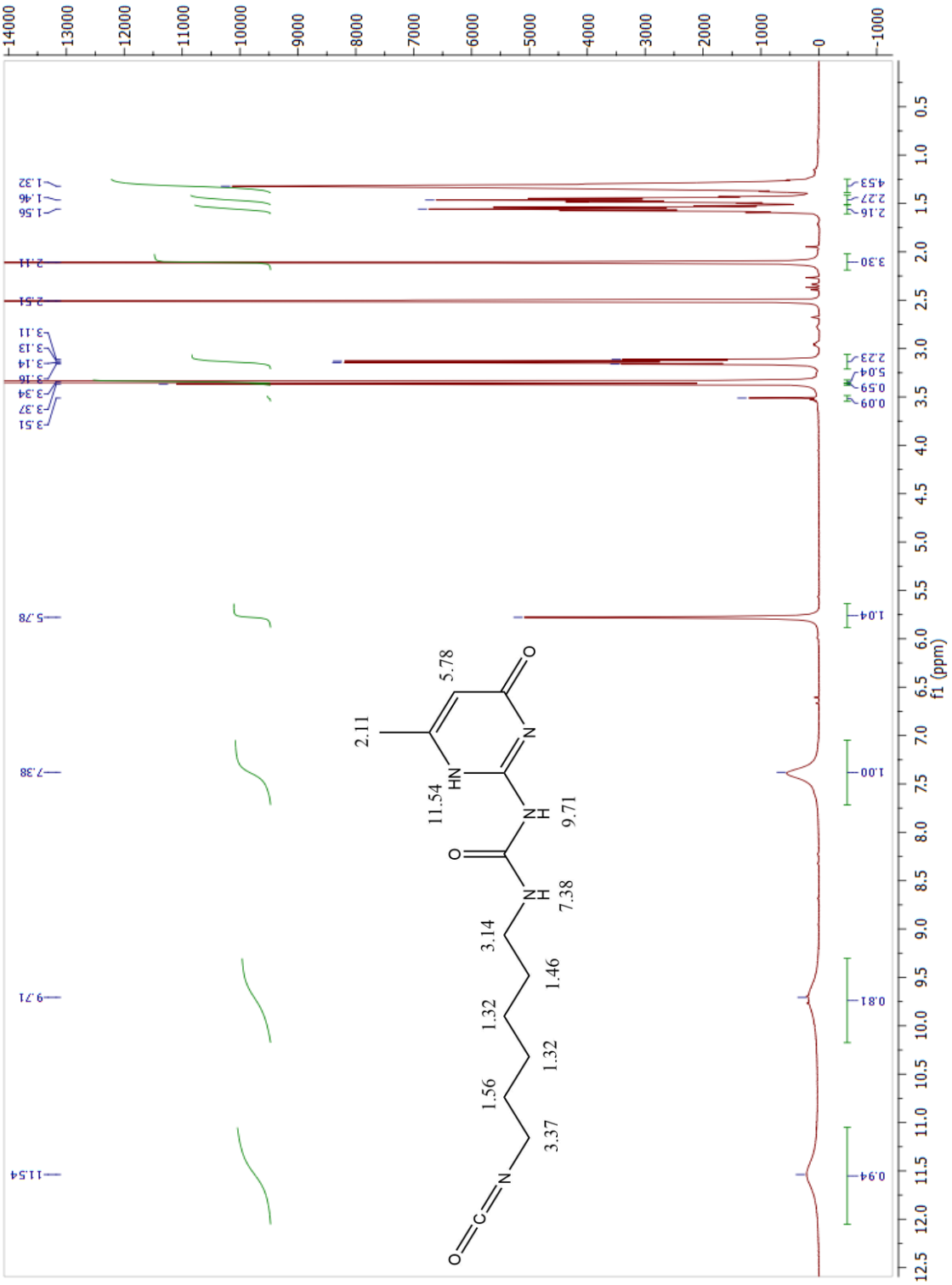

**Attachment 6.** Zoom of $^{1}$H-NMR of UPy-NCO

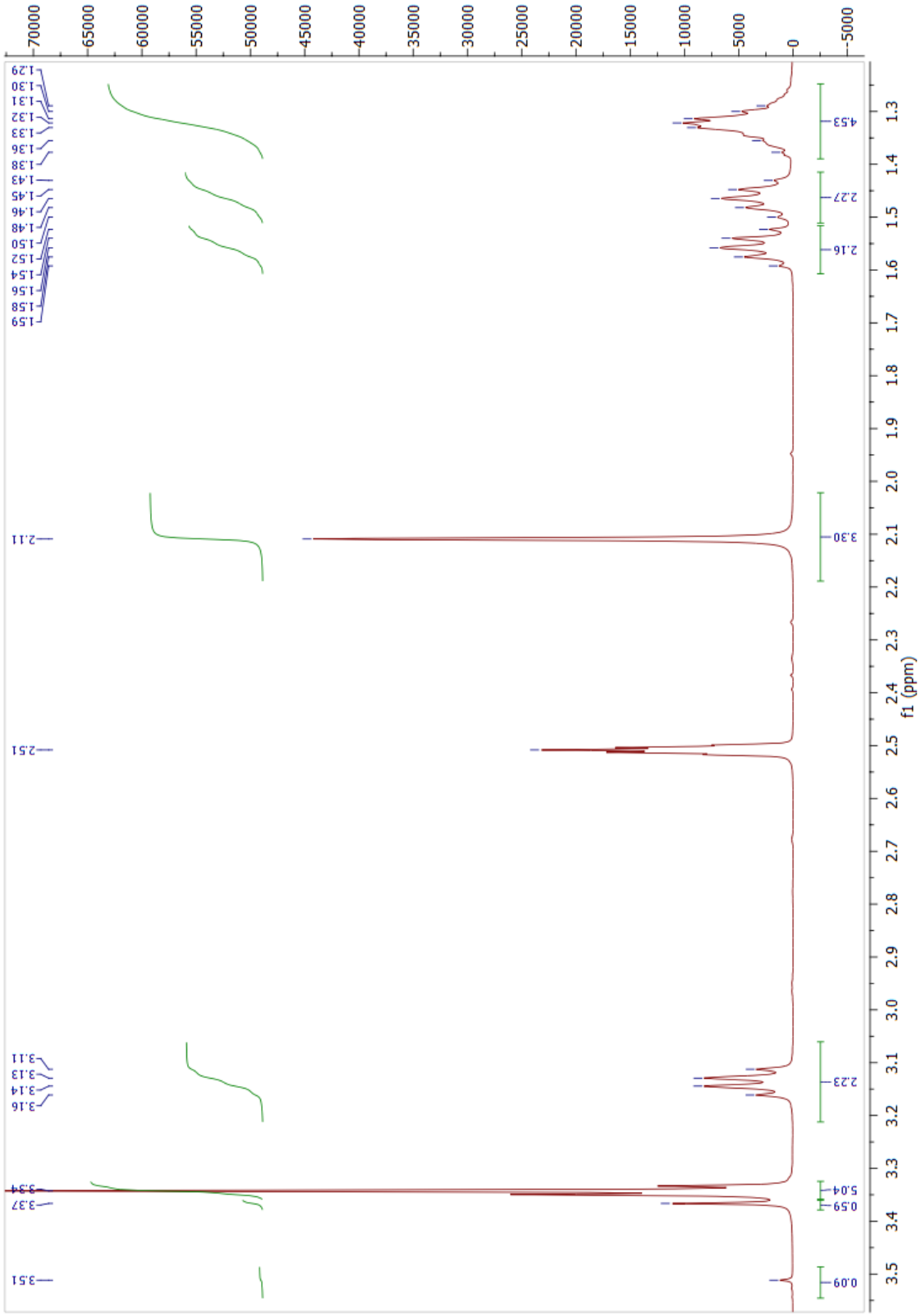

**Attachment 7.** $^{1}$H-NMR spectra of pristine HEMA-PEG-HEMA (in MeOD)

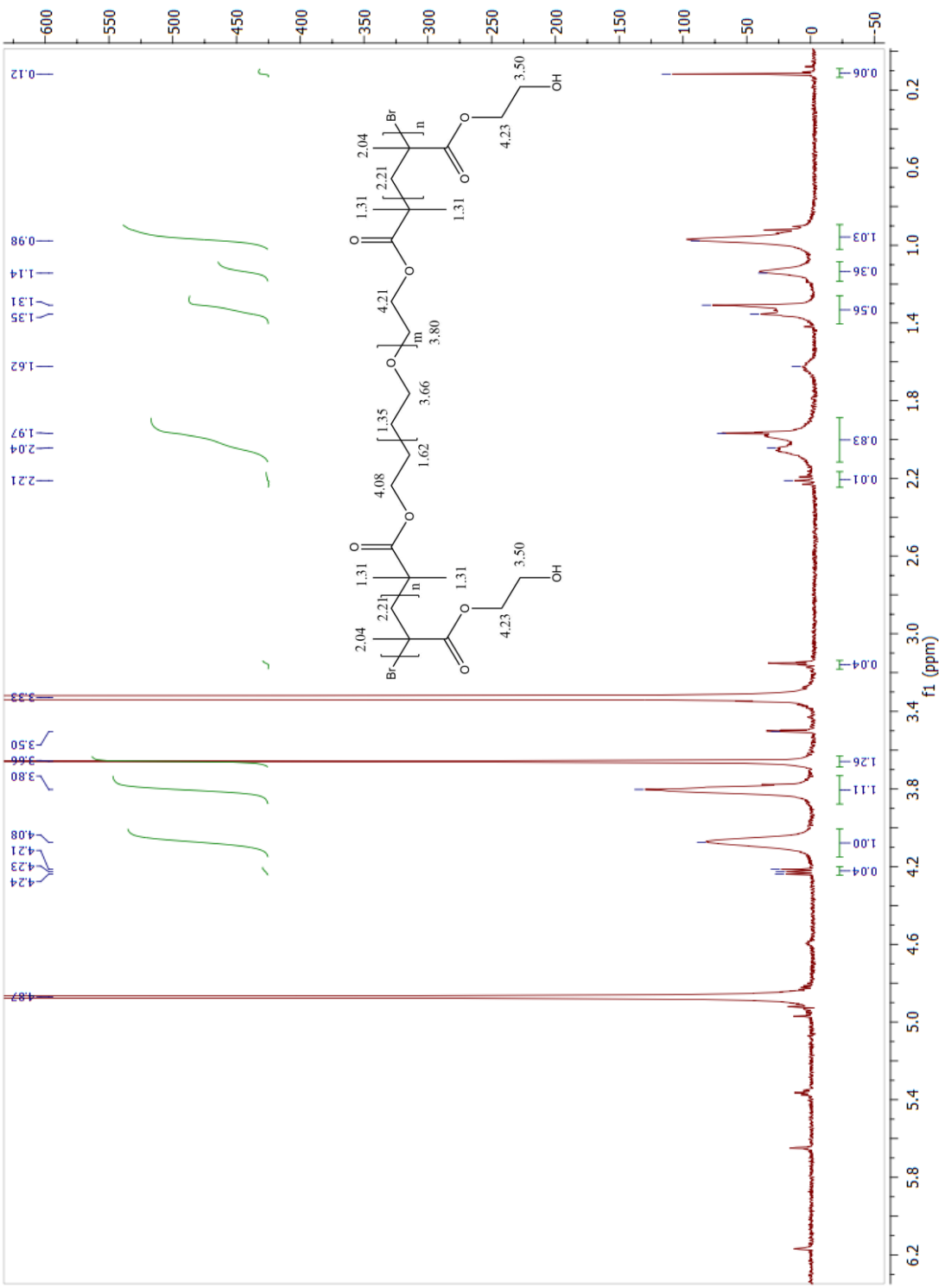

**Attachment 8.** $^{1}$H-NMR spectra of HEMA-PEG-HEMA-Upy (in DMSO-$d_6$)

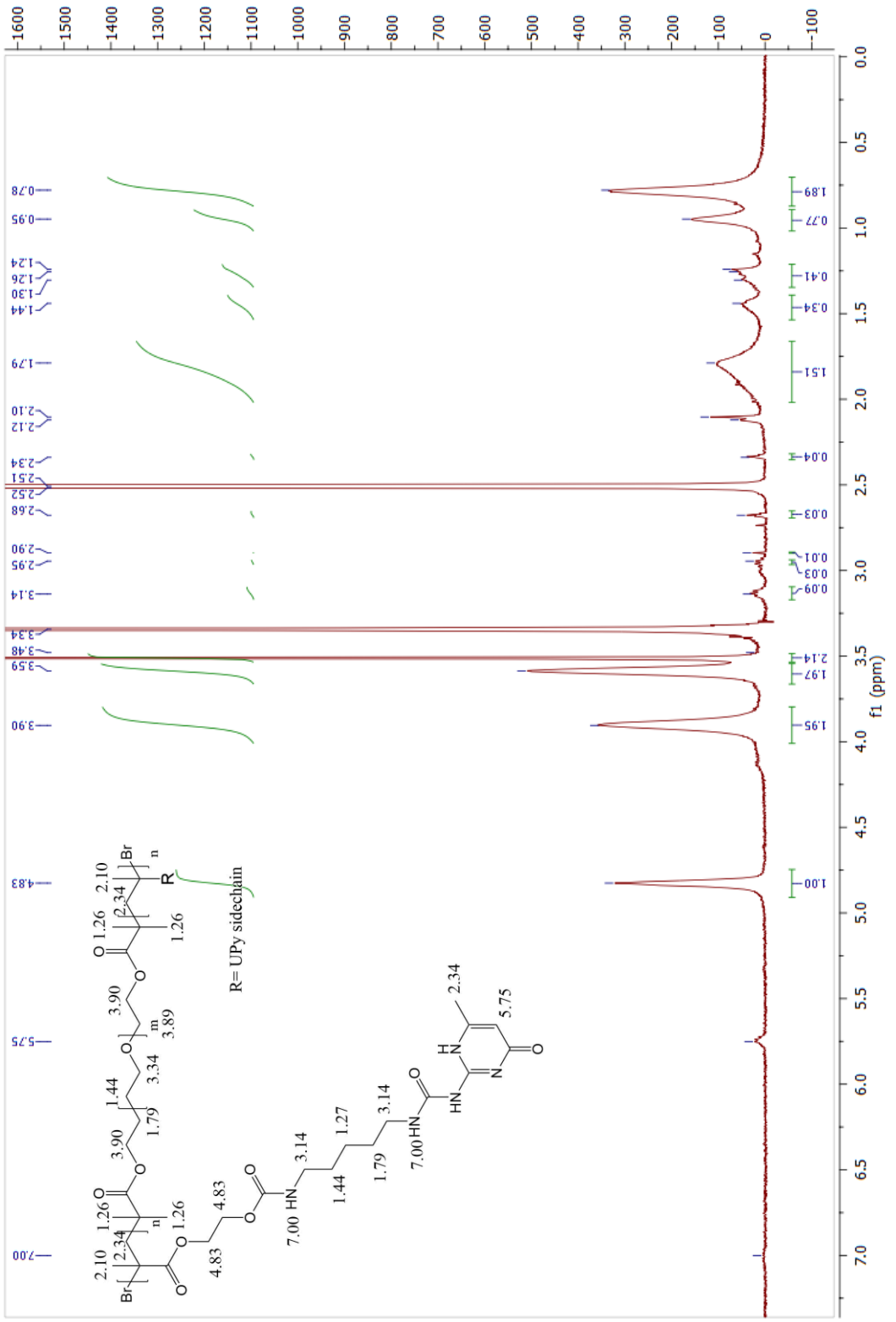

**Attachment 9.** $^{1}$H-NMR spectra of 20 kDa pHEMA (in DMSO-$d_6$).

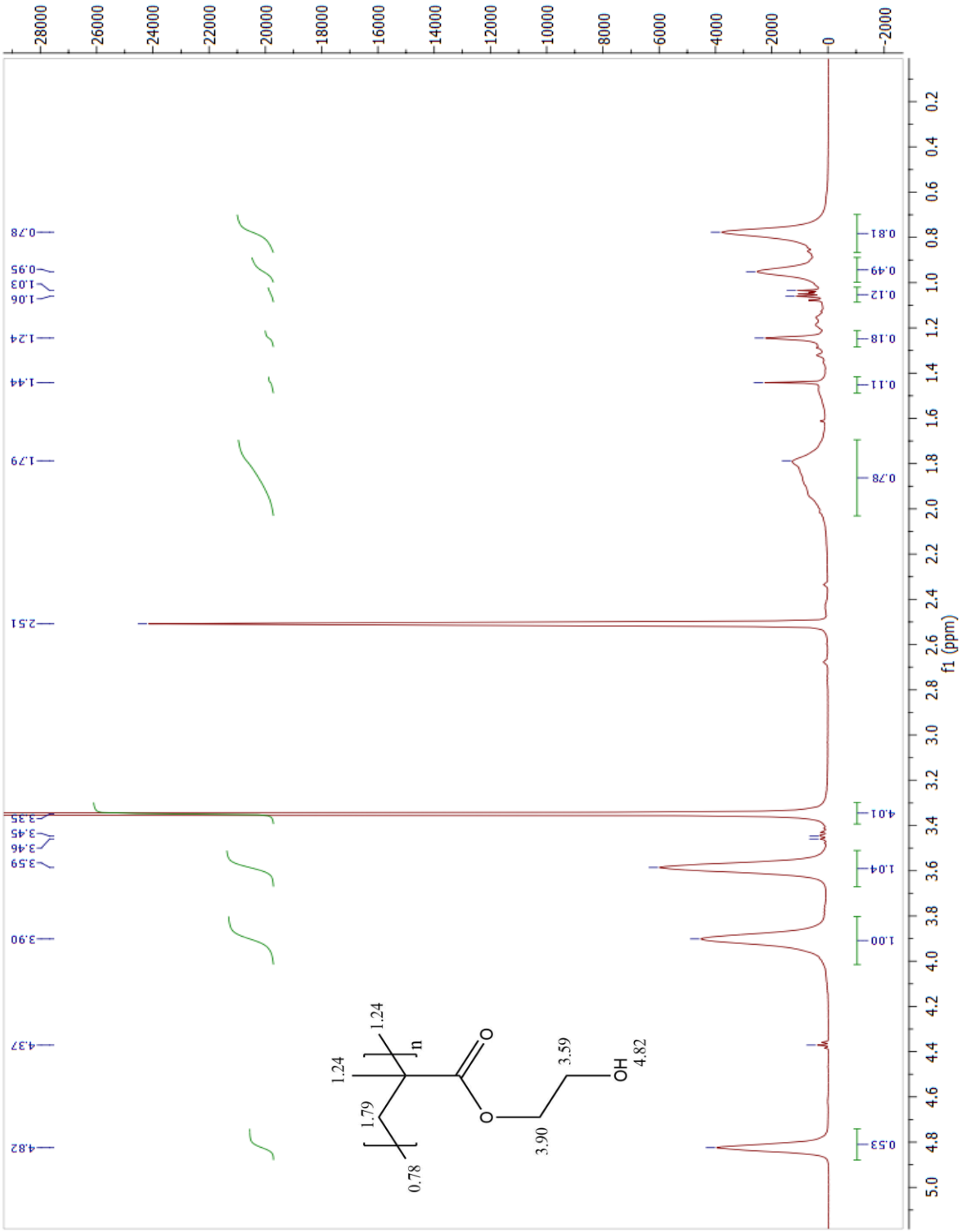

**Attachment 10.** $^{1}$H-NMR spectra of 1 MDa pHEMA (in DMSO-$d_6$).

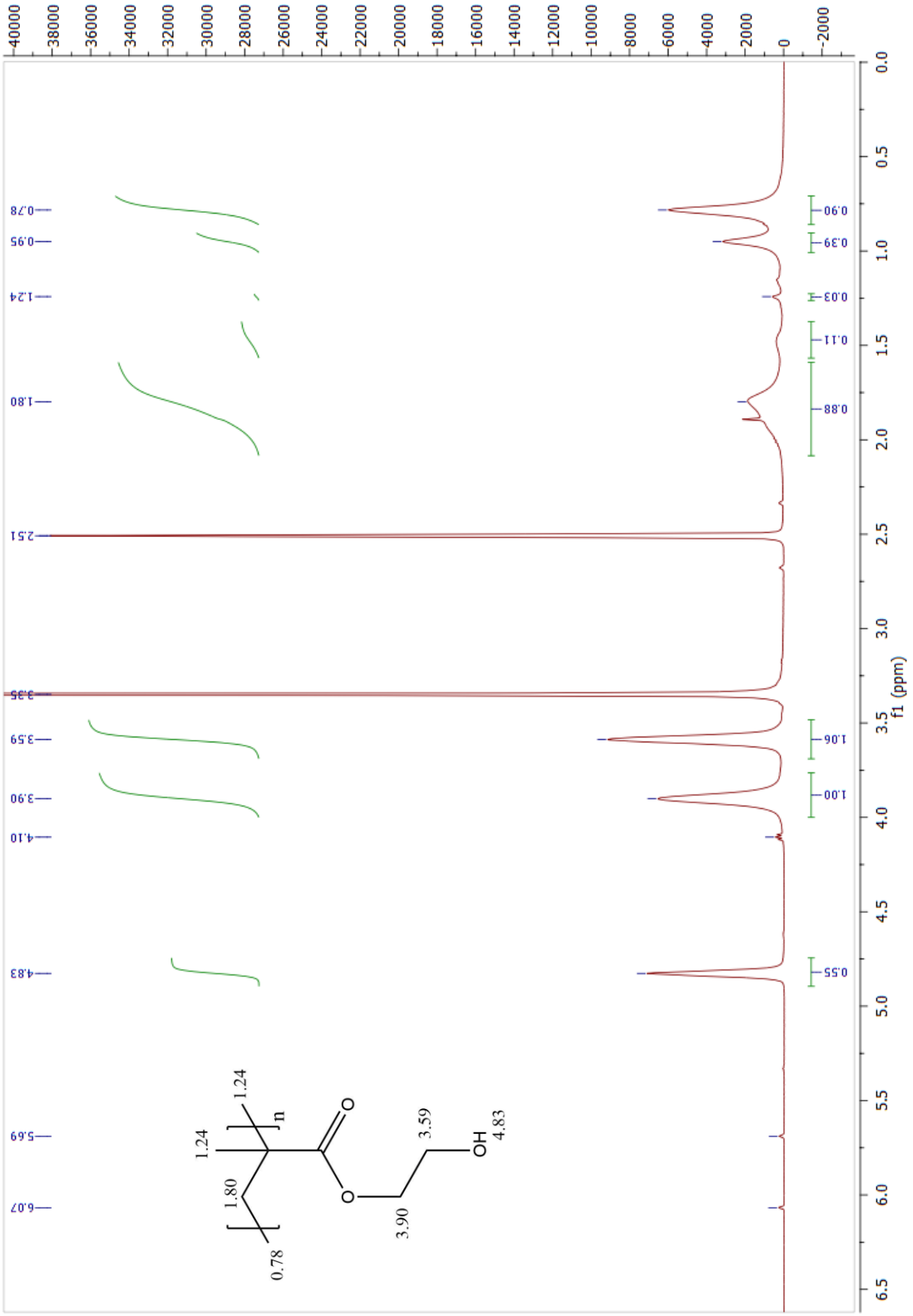

**Attachment 11.** $^{1}$H-NMR spectra of 1 % pHEMA-UPy (20 kDa pHEMA) (in DMSO-$d_6$).

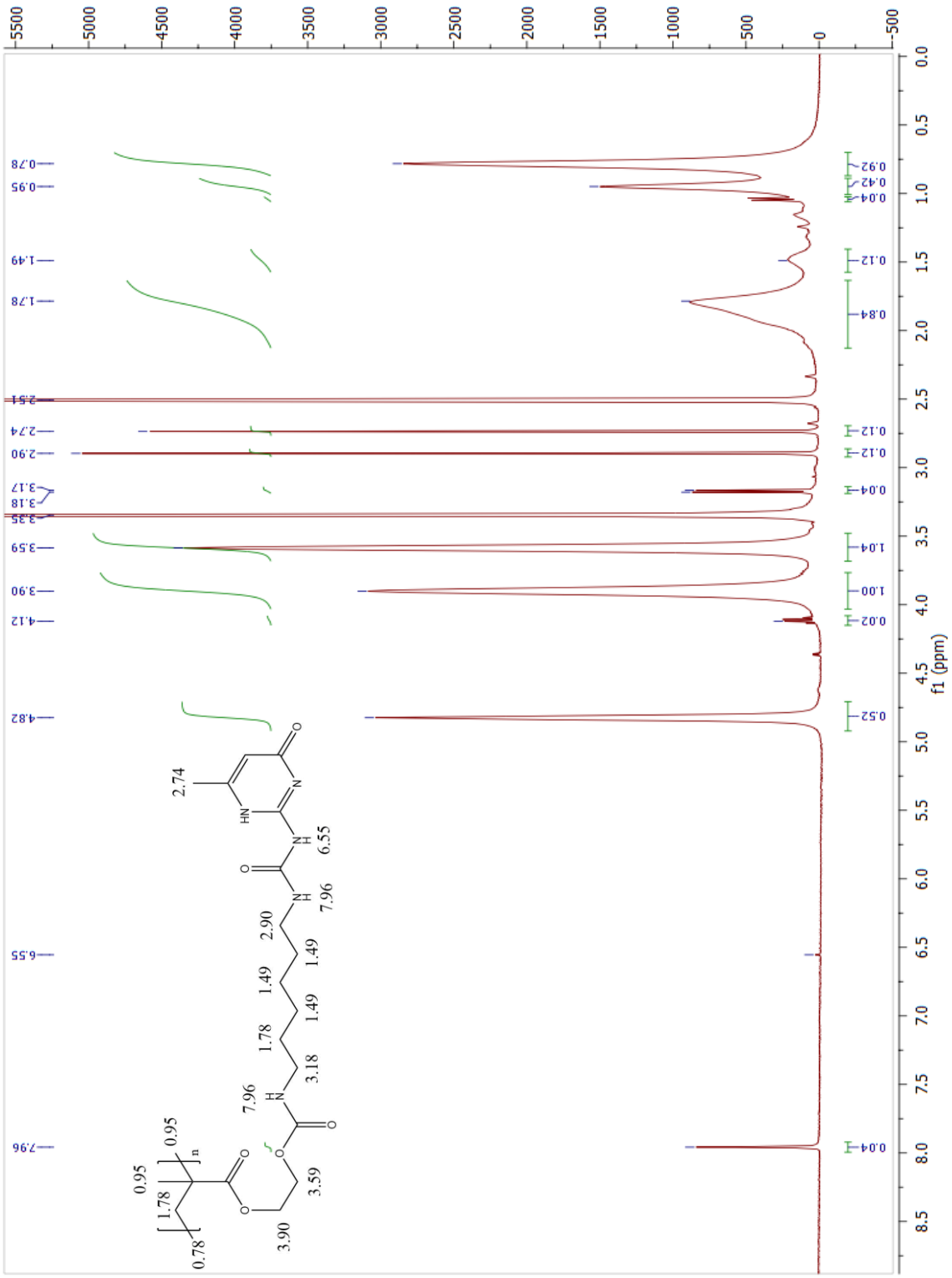

**Attachment 12.** $^{1}$H-NMR spectra of 1 % pHEMA-UPy (1 MDa pHEMA) (in DMSO-$d_6$).

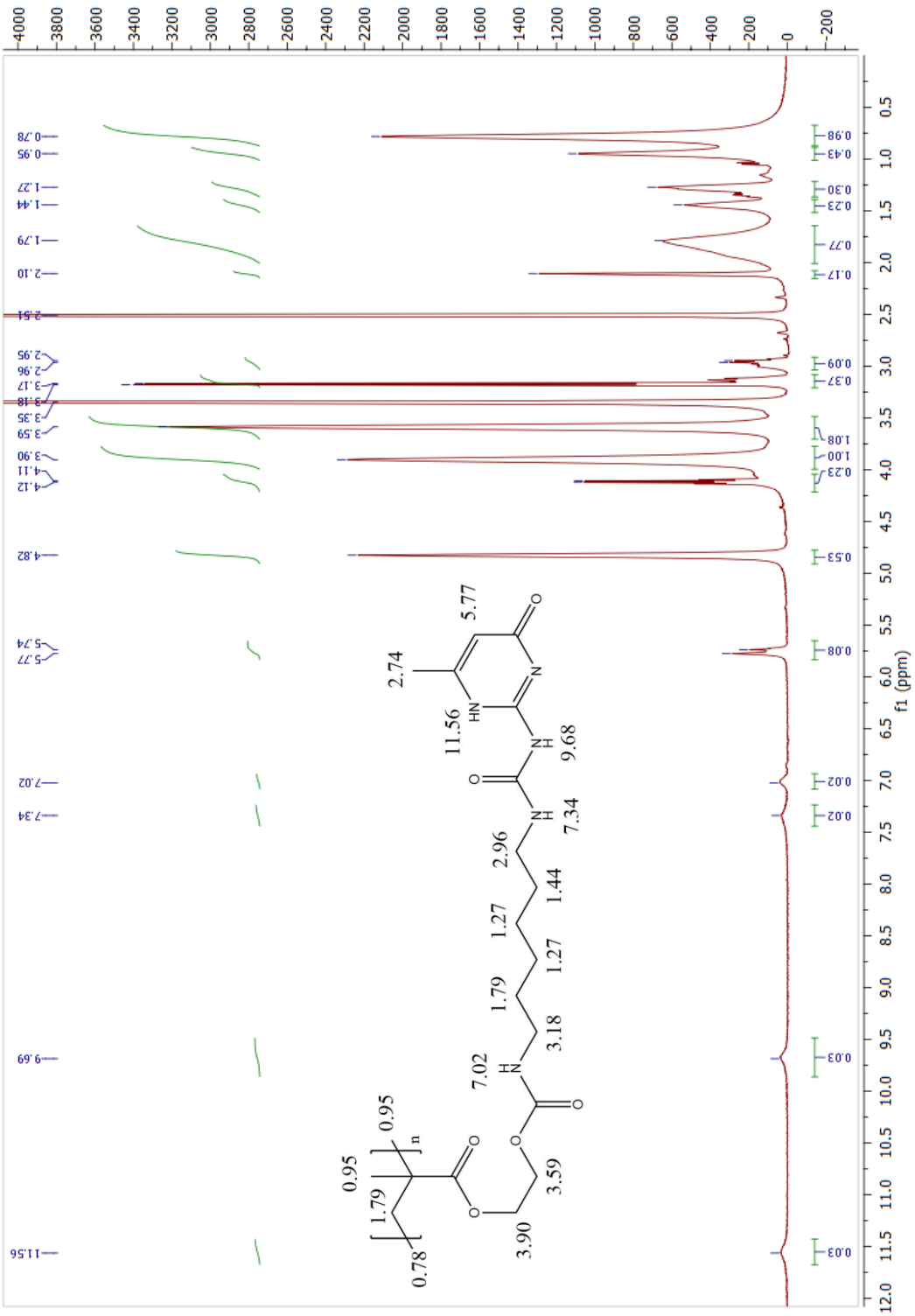

**Attachment 13.** $^{1}$H-NMR spectra of 10 % pHEMA-UPy (20 kDa pHEMA) (in DMSO-$d_6$).

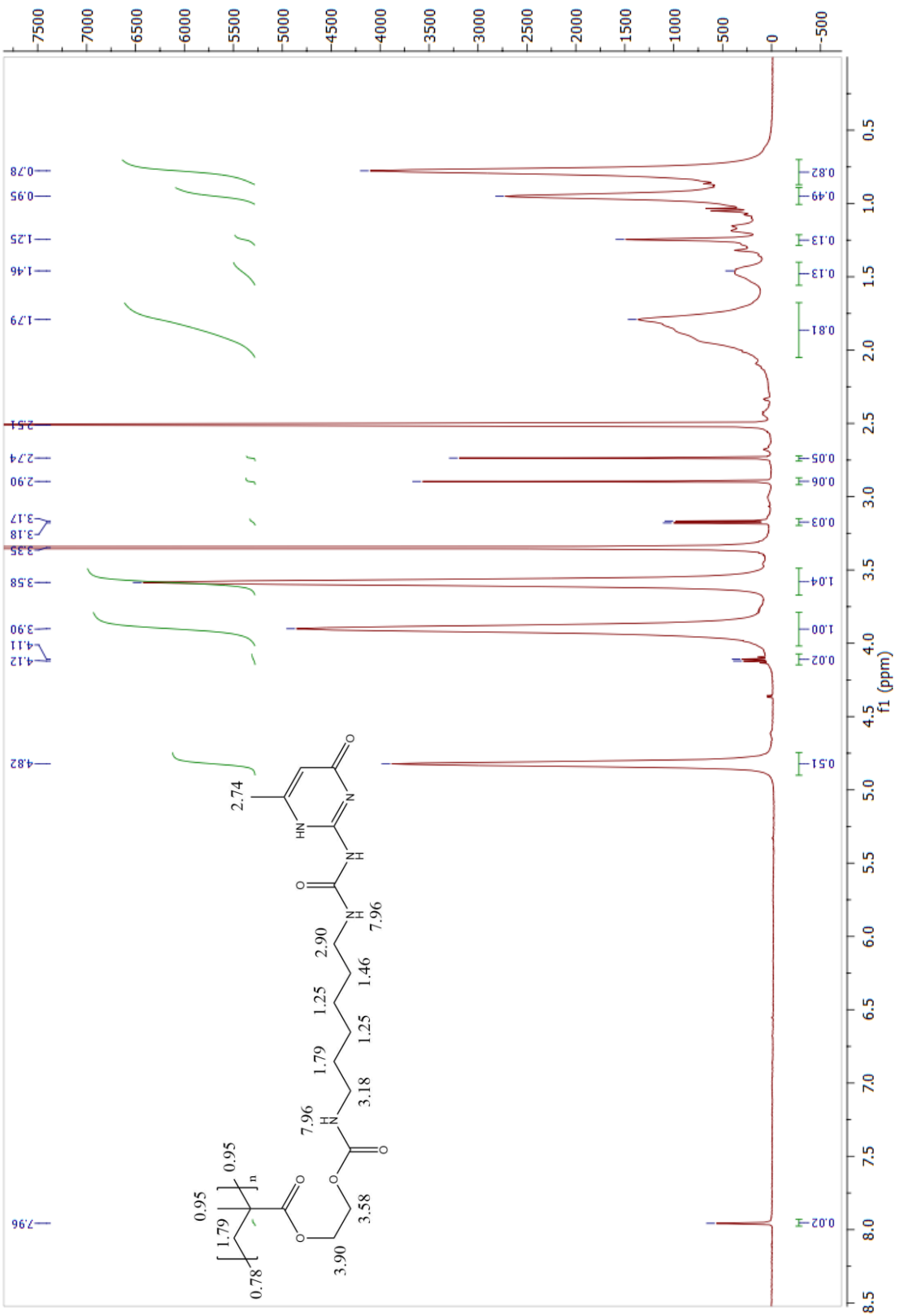

**Attachment 14.** $^{1}$H-NMR spectra of 10 % pHEMA-UPy (1 MDa pHEMA) (in DMSO-$d_6$).

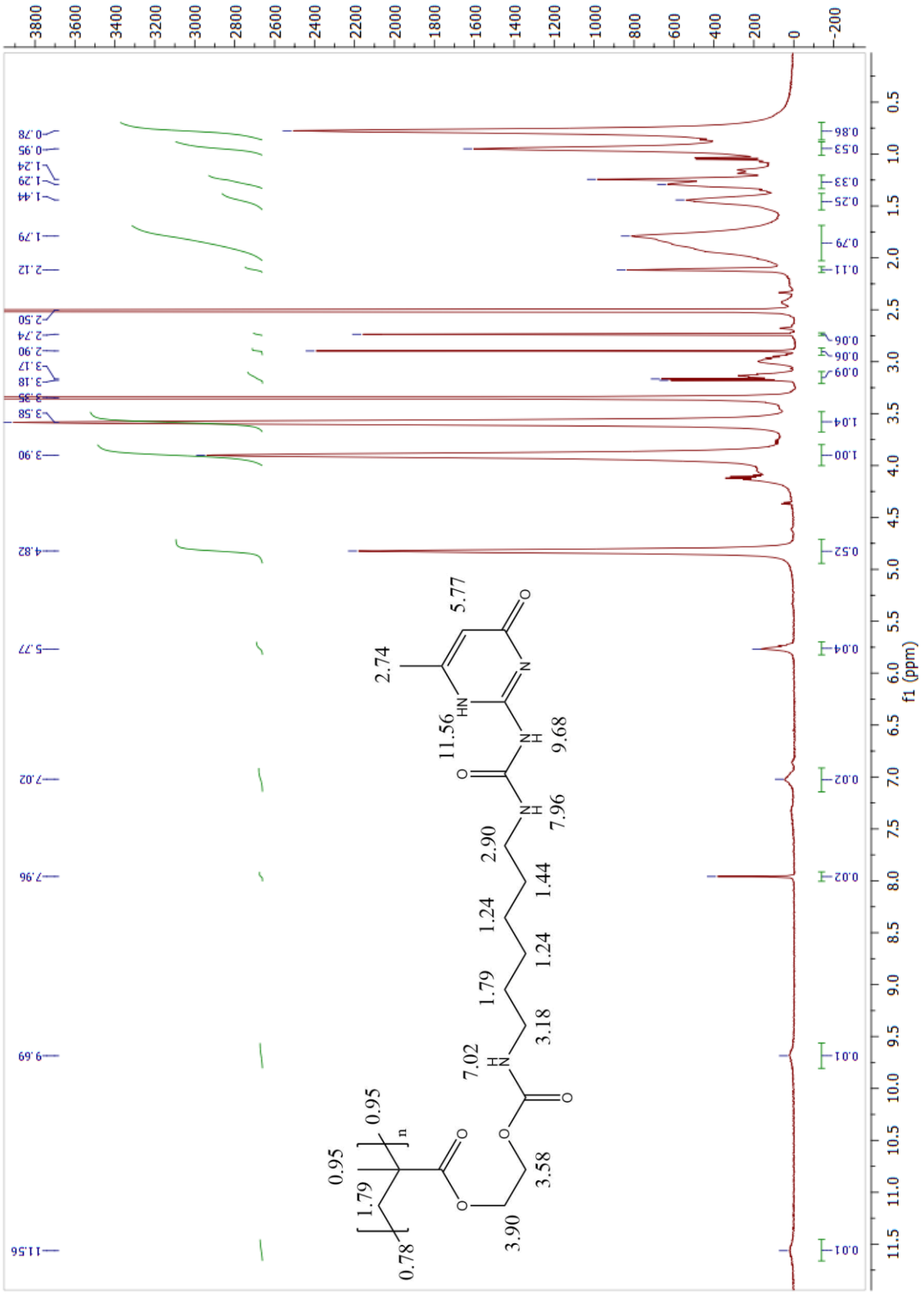

## C. Tensile testing

**Attachment 15.** Stress strain curve of 1MDa poly(2-hydroxyethylmethacrylate) polymer.

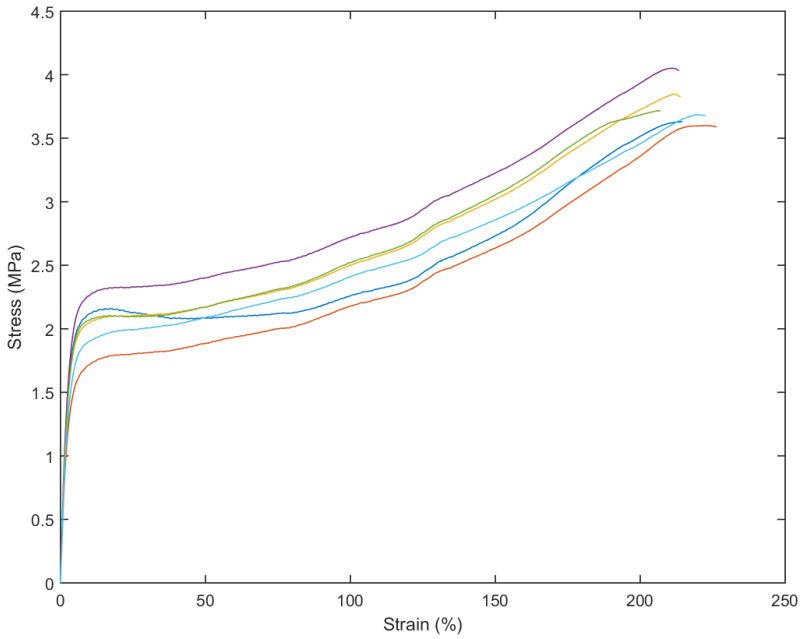


**Attachment 16.** Stress-strain curve of 1 % pHEMA-UPy derivative (1 MDa pHEMA).

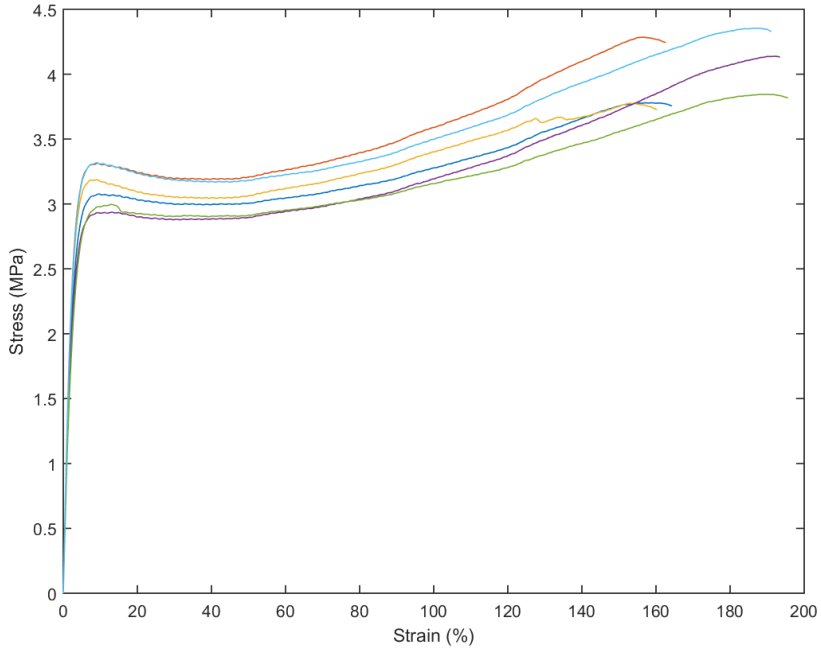

**Attachment 17.** Stress-strain curve of 10 % pHEMA-UPy derivative (1 MDa pHEMA).

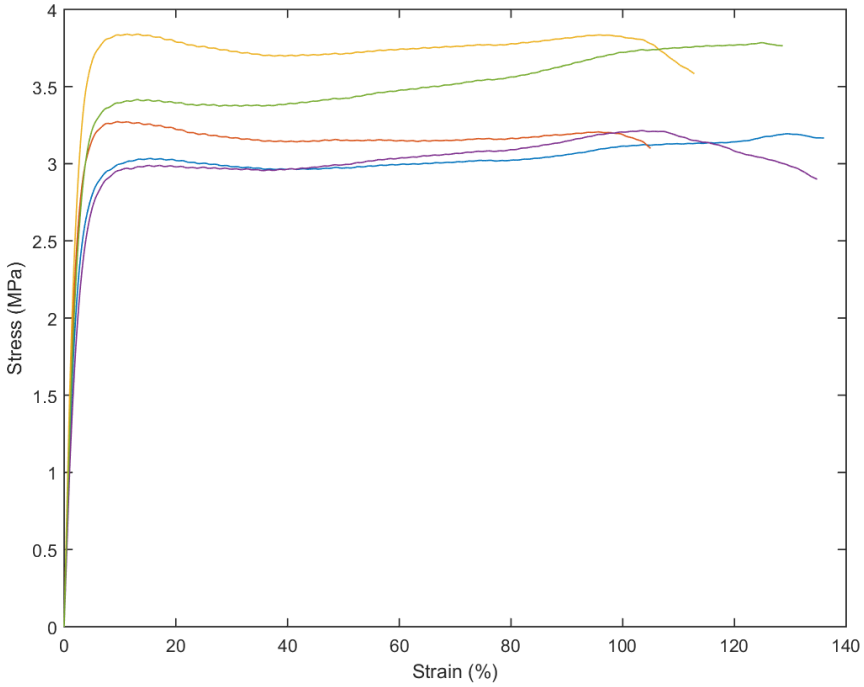


**Attachment 18.** Stress-strain curve of pHEMA (1 MDa) / 1 % w/w ox-CNT composite.

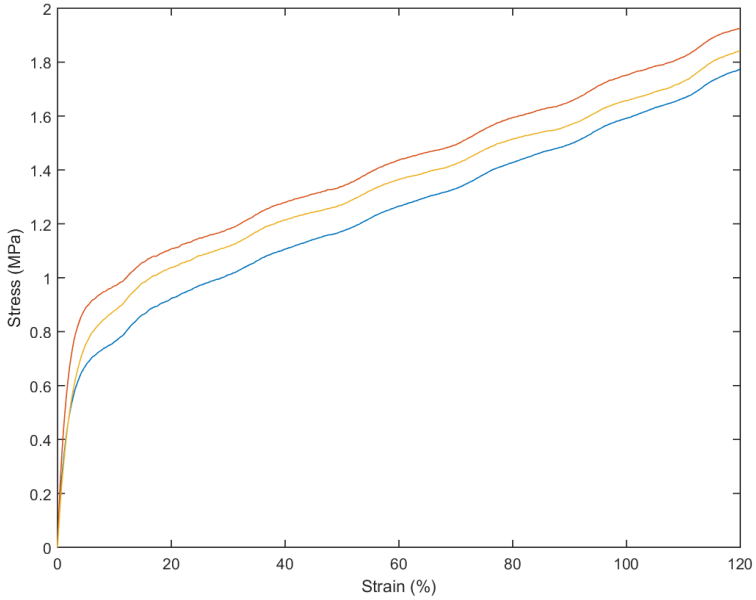

**Attachment 19.** Stress-strain curve of 1 % pHEMA-UPy / 1 % w/w CNT-UPy composite (5mm samples)

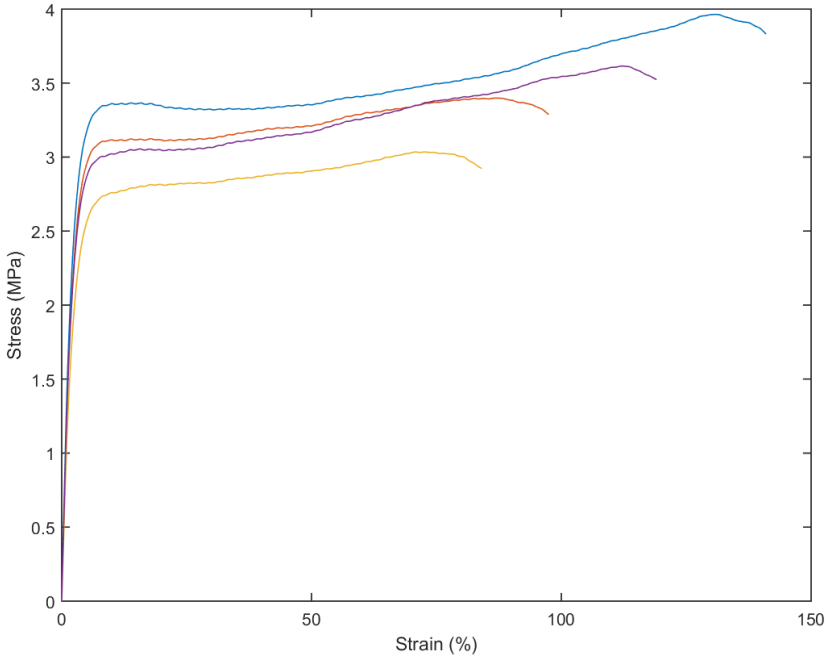


**Attachment 20.** Stress-strain curve of 1 % pHEMA-UPy / 5 % w/w CNT-UPy composite.

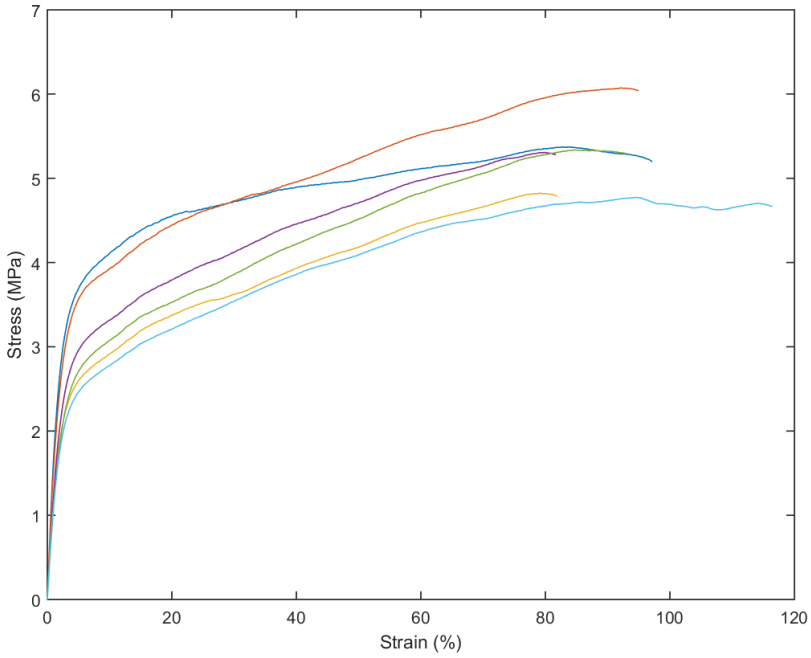

**Attachment 21.** Stress-strain curve of 10 % pHEMA-UPy / 1 % w/w CNT-UPy composite.

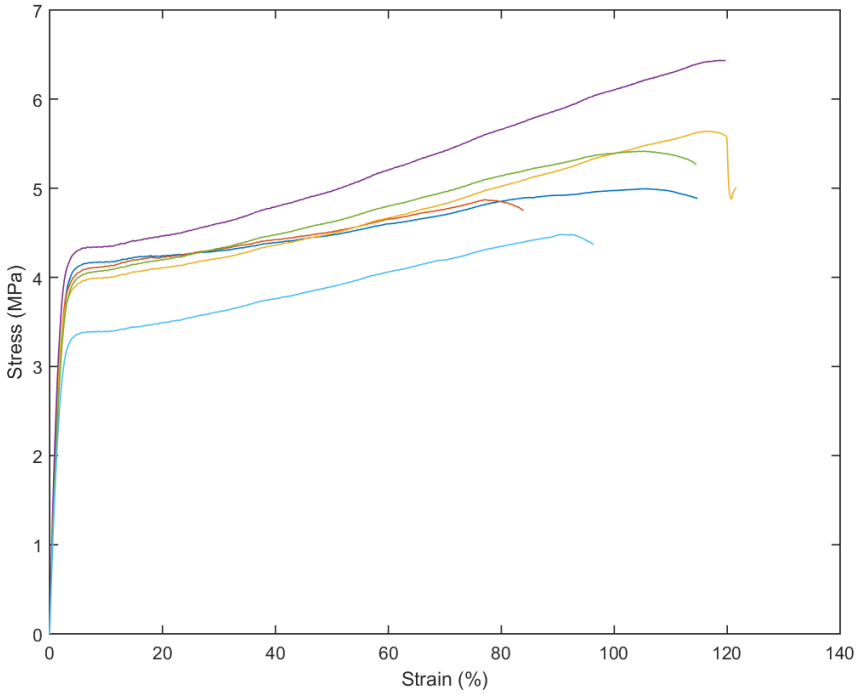


**Attachment 22.** Stress-strain curve of heat pressed 10 % pHEMA-UPy derivative (1 MDa pHEMA).

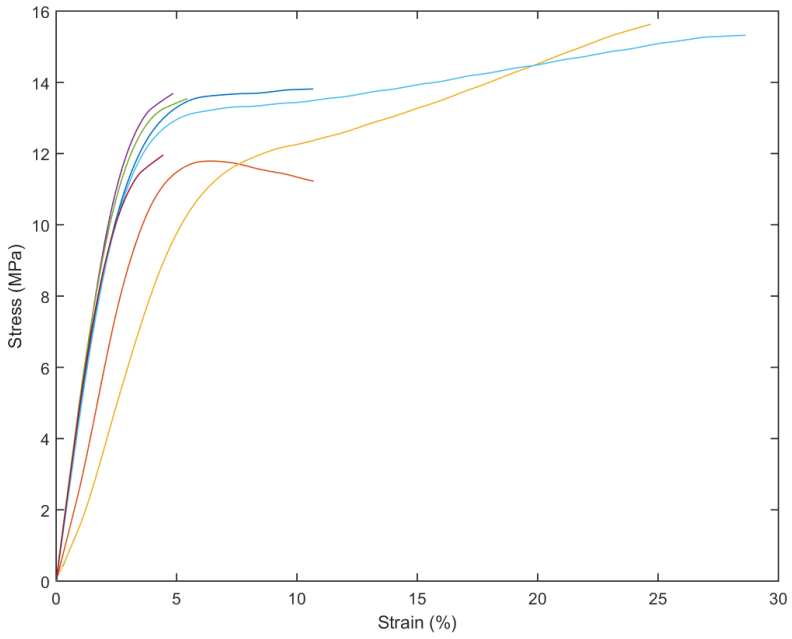

**Attachment 23.** Stress-strain curve of heat pressed 10 % pHEMA-UPy / 1 % w/w CNT-UPy composite.